PRODUCTION OF BIO-JET FUEL FROM PALM FATTY ACID DISTILLATE OVER BI-FUNCTIONAL CoPd/HZSM-12 CATALYSTS

Jarujit Chaowichitra

A Thesis Submitted in Partial Fulfillment of the Requirements
for the Degree of Master of Science
The Petroleum and Petrochemical College, Chulalongkorn University
in Academic Partnership with
The University of Michigan, The University of Oklahoma,
Case Western Reserve University, and Institut Français du Pétrole
2020

2503957090
CU iThesis 6171003063 thesis / recv: 27072563 17:27:35 / seq: 25

บทคัดย่อและแฟ้มข้อมูลฉบับเต็มของวิทยานิพนธ์ตั้งแต่ปีการศึกษา 2554 ที่ให้บริการในคลังปัญญาจุฬาฯ (CUIR)
เป็นแฟ้มข้อมูลของนิสิตเจ้าของวิทยานิพนธ์ที่ส่งผ่านทางบัณฑิตวิทยาลัย
The abstract and full text of theses from the academic year 2011 in Chulalongkorn University Intellectual Repository(CUIR)
are the thesis authors' files submitted through the Graduate School.

Production of Bio-jet Fuel from Palm Fatty Acid Distillate over Bi-functional CoPd/HZSM-12 Catalysts

2503957090 CU iThesis 6171003063 thesis / recv: 27072563 17:27:35 / seq: 25

Miss Jarujit Chaowichitra

A Thesis Submitted in Partial Fulfillment of the Requirements
for the Degree of Master of Science in Petrochemical Technology
Common Course
the Petroleum and Petrochemical College
Chulalongkorn University
Academic Year 2019
Copyright of Chulalongkorn University

การสังเคราะห์น้ำมันไบโอเจ็ทจากกรดไขมันปาล์มโดยใช้ตัวเร่งปฏิกิริยาโคบอลต์แพลเลเดียมบนตัวรองรับซีโอไลต์เอชซีเอสเอ็มทเวลฟ์

น.ส.จารุจิต เชาวน์วิจิตร

วิทยานิพนธ์นี้เป็นส่วนหนึ่งของการศึกษาตามหลักสูตรปริญญาวิทยาศาสตรมหาบัณฑิต
สาขาวิชาเทคโนโลยีปิโตรเคมี ไม่สังกัดภาควิชา/...
วิทยาลัยปิโตรเลียมและปิโตรเคมี จุฬาลงกรณ์มหาวิทยาลัย
ปีการศึกษา 2562
ลิขสิทธิ์ของจุฬาลงกรณ์มหาวิทยาลัย

2503957090 CU iThesis 6171003063 thesis / recv: 27072563 17:27:35 / seq: 25

Thesis Title	Production of Bio-jet Fuel from Palm Fatty Acid Distillate over Bi-functional CoPd/HZSM-12 Catalysts
By	Miss Jarujit Chaowichitra
Field of Study	Petrochemical Technology
Thesis Advisor	Associate Professor SIRIPORN JONGPATIWUT, Ph.D.

Accepted by the the Petroleum and Petrochemical College, Chulalongkorn University in Partial Fulfillment of the Requirement for the Master of Science

..... Dean of the the Petroleum and Petrochemical College
(Professor SUWABUN CHIRACHANCHAI, Ph.D.)

THESIS COMMITTEE

..... Chairman
(Professor THIRASAK RIRKSOMBOON, Ph.D.)

..... Thesis Advisor
(Associate Professor SIRIPORN JONGPATIWUT, Ph.D.)

..... External Examiner
(Professor Tawan Sooknoi, Ph.D.)

2503957090 CU iThesis 6171003063 thesis / recv: 27072563 17:27:35 / seq: 25

Graphical abstract

Catalyst Activity Testing

- Metal Loading
- Catalyst Support
- Reaction Temperature
- Reaction Pressure
- LHSV (h^{-1})

The optimal condition for 10Co1Pd/HZSM-12 was 350 °C, 30 bar, LHSV of 1.5 h^{-1}, and H_2/feed ratio of 8, giving 55% bio-jet fuel.

The presence of bimetallic **CoPd** on HZSM-12 zeolite support enhanced the acidity and deoxygenation activity for bio-jet fuel production. Moreover, it exhibited high stability due to its low coke formation.

10Co1Pd/HZSM-5 had high acidity, lowering bio-jet fuel yield while **10Co1Pd/HY** had a large pore size, giving a low cracking for producing jet fuel and occurring high coke deposition.

จารุจิต เชาวน์วิจิตร : การสังเคราะห์น้ำมันไบโอเจ็ทจากกรดไขมันปาล์มโดยใช้ตัวเร่งปฏิกิริยาโคบอลต์แพลเลเดียมบนตัวรองรับซีโอไลต์เอชซีเอสเอ็มทเวลฟ์. (
Production of Bio-jet Fuel from Palm Fatty Acid Distillate over Bi-functional CoPd/HZSM-12 Catalysts)
อ.ที่ปรึกษาหลัก : รศ. ดร.ศิริพร จงผาติวุฒิ

น้ำมันเจ็ทเป็นหนึ่งในผลิตภัณฑ์หลักจากอุตสาหกรรมการกลั่น ซึ่งมีการปล่อยแก๊สจากการเผาไหม้ส่งผลให้เกิดสภาวะโลกร้อน ดังนั้นน้ำมันไบโอเจ็ทจึงถูกนำมาศึกษาเพื่อแก้ปัญหาดังกล่าว กรดไขมันปาล์มเป็นสารตั้งต้นที่น่าสนใจในการเปลี่ยนเป็นน้ำมันไบโอเจ็ทโดยผ่านปฏิกิริยาดีออกซิจิเนชัน ไฮโดรแครกกิง และไอโซเมอไรเซชัน ในงานวิจัยนี้ศึกษาตัวเร่งปฏิกิริยาซึ่งประกอบด้วยโลหะเดี่ยวของโคบอลต์ (Co) และแพลเลเดียม (Pd) โลหะคู่ของโคบอลต์แพลเลเดียม (CoPd) นิกเกิลแพลเลเดียม (NiPd) บนตัวรองรับเอชซีเอสเอ็มทเวลฟ์ (HZSM-12) ที่ปริมาณต่าง ๆ และผลของโลหะคู่ CoPd บนตัวรองรับซีโอไลต์ซึ่งประกอบไปด้วยเอชซีเอสเอ็มทเวลฟ์ (HZSM-12) เอชซีเอสเอ็มไฟว์ (HZSM-5) และซีโอไลต์วาย (HY) โดยผ่านเครื่องปฏิกรณ์แบบทริคเกิลเบดชนิดไหลอย่างต่อเนื่อง การมี CoPd บนตัวรองรับ HZSM-12 ช่วยเพิ่มปฏิกิริยาดีออกซิจิเนชันและความเป็นกรดสำหรับการผลิตน้ำมันไบโอเจ็ท นอกจากนี้ 10Co1Pd/HZSM-12 แสดงความเสถียรสูงเนื่องจากเกิดโค้กน้อย 10Ni1Pd/HZSM-12 แสดงความสามารถในทำปฏิกิริยาดีออกซิจิเนชันสูงแต่ไฮโดรแครกกิงต่ำทำให้ได้ไบโอดีเซลสูง 10Co1Pd/HZSM-5 มีความเป็นกรดที่สูงทำให้มีการตัดพันธะสูงส่งผลให้เกิดน้ำมันไบโอเจ็ทน้อยลง 10Co1Pd/HY มีขนาดรูพรุนที่ใหญ่และต่อถึงกันทำให้เกิดน้ำมันไบโอเจ็ทได้ต่ำและเกิดโค้กสูง จากการศึกษาพบว่าสภาวะที่เหมาะสมในการผลิตน้ำมันไบโอเจ็ทจาก 10Co1Pd/HZSM-12 คือที่อุณหภูมิ 350 องศาเซลเซียส ความดัน 30 บาร์ สัดส่วนสารป้อนต่อปริมาณตัวเร่งปฏิกิริยา 1.5 ต่อชั่วโมง สัดส่วนโดยโมลของไฮโดรเจนต่อสารตั้งต้นเท่ากับ 8 โดยผลิตได้ถึงร้อยละ 55

สาขาวิชา เทคโนโลยีปิโตรเคมี ลายมือชื่อนิสิต

.....

ปีการศึกษา 2562 ลายมือชื่อ อ.ที่ปรึกษาหลัก

.....

2503957090 CU iThesis 6171003063 thesis / recv: 27072563 17:27:35 / seq: 25

6171003063 : MAJOR PETROCHEMICAL TECHNOLOGY
KEYWORD: Palm fatty acid distillate (PFAD)/ Bio-jet fuel/ Deoxygenation/ Cobalt/ Palladium/ HZSM-12 zeolite/

Jarujit Chaowichitra : Production of Bio-jet Fuel from Palm Fatty Acid Distillate over Bi-functional CoPd/HZSM-12 Catalysts. Advisor: Assoc. Prof. SIRIPORN JONGPATIWUT, Ph.D.

Jet fuel is one of the major products from a petroleum refinery, its combustion emissions contribute to global warming. Therefore, bio-jet fuel is introduced to solve this problem. Palm fatty acid distillate (PFAD) is an interesting feedstock for bio-jet fuel production via three reactions including deoxygenation, hydrocracking, and isomerization. In this study, the monometallic (Co and Pd) and bimetallic (CoPd and NiPd) supported on HZSM-12 zeolite with various metal loadings and bimetallic CoPd with various zeolite supports (HZSM-12, HZSM-5, and HY) were investigated in a continuous flow trickle bed reactor. The presence of bimetallic CoPd on HZSM-12 zeolite support enhanced the deoxygenation activity and acidity for bio-jet fuel production. Moreover, 10Co1Pd/HZSM-12 exhibited high stability due to its low coke formation. 10Ni1Pd/HZSM-12 catalyst showed high deoxygenation reaction but low hydrocracking thus it produced a high amount of biodiesel. The 10Co1Pd/HZSM-5 catalyst had high acidity which excessively cracked, resulting in a low quantity of bio-jet fuel, while the 10Co1Pd/HY catalyst had a big 3-dimensional pore size that caused a low selectivity to bio-jet fuel production and high coke formation. Furthermore, the optimal condition for bio-jet fuel production over 10Co1Pd/HZSM-12 catalyst was found at 350 °C, 30 bar, LHSV of 1.5 h^{-1}, and H_2/feed molar ratio of 8, giving 55 % bio-jet fuel yield.

Field of Study:	Petrochemical Technology	Student's Signature .....
Academic Year:	2019	Advisor's Signature .....

2503957090 CU iThesis 6171003063 thesis / recv: 27072563 17:27:35 / seq: 25

ACKNOWLEDGEMENTS

I am grateful for the full scholarship and full funding of the thesis work provided by the Petroleum and Petrochemical College and Center of Excellence on Petrochemical and Materials Technology.

This project cannot be completed without guidance and assistance from the following people.

I am deeply grateful to my advisor, Assoc. Prof. Siriporn Jongpatiwut for giving me an opportunity to do this project, giving suggestions and providing all supports until the completion of this project.

I would like to thank Prof. Thirasak Rirksomboon and Prof. Tawan Sooknoi for being my thesis committee and for giving me the suggestion for my project.

I am grateful to Global Green Chemicals Public Co., Ltd. who provides palm fatty acid distillate (PFAD) for using in this research.

I am thankful to Mr. Katipot Inkong who guides and teaches me to know about the mechanical skills for modifying the pipeline system until complete.

Moreover, I would like to thank all of my friends in Lab 604, including Titipan, Kan, Bharanabha, Chakorn, Ariya for their friendship and assistance.

Finally, I extend my gratitude to my parents for their love, support, inspiration, encouragement to me every way since I was young until I complete this project.

Jarujit Chaowichitra

2503957090 CU iThesis 6171003063 thesis / recv: 27072563 17:27:35 / seq: 25

TABLE OF CONTENTS

Page

ABSTRACT (THAI) iii

ABSTRACT (ENGLISH) iv

ACKNOWLEDGEMENTS v

TABLE OF CONTENTS vi

LIST OF TABLES x

LIST OF FIGURES xii

CHAPTER 1 INTRODUCTION 1

CHAPTER 2 LITERATURE REVIEW 3

2.1 Jet Fuel 3

2.2 Bio-jet Fuel 5

2.2.1 Biomass-derived Aviation Fuels 5

2.2.2 Vegetable Oil 8

2.3 Palm Fatty Acid Distillate Feedstock 10

2.4 The Overall Reaction for Bio-jet Fuel Production 15

2.4.1 Deoxygenation Reaction 15

2.4.1.1 Decarbonylation (DCN) 16

2.4.1.2 Decarboxylation (DCX) 16

2.4.1.3 Hydrodeoxygenation (HDO) 16

2.4.2 Methanation and Water-Gas-Shift Reactions 17

2.4.3 Hydrocracking and Isomerization Reactions 18

2.5 The Catalyst for Bio-jet Fuel Production 21

2.5.1 Zeolite as a Support Catalyst for Biojet Fuel Production 21

2.5.2 Active Metal and Promoter 25

CHAPTER 3 EXPERIMENTAL 26

3.1 Materials and Equipment 26

2503957090 CU iThesis 6171003063 thesis / recv: 27072563 17:27:35 / seq: 25

3.2 Experimental Procedures....28
3.2.1 Catalyst Preparation....28
3.2.1.1 Synthesis of ZSM-12 Catalyst....28
3.2.1.2 Treatment of ZSM-12 with Ammonium Nitrate....28
3.2.1.3 Preparation of HZSM-5 and HY Catalysts....28
3.2.2 Metal Loading on Zeolite Supports....29
3.3 Catalyst Characterizations....29
3.3.1 X-ray Diffraction (XRD)....29
3.3.2 X-ray Fluorescence (XRF)....29
3.3.3 Surface Analysis....29
3.3.4 Temperature Programmed Reduction (TPR)....30
3.3.5 Temperature Programmed Desorption (TPD)....30
3.3.6 Transmission Electron Microscopy (TEM)....30
3.3.7 Temperature Programmed Oxidation (TPO)....30
3.3.8 CHNS Analyzer....31
3.4 Catalytic Activity Testing....31
3.5 Product Analysis....33
3.5.1 Liquid Products Analysis....33
3.5.2 Gas Products Analysis....35
CHAPTER 4 RESULTS AND DISCUSSION....37
4.1 Characterization of Catalysts....37
4.1.1 X-ray Diffraction (XRD)....37
4.1.2 X-ray Fluorescence (XRF)....39
4.1.3 Brunauer-Emmett-Teller (BET)....40
4.1.4 Temperature Programmed Reduction (TPR)....41
4.1.5 Temperature Programmed Desorption (TPD) of Ammonia....42
4.1.6 Transmission Electron Microscopy (TEM)....44
4.1.7 Temperature Programmed Oxidation (TPO)....45
4.1.8 CHNS Analyzer....46

2503957090 CU iThesis 6171003063 thesis / recv: 27072563 17:27:35 / seq: 25

4.2 Gas Chromatography of Feed and Standard Analysis 47
4.2.1 Feed Analysis 47
4.2.2 Standard Analysis 48
4.3 Catalyst Activity Testing 50
4.3.1 Effect of Metal Loading 50
4.3.1.1 Effect of Mono- and Bi-metallic CoPd Supported on HZSM-12 50
4.3.1.2 Effect of Co Loading on CoPd/HZSM-12 Catalysts 53
4.3.1.3 Comparison CoPd/HZSM-12 and NiPd/HZSM-12 Catalysts 54
4.3.2 Effect of Zeolite Supports 55
4.3.3 Effect of Reaction Temperature 58
4.3.4 Effect of Reaction Pressure 59
4.3.5 Effect of Liquid Hourly Space Velocity (LHSV) 60
4.4 The Proposed Reaction Pathway 61
CHAPTER 5 CONCLUSIONS AND RECOMMENDATIONS 63
5.1 Conclusions 63
5.2 Recommendations 63
APPENDICES 64
Appendix A1 Overall Mass Balance of Deoxygenation-hydroprocessing at Mono- and Bi-metallic CoPd supported on HZSM-12 64
Appendix A2 Overall Mass Balance of Deoxygenation-hydroprocessing at Different Co loading on CoPd/HZSM-12 Catalysts 66
Appendix A3 Overall Mass Balance of Deoxygenation-hydroprocessing at CoPd/HZSM-12 and NiPd/HZSM-12 Catalysts 68
Appendix A4 Overall Mass Balance of Deoxygenation-hydroprocessing at Different Zeolite Supports 70
Appendix A5 Overall Mass Balance of Deoxygenation-hydroprocessing at Different in Temperature 72
Appendix A6 Overall Mass Balance of Deoxygenation-hydroprocessing at Different in Pressure 74
Appendix A7 Overall Mass Balance of Deoxygenation-hydroprocessing at Different Liquid Hourly Space Velocity 76

2503957090 CU iThesis 6171003063 thesis / recv: 27072563 17:27:35 / seq: 25

REFERENCES 78
VITA 83

2503957090
CU iThesis 6171003063 thesis / recv: 27072563 17:27:35 / seq: 25

LIST OF TABLES

PAGE

Table 2.1 Recent research on the conversion of lipid to bio-aviation fuel (2010 to 2018) (Wang *et al.*, 2019) 6

Table 2.2 Chemical structure for common vegetable oil of fatty acids (Ong *et al.*, 2011) 9

Table 2.3 Oil palm biomass components and potential energy generated (Ong *et al.*, 2011) 13

Table 2.4 Refining volumes (tonnes) and value of palm oil & PFAD in Malaysia. 2012 – 2015 average (Ab Gapor Md, 2010) 15

Table 2.5 Methanation and water-gas-shift reactions (Feng *et al.*, 2019) 17

Table 2.6 The topology, channel structure, size, and pore model of zeolites (Zhang *et al.*, 2016) 22

Table 3.1 The description of system in flow diagram of the continuous flow trickle-bed reactor 32

Table 3.2 The reaction conditions for hydroprocessing of PFAD in continuous flow trickle-bed reactor 33

Table 3.3 The chromatographic temperature program for liquid product analysis 34

Table 3.4 The chromatographic temperature program for gas-phase product analysis 35

Table 4.1 XRD data of the prepared HZSM-12 38

Table 4.2 Chemical composition of the prepared catalysts 39

Table 4.3 Physical characteristics of the prepared catalysts 40

Table 4.4 Acidity of parent HZSM-12, 10Co1Pd/HZSM-12, 10Co/HZSM-12, 1Pd/HZSM-12, 10Ni1Pd/HZSM-12, 10Co1Pd/HZSM-5, and 10Co1Pd/HY from NH_3-TPD 43

Table 4.5 Amount of carbon deposits on spent catalysts from CHNS analyzer 47

Table 4.6 Composition of PFAD feedstock 48

Table A1 Overall mass balance of deoxygenation-hydroprocessing one-pot reaction over 10Co/HZSM-12, 1Pd/HZSM-12, and 10Co1Pd/HZSM-12 catalysts (Reaction

2503957090 CU iThesis 6171003063 thesis / recv: 27072563 17:27:35 / seq: 25

conditions: 350°C, 30 bar, H_2/Feed molar ratio of 8, LHSV of 1.5 h^{-1}, and TOS = 6 h) 64

Table A2 Overall mass balance of deoxygenation-hydroprocessing one-pot reaction over 5Co1Pd/HZSM-12, 10Co1Pd/HZSM-12, and 15Co1Pd/HZSM-12 catalysts (Reaction conditions: 350°C, 30 bar, H_2/Feed molar ratio of 8, LHSV of 1.5 h^{-1}, and TOS = 6 h) 66

Table A3 Overall mass balance of deoxygenation-hydroprocessing one-pot reaction over 10Co1Pd/HZSM-12 and 10Ni1Pd/HZSM-12 catalysts (Reaction conditions: 350°C, 30 bar, H_2/Feed molar ratio of 8, LHSV of 1.5 h^{-1}, and TOS = 6 h) 68

Table A4 Overall mass balance of deoxygenation-hydroprocessing one-pot reaction over 10Co1Pd/HY, 10Co1Pd/HZSM-12, and 10Co1Pd/HZSM-5 catalysts (Reaction conditions: 350°C, 30 bar, H_2/Feed molar ratio of 8, LHSV of 1.5 h^{-1}, and TOS = 6 h) 70

Table A5 Overall mass balance of deoxygenation-hydroprocessing one-pot reaction over 10Co1Pd/HZSM-12 catalyst in different temperature (Reaction conditions: 30 bar, H_2/Feed molar ratio of 8, LHSV of 1.5 h^{-1}, and TOS = 6 h) 72

Table A6 Overall mass balance of deoxygenation-hydroprocessing one-pot reaction over 10Co1Pd/HZSM-12 catalyst in different pressure (Reaction conditions: 350°C, H_2/Feed molar ratio of 8, LHSV of 1.5 h^{-1}, and TOS = 6 h).....74

Table A7 Overall mass balance of deoxygenation-hydroprocessing one-pot reaction over 10Co1Pd/HZSM-12 catalyst in different liquid hourly space velocity (Reaction conditions: 350°C, 30 bar, H_2/Feed molar ratio of 8, and TOS = 6 h) 76

2503957090 CU iThesis 6171003063 thesis / recv: 27072563 17:27:35 / seq: 25

LIST OF FIGURES

PAGE

Figure 2.1 Expected growth of the aviation sector. Left: Passenger Traffic Forecast in billion revenue passengers kilometers (RPK) (most likely scenario/central forecast). Right: Aviation oil consumption [Mtoe] by region (New Policies Scenario) (Thrän et al., 2016). 4

Figure 2.2 Typical structure of a triglyceride molecule (Ong et al., 2011). 9

Figure 2.3 Oil palm tree and fruits (Ong *et al.*, 2011). 11

Figure 2.4 Fresh oil palm fruit and its longitudinal section (Ong *et al.*, 2011). 11

Figure 2.5 Production oil yield for various sources of biodiesel feedstock (Ong *et al.*, 2011). 12

Figure 2.6 World palm oil production 2009 (Ong *et al.*, 2011). 13

Figure 2.7 Physical refining process of crude palm oil (Kiatkittipong *et al.*, 2013)...14

Figure 2.8 Various deoxygenation reaction schemes with other possible reactions including thermodynamic data (ΔG_{573} in kJ/mol at 1 bar) (Pattanaik et al., 2017). 16

Figure 2.9 Methanation and water-gas-shift reactions (Khan *et al.*, 2019). 18

Figure 2.10 Composition of zeolites: from primary building unit to zeolite cage-like frameworks (Ramsay *et al.*, 2000). 21

Figure 2.11 The yield of di-branched C10 as a function of monobranched C10 in n-decane hydroisomerization at 5% isomerization yield. Conditions: 4.5 bar, 300 °C, H_2/n-C_{10} molar ratio of 214, WHSV of 0.37 h^{-1} (Mäki-Arvela et al., 2018). 24

Figure 3.1 The schematic diagram of the reactor system. 32

Figure 4.1 XRD patterns of synthesized catalysts. 38

Figure 4.2 H_2-TPR profiles of 10Co1Pd/HZSM-12, 10Co/HZSM-12, 1Pd/HZSM-12, and 10Ni1Pd/HZSM-12. 41

Figure 4.3 NH_3-TPD profiles of parent HZSM-12, 1Pd/HZSM-12, 10Co/HZSM-12, 10Co1Pd/HZSM-12, 10Co1Pd /HZSM-5, and 10Co1Pd /HY catalysts. 43

Figure 4.4 TEM images of (a) calcined HZSM-12 zeolite, (b) 5Co1Pd/ HZSM-12 zeolite, (c) 10Co1Pd/ HZSM-12 zeolite, and (d) 15Co1Pd/ HZSM-12 catalysts....44

2503957090 CU iThesis 6171003063 thesis / recv: 27072563 17:27:35 / seq: 25

Figure 4.5 Temperature Programmed Oxidation of 1Pd/HZSM-12, 10Co/HZSM-12, 10Co1Pd/HZSM-12, 10Ni1Pd/HZSM-12, 10Co1Pd/HZSM-5, and 10Co1Pd/HY catalysts. 46

Figure 4.6 The chromatogram of various components in PFAD range analyzed by a GC/FID. 48

Figure 4.7 The chromatogram of various *n*-alkane components in ASTM 2887 standard analyzed by a GC/FID. 49

Figure 4.8 The chromatogram of oxygenated compounds standard analyzed by a GC/FID. 50

Figure 4.9 The conversion of PFAD and product yield obtained over (a) 1Pd/HZSM-12, (b) 10Co/HZSM-12, and (c) 10Co1Pd/HZSM-12 (Reaction condition: 350°C, 30 bar, LHSV= 1.5 h^{-1}, and H_2/feed molar ratio of 8). 52

Figure 4.10 The conversion and yield of products over 1Pd/HZSM-12, 10Co /HZSM-12, and 10Co1Pd/HZSM-12 catalysts (Reaction condition: 350°C, 30 bar, LHSV= 1.5 h^{-1}, H_2/feed molar ratio of 8, and TOS= 6 h). 53

Figure 4.11 The conversion and yield of products over 5Co1Pd/HZSM-12, 10Co1Pd/HZSM-12, and 15Co1Pd/HZSM-12 catalysts (Reaction condition: 350°C, 30 bar, LHSV= 1.5 h^{-1}, H_2/feed molar ratio of 8, and TOS= 6 h). 54

Figure 4.12 The conversion and yield of products over 10Ni1Pd/HZSM-12 and 10Co1Pd/HZSM-12 catalysts (Reaction condition: 350°C, 30 bar, LHSV= 1.5 h^{-1}, H_2/feed molar ratio of 8, and TOS= 6 h). 55

Figure 4.13 The appearance of liquid products obtained over different supports (a) 10Co1Pd/HZSM-12, (b) 10Co1Pd/HZSM-5, and (c) 10Co1Pd/HY (Reaction condition: 350°C, 30 bar, LHSV= 1.5 h^{-1}, and H_2/feed molar ratio of 8)..... 56

Figure 4.14 The Conversion of PFAD and product yield obtained over (a) 10Co1Pd/HZSM-12, (b) 10Co1Pd/HZSM-5, and (c) 10Co1Pd/HY (Reaction condition: 350°C, 30 bar, LHSV= 1.5 h^{-1}, and H_2/feed molar ratio of 8)..... 57

Figure 4.15 The conversion and yield of products over 10Co1Pd/HZSM-5, 10Co1Pd/HZSM-12, and 10Co1Pd/HY catalysts (Reaction condition: 350°C, 30 bar, LHSV= 1.5 h^{-1}, H_2/feed molar ratio of 8, and TOS= 6 h). 58

Figure 4.16 The conversion and yield of products over 10Co1Pd/HZSM-12 catalyst with different temperatures (Reaction condition: 30 bar, LHSV= 1.5 h^{-1}, H_2/feed molar ratio of 8, and TOS= 6 h)..... 59

2503957090 CU iThesis 6171003063 thesis / recv: 27072563 17:27:35 / seq: 25

Figure 4.17 The conversion and yield of products over 10Co1Pd/HZSM-12 catalyst with different pressure (Reaction condition: 350°C, LHSV= 1.5 h^{-1}, H_2/feed molar ratio of 8, and TOS= 6 h). 60

Figure 4.18 The conversion and yield of products over 10Co1Pd/HZSM-12 catalysts with different LHSV (Reaction condition: 350°C, 30 bar, H_2/feed molar ratio of 8, and TOS= 6 h). 61

Figure 4.19 The proposed reaction pathway of bio-jet fuel production from palmitic acid over bi-functional catalysts. 62

2503957090 CU iThesis 6171003063 thesis / recv: 27072563 17:27:35 / seq: 25

2503957090 CU iThesis 6171003063 thesis / recv: 27072563 17:27:35 / seq: 25

CHAPTER 1
INTRODUCTION

Nowadays, transportation by airplane has been increasing due to increasing industrialization and motorization. Jet fuel, referred to as aviation fuel, is one of the major products from petroleum refinery. The combustion of fossil fuels has come into considerable attention because of the impact on environment and health, the combustion of fossil fuels has released greenhouse gases (GHG) including a myriad of toxic air pollutants and carbon dioxide (CO_2). Thus, alternative energy is necessary for solving this problem. There are many types of research attempting to develop new alternative energy for replacing the rising of petroleum-based fuel demand and the fluctuation of oil prices.

One of the most appropriate raw materials for renewable aviation fuels is the vegetable oil which contains fatty acid in the proper carbon chain range and offers a simpler approach to the production of bio-jet fuel. Palm fatty acid distillate or PFAD is a by-product from the crude palm oil refinery process that is normally used in soap and animal food industries. PFAD has become an attractive raw material since its cost is low and it does not affect to food chain. The main component in PFAD is free fatty acids which are oleic, stearic, and palmitic acids.

Bi-functional catalysts, containing metal site and acid site, comes into consideration to produce hydrocarbon in the jet fuel range ($C_9 - C_{14}$) from PFAD via deoxygenation process (DO) and C arrangement. In the DO process, fatty acids are transformed into saturated hydrocarbons through three possible pathways: decarboxylation, decarbonylation, and hydrodeoxygenation reactions. Then, the saturated hydrocarbons can be further converted into bio-jet fuel by hydrocracking and hydroisomerization. Pd is a noble metal highly active and selective for the DO process through decarboxylation pathway. Co is a non-noble metal which exhibits high stability and presents high performance for hydrodeoxygenation pathway at high reaction pressure. Ni is a non-noble metal selective to decarboxylation pathway and mainly taken part in hydrogenation. Therefore, side reaction such as methanation occurs which could reduce coke deposition. In addition, metals increase the acid

strength which shifts the reaction towards the hydrocracking to produce alkane which has appropriate hydrocarbons in jet fuel range. HZSM-12 is an attractive acid catalyst support because of its good stability, resistance to deposit hard coke, and excellent catalytic performance. Beside HZSM-12, HZSM-5 and HY which are commercially used as catalyst support are also studied to investigate the effect of pore size, dimensional structure, and acidity.

In this study, the conversion of PFAD to bio-jet fuels was investigated in a trickle bed reactor. The monometallic (Co and Pd) and bimetallic (CoPd and NiPd) supported on HZSM-12 zeolite with various metal loadings and bimetallic CoPd with various zeolite supports (HZSM-12, HZSM-5, and HY) were prepared by incipient wetness impregnation. The catalysts were used to investigate the conversion and products selectivity during the catalysts activity testing. The fresh catalysts were characterized by X-ray diffraction (XRD), X-ray fluorescence (XRF), Brunauer-Emmett-Teller (BET), temperature programmed reduction (TPR), temperature programmed desorption (TPD) of ammonia, and transmission electron microscopy (TEM). Furthermore, the spent catalysts were characterized by temperature programmed oxidation (TPO) and CHNS analyzer. Moreover, the optimum operating conditions (i.e. temperature, pressure, and LHSV) for producing bio-jet fuel were also investigated.

2503957090 CU iThesis 6171003063 thesis / recv: 27072563 17:27:35 / seq: 25

2503957090 CU iThesis 6171003063 thesis / recv: 27072563 17:27:35 / seq: 25

CHAPTER 2
LITERATURE REVIEW

2.1 Jet Fuel

Jet fuel is a common name for aviation fuels used in gas-turbine engine powered aircraft. Traditionally jet fuel has main components which consist of linear alkanes, branched alkanes (around 70 to 85%), and cycloalkanes. Jet fuel typically composed a carbon number in range C_9–C_{14}. Typically, jet fuel (or 'kerosene') corresponds to the kerosene distillation fraction of crude oil (~150 – 275 °C). Physicochemical properties of jet fuel differ from other combustion engine fuels in terms of operational conditions and engine specific technical requirements. Moreover, the relative proportion of several hydrocarbons affects the properties of jet fuel such as energy content, combustibility, density, and fluidity. Jet fuel requires the minimal composition of sulfur, oxygen, and nitrogen hetero compounds since they influence fuel stability, lubricity, corrosivity, and cooling characteristics that affect the combustion properties and the environmental impact (Kallio *et al.*, 2014). There are two main standard international specifications of aviation in the market which compose of Jet A/Jet A–1 and Jet B. Firstly, Jet A and Jet A–1 are kerosene type fuels that have the different freezing points. For Jet A, it is used in commercial flights in the United States and it has a freezing point of -40 °C or below with no additive contain while Jet A–1 have a freeze point of -47 °C or below and normally contains static dissipator additive thus it appropriate for intercontinental flights. Secondly, Jet B is jet fuel blending between naphtha and kerosene which has a low freezing point of -60 °C so it suitable for use in cold weather (Zhang *et al.*, 2016)

A strong increase in aviation transport is expected for the future as shown in Figure 2.1. It is expected that passenger transport growth of 5% per year from 2010 to 2030 and air traffic is expected to increase from 3.8% to 5.1% per year thus in 2040 RPK can reach over 18 billion PRK. For jet fuel demand, it expects to increase only 1.5% per year between 2010 and 2035 because of increasing improvements in the specific fuel (Thrän *et al.*, 2016).

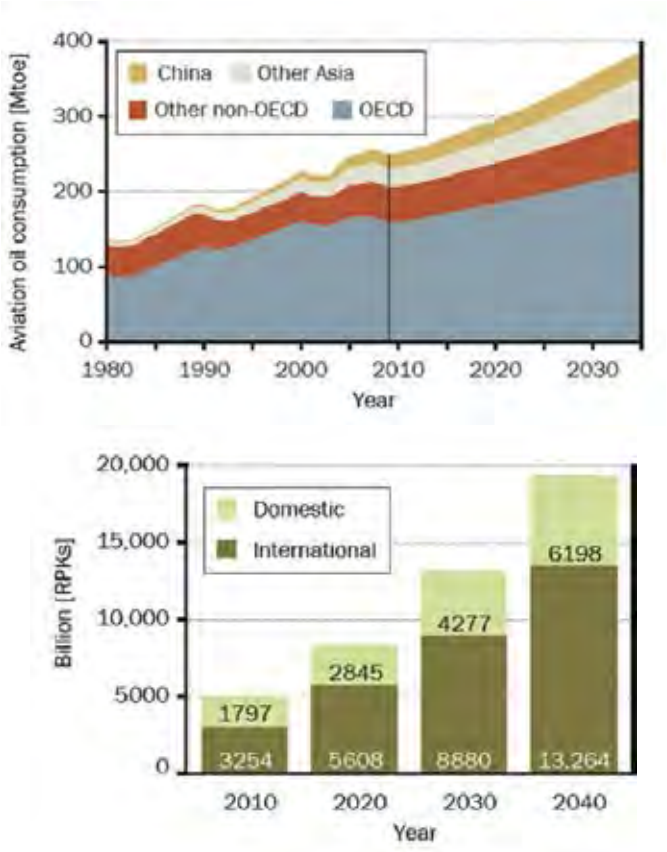

Figure 2.1 Expected growth of the aviation sector. Left: Passenger Traffic Forecast in billion revenue passengers kilometers (RPK) (most likely scenario/central forecast). Right: Aviation oil consumption [Mtoe] by region (New Policies Scenario) (Thrän et al., 2016).

Aviation transport activity and energy consumption offsetting efficiency gains of new aircraft are rapidly grown, the increase of environmental impacts must also be considered. Many greenhouse gases are released from aircraft engine and these include carbon dioxide (CO_2) and nitrogen oxides (NO_x) which have influence atmospheric chemistry and result in changes in the abundance of ozone (O_3) and methane (CH_4). CO_2 becomes the main contributor to climate change and it is included in the EU Emissions Trading Scheme (EU ETS). Airline operations worldwide produced CO_2 about 689 million tonnes and 705 million tonnes in 2012 and 2013, respectively. International Civil Aviation Organization (ICAO) (2009) forecasts that in 2050 aviation emission could be increased around 300 – 700% compared to 2005. The benefits of aviation transport will come as a cost to solve

2503957090 CU iThesis 6171003063 thesis / recv: 27072563 17:27:35 / seq: 25

GHG emissions. Therefore, aviation is striving to reduce the problem in the short and mid-term while at the same time they aim to find lower fuel cost burdens over the long term (Kousoulidou *et al.*, 2016).

The increase of aviation fuel application and green-house gas emissions occurred so it contributes to finding ways to solve them. The process of finding a solution includes finding alternative sustainable resources that are friendly to environmental, low cost, and reach the specific condition of jet fuel.

The increase of aviation fuel application and green-house gas emissions occurred so it contributes to finding ways to solve them. The process of finding a solution includes finding alternative sustainable resources that are friendly to environmental, low cost, and reach the specific condition of jet fuel.

2503957090 CU iThesis 6171003063 thesis / recv: 27072563 17:27:35 / seq: 25

2.2 Bio-jet Fuel

Biomass and liquid biofuels become attractive because of carbon neutral properties in terms of CO_2 emissions, reduced soot emissions, enhanced ignition, and it can replace the existing petroleum-derived fuels. Moreover, many sources (such as animal and plant) can use to produce liquid fuels with various properties that suitable for bio-jet fuel. (Han *et al.*, 2018)

2.2.1 Biomass-derived Aviation Fuels

Lipids are studied and used to be a feedstock for bio-jet fuel production as shown in Table 2.1. Lipids come from many raw materials such as vegetable oil, waste cooking oil, algae oil, or fermented lipids. A single step catalyst process can produce jet fuel range alkane and diesel type alkane. However, the yield of aviation fuel from common lipid which mainly C_{18} fatty acid is low around 40 wt.%, the low yield is obstructive the use of large-scale application thus it must improve the product properties and process efficiency such as hydrocracking to convert C_{17} and C_{18} into aviation fuel range ($C_9 - C_{14}$) and avoid non-selective cracking of fatty acids. During the development of bio-aviation fuel, the control of the aromatics percentage also should be carefully considered.

Table 2.1 Recent research on the conversion of lipid to bio-aviation fuel (2010 to 2018) (Wang *et al.*, 2019)

Raw materials	**Catalysts**	**Conversion/results/scale**
Castor oil	$PtAl_2O_3$ and Pt/ZSM-22	The castor oil to jet fuel process has a carbon selectivity of about 90% in laboratory scale experiments.
Macauba oils; almond oils	Pd/C	Hydrocarbon contents exceeded 65% in laboratory scale experiments.
Sunflower oil	ZSM-5	Yields of hydrocarbon fuels were 59.4 % —73.9 % in laboratory scale experiments.
Jatropha oils	BASF Nysofact 120	JP-8, naval distillate, and gasoline fractions were produced at a conservative total yield between 40 and 52 % in laboratory scale experiments.
	Sulphided NiMo and NiW supported on hierarchical mesoporous SAPO-11	Liquid hydrocarbon products were about 84 wt %, with 20 % gasoline range hydrocarbons, about 40% diesel, and about 40% aviation kerosene. Laboratory scale experiments.
	Ni-W/ZSM-5	Jet-fuel range hydrocarbons were obtained at 40 — 45 %. Laboratory scale experiments.
	Ni-W/SiO_2 - Al_2O_3;	A Ni-Mo catalyst demonstrated the highest C_{15} — C_{18} hydrocarbon yield of about 97.9 % in laboratory scale experiments.
	Co-Mo/ Al_2O_3; Ni-Mo/ Al_2O_3	A Ni-Mo catalyst demonstrated the highest C_{15} – C_{18} hydrocarbon yield of about 97.9 % in laboratory scale experiments.

2503957090 CU iThesis 6171003063 thesis / recv: 27072563 17:27:35 / seq: 25

Table 2.1 (cont.) Recent research on conversion of lipid to bio-aviation fuel (2010 to 2018) (Wang *et al.*, 2019)

Raw materials	Catalysts	Conversion/results/scale
Jatropha oils	Sulfided Ni-Mo/Al_2O_3	Cracked product yield was 20 − 45% in laboratory scale experiments.
	Pt/Al_2O_3; Rh/Al_2O_3 and $NiMo/Al_2O_3$	The highest hydrocarbon was obtained at 76.5% in laboratory scale experiments.
Microalgae oil and soybean oil	Pt/MWCNTs	The selectivity of the hydrothermal decarboxylation of stearic acid reached 97% in laboratory scale experiments.
	Pt/Al_2O_3/SAPO-11 for HDO and Ni_2P/HY for hydrocracking	Fractionation resulted in 42 − 48 wt% of jet fuel with > 12% aromatics in laboratory scale experiments.
Vacuum distillate and vegetable oil mixtures	Commercial presulphided catalysts (not detailed by author)	The maximum naphtha conversion was ~65% and the highest naphtha selectivity was ~50%. Pilot scale experiments were performed.
Waste soybean oil (SBO) and palm fatty acid distillate (PFAD)	Pd/beta-zeolite catalyst	The deoxygenations of SBO and PFAD were 95.5% and 94.3%, respectively. Jet-fuel range hydrocarbons reached 69.3% in laboratory scale experiments.
Waste cooking oil	Sulfur-free Ni-Mo/γ-Al_2O_3	Hydrodeoxygenation of enzymatically pre-treated waste cooking oil achieved a yield of ~ 97% in laboratory scale experiments.

2503957090 CU iThesis 6171003063 thesis / recv: 27072563 17:27:35 / seq: 25

Table 2.1 (cont.) Recent research on conversion of lipid to bio-aviation fuel (2010 to 2018). (Wang *et al.*, 2019)

Raw materials	Catalysts	Conversion/results/scale
Waste cooking oil	Sulfur-free Ni-Mo/γ-Al_2O_3	Hydrodeoxygenation of enzymatically pre-treated waste cooking oil achieved a yield of ~ 97% in laboratory scale experiments.
	Ni/Meso-Y; Ni/SAPO-34; Ni/HY	Jet range alkanes were produced using Ni/HY, Ni/SAPO-34 and Ni/Meso-Y catalysts in laboratory scale experiments. The selectivities were 53%, 58% and 53%, respectively.
Waste soybean oil (SBO) and palm fatty acid distillate (PFAD)	Pd/beta-zeolite catalyst	The deoxygenations of SBO and PFAD were 95.5% and 94.3%, respectively. Jet-fuel range hydrocarbons reached 69.3% in laboratory scale experiments.
Waste soybean oil (SBO) and palm fatty acid distillate	Pd/beta-zeolite catalyst	The deoxygenations of SBO and PFAD were 95.5% and 94.3%, respectively. Jet-fuel reached 69.3% in laboratory scale.

2.2.2 Vegetable Oil

Nowadays, many kinds of research interests on biofuels production from several renewable feedstocks thus vegetable oil comes into attention for being feedstock. Vegetable oils with different origins have gained immense popularity as sustainable resources for biofuel production due to their high energy density and similarity in molecular structure with petroleum-based fuels. Vegetable oil has the chemical structure as shown in Figure 2.2, consisting of 98% triglycerides and other which is mono and diglycerides. Vegetable oil contains fatty acid, phospholipids,

2503957090 CU iThesis 6171003063 thesis / recv: 27072563 17:27:35 / seq: 25

phosphatides, carotenes, tocopherols, sulfur compounds, and traces of water (Ong *et al.*, 2011).

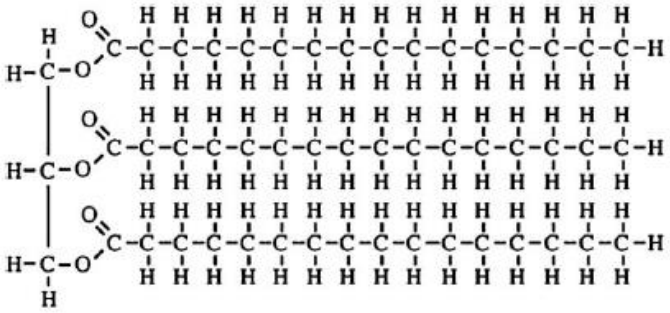

Figure 2.2 Typical structure of a triglyceride molecule (Ong et al., 2011).

The vegetable oil commonly has fatty acids which are stearic, palmitic, oleic, linoleic, and linolenic acids. Table 2.2 shows the summary of the fatty acid composition in some common vegetable oil. Vegetable oil can be used in several paths such as straight vegetable oil, oil blends, pyrolysis, micro-emulsification, and transesterification in a diesel engine (Ong *et al.*, 2011).

Table 2.2 Chemical structure for common vegetable oil of fatty acids (Ong *et al.*, 2011)

Name	**Chemical name**	**Structure (carbon atom : double bond)**	**Formula**
Lauric	Dodecanoic	12:0	$C_{12}H_{24}O_2$
Myristic	Tetradecanoic	14:0	$C_{14}H_{28}O_2$
Palmitic	Hexadecanoic	16:0	$C_{16}H_{32}O_2$
Stearic	Octadecanoic	18:0	$C_{18}H_{36}O_2$
Oleic	cis-9-Octadecenoic	18:1	$C_{18}H_{34}O_2$

2503957090 CU iThesis 6171003063 thesis / recv: 27072563 17:27:35 / seq: 25

Table 2.2 (cont.) Chemical structure for common vegetable oil of fatty acids (Ong et al., 2011)

Name	Chemical name	Structure (carbon atom : double bond)	Formula
Linoleic	cis-9,cis-12-Octadecadienoic	18:2	$C_{18}H_{32}O_2$
Linolenic	cis-9,cis-l2,cis-15-Octadecatrienoic	18:3	$C_{18}H_{30}O_2$
Arachidic	Eicosanoic	20:0	$C_{20}H_{40}O_2$
Gadoleic	11-eicosenoic	20:1	$C_{20}H_{38}O_2$
Behenic	Docosanoic	22:0	$C_{22}H_{44}O_2$
Erucle	cis-13-Docosenoic	22:1	$C_{22}H_{42}O_2$
Lignoceric	Tetracosanoic	24:0	$C_{24}H_{48}O_2$

2.3 Palm Fatty Acid Distillate Feedstock

Palm oil is a tropical plant that grows in lowland with humidity as shown in Figure 2.3. The fruit consists of a fibrous mesocarp layer and the endocarp (shell) containing the kernel which contains oil and carbohydrate reserves for the embryo as shown in Figure 2.4. Palm oil is used mainly in food application and this edible oil production comes into attention for feedstock. The palm oil processing industry began in Malaysia around the 1970s and then used in the processes of refining and fractionation, alone or in combination (Ong *et al.*, 2011).

2503957090 CU iThesis 6171003063 thesis / recv: 27072563 17:27:35 / seq: 25

Figure 2.3 Oil palm tree and fruits (Ong *et al.*, 2011).

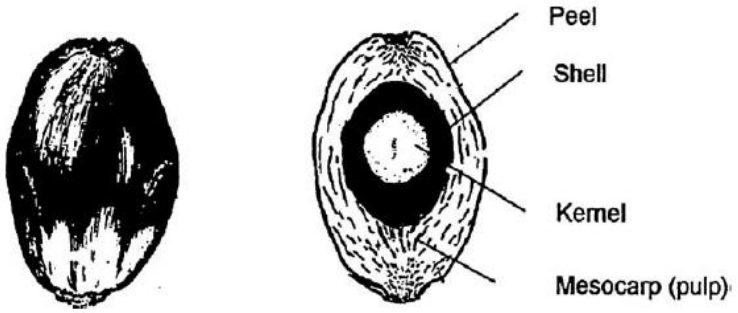

Figure 2.4 Fresh oil palm fruit and its longitudinal section (Ong *et al.*, 2011).

Production oil yield for various sources of biodiesel feedstock as shown in Figure 2.5. soybean, palm, sunflower, rapeseed and peanut oil are considered as an alternative fuel for the diesel engine. Moreover, many interesting alternative fuels come into attention such as mustard seed, Jatropha curcas, cottonseed, and Calophyllum inophyllum oil. They can drive in current situations which have an increasing population, rising standards of living, and increasing incomes in developing countries. From all of this, palm oil gives high potential products, high production rates, and high oil content that have ability to meet the future demand. As shown in Figure 2.5, oil palm gives high potential productivity of 5,950 liters per hectare which is 13 times higher than soybean oil and the following high oil productivity is Calophyllum inophyllum oil. Life cycle analysis (LCA) conducted on various biodiesels and the result showed that palm oil-based biodiesel can reduce

2503957090 CU iThesis 6171003063 thesis / recv: 27072563 17:27:35 / seq: 25

greenhouse gases (GHG) emission by 62% as compared to soybean oil (40%), rapeseed oil (45%) and sunflower oil (58%).

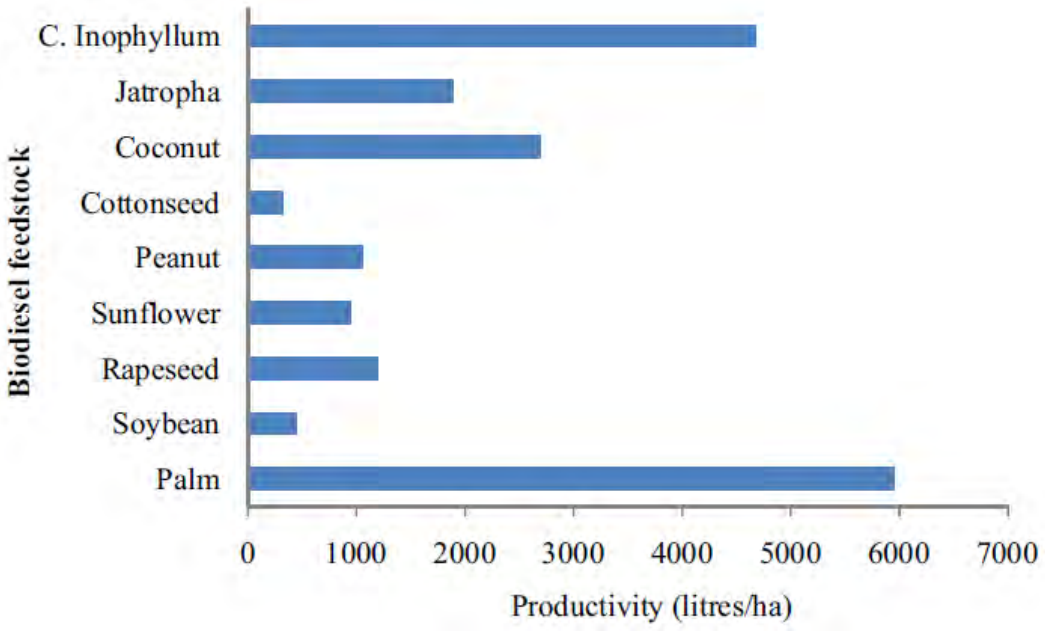

Figure 2.5 Production oil yield for various sources of biodiesel feedstock (Ong *et al.*, 2011).

In these few decades, global demand for edible oil is increasing and there causes a high rate of increase in the area of oil crop cultivation especially soybean and oil palm. The world production of palm oil is 45 million tonnes and the highest production is in South East Asia with a total of 89% of total palm oil production which consists of 40% in Malaysia, 46% in Indonesia, 3% in Thailand as shown in Figure 2.6. The highest land using for oil palm cultivation is Malaysia about 4.5 million hectares. It produced 17.73 million tonnes of palm oil and contributed about 65.19 billion to the Malaysia export in 2008. Malaysia has approximately 362 palm oil mills and processing 71.3 million tonnes of fresh fruit bunch. Moreover, producing an estimated 19 million tonnes of crop residue annually in the form of empty fruit fiber, bunch, and shell. Table 2.3 shows oil palm biomass components, quantity, calorific values, and moisture content that can be used for electricity. Palm oil is one of the most efficient oil because of land utilization, efficiency, and productivity (Ong *et al.*, 2011).

2503957090 CU iThesis 6171003063 thesis / recv: 27072563 17:27:35 / seq: 25

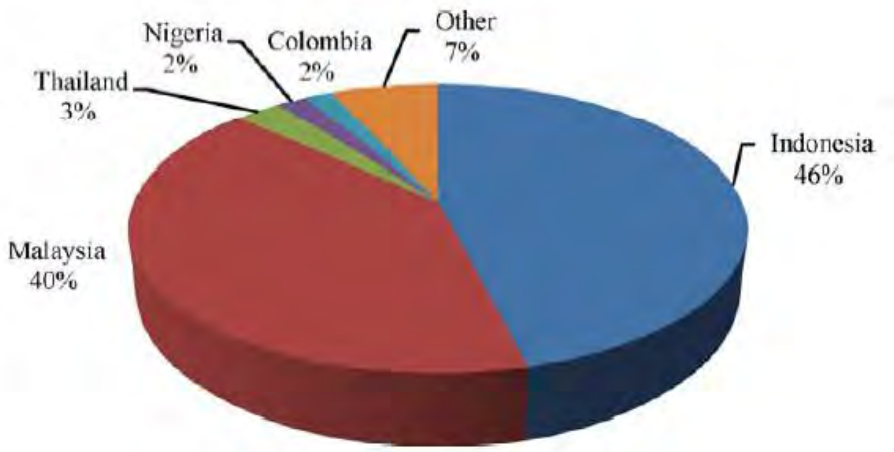

Figure 2.6 World palm oil production 2009 (Ong *et al.*, 2011).

Table 2.3 Oil palm biomass components and potential energy generated (Ong *et al.*, 2011)

Oil palm component	**Quantity (million tonnes)**	**Calorific value (kJ/kg)**	**Potential energy generated (Mtoe)**
Empty fruit bunch	17.00	18,838	7.65
Mesocarp fibre	9.6	19,096	4.37
Shell	5.92	20,108	2.84
Palm kernel	2.11	18,900	0.95
Total	34.63		15.81

The crude palm oil (CPO) is physically refined by removing impurities to reach acceptable levels. The refinery process of palm oil was shown in Figure 2.7. Firstly, the process removes an impurity called gum (phospholipids, phosphatides) in crude palm oil by precipitation process. The appropriate temperature for precipitation usually occurs at 90 – 130 °C and uses phosphoric acid as a precipitant. Then, CPO goes to the degummed palm oil (DPO) process. The degummed palm oil is bleached

2503957090 CU iThesis 6171003063 thesis / recv: 27072563 17:27:35 / seq: 25

for removing any undesirable impurities such as pigments and trace metals. The output of this process is bleached palm oil (BPO). Next, BPO is deodorized to eliminate free fatty acid content. This step including refined, bleached, and deodorized palm oil (RBDPO) gives palm fatty acid distillate (PFAD) as a by-product. Finally, the RBDPO is fractionated to give refined palm olein (RPO) and refined palm Stearin (RPS) (Kiatkittipong *et al.*, 2013).

2503957090 CU iThesis 6171003063 thesis / recv: 27072563 17:27:35 / seq: 25

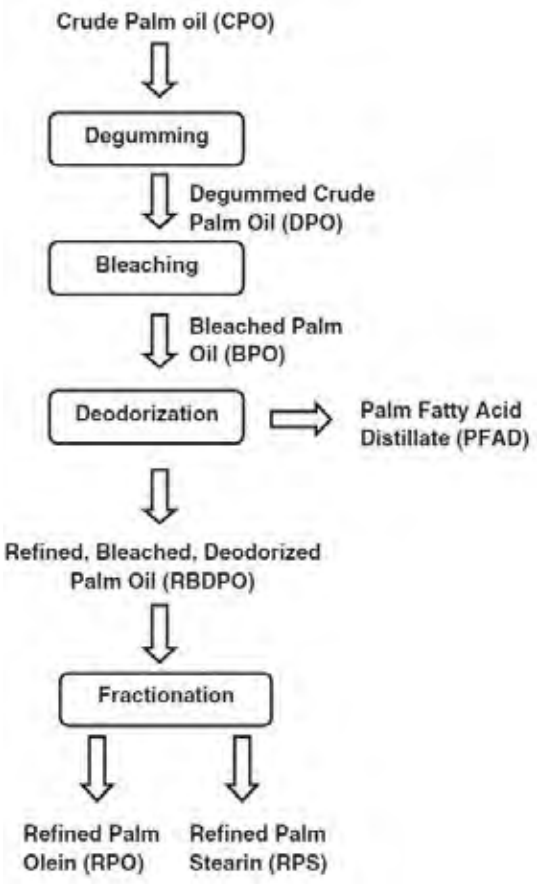

Figure 2.7 Physical refining process of crude palm oil (Kiatkittipong *et al.*, 2013).

Palm fatty acid distillation or PFAD is a by-product of crude palm oil production. PFAD has a highly odoriferous product that also contains a minor component of glycerol esters with the feedstocks. PFAD has a light brown solid at room temperature and melting to a brown liquid on heating about 83 ˚C. It is no official production data on PFAD to be available unlike the crude palm oil and

processed palm oil products, but PFAD has estimated information of volume and values that are given in Table 2.4.

Table 2.4 Refining volumes (tonnes) and value of palm oil & PFAD in Malaysia. 2012 – 2015 average (Ab Gapor Md, 2010)

	Refining output	**Value (theoretical)**
Refined, Bleached and Deodorised Palm Oil	13,966,000 ton	$10,810,000,000
PFAD	678,000 ton	$445,000,000

2503957090 CU iThesis 6171003063 thesis / recv: 27072563 17:27:35 / seq: 25

2.4 The Overall Reaction for Bio-jet Fuel Production

2.4.1 Deoxygenation Reaction

The deoxygenation method converts fatty acid to produce linear long chain hydrocarbon in the presence of both H_2 and H_2-free environments. During the catalytic deoxygenation process, oxygen is removed from fatty acid to get pure hydrocarbon fuels that are fully compatible with diesel. Deoxygenation process has three possible pathways which consist of decarboxylation (DCX), decarbonylation (DCN), and hydrodeoxygenation (HDO) reactions, where the H_2 consumption for the reaction follows the order of DCX < DCN < HDO. Decarboxylation and decarbonylation in liquid phase produce gas phase CO_2, CO, H_2, and H_2O which can further occur water-gas-shift reaction and methanation of CO_2 and CO. A detailed scheme for various deoxygenation pathways along with other possible reactions like the water-gas-shift reaction and hydrogenation occurring in the process is shown in Figure 2.8 (Pattanaik *et al.*, 2017).

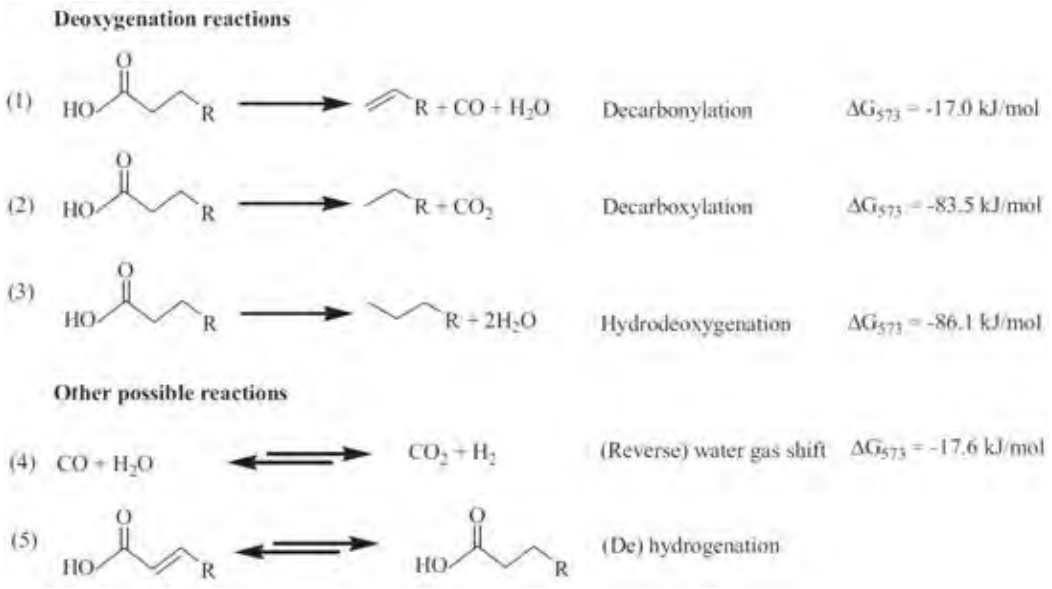

Figure 2.8 Various deoxygenation reaction schemes with other possible reactions including thermodynamic data (ΔG_{573} in kJ/mol at 1 bar) (Pattanaik et al., 2017).

2.4.1.1 Decarbonylation (DCN)

Decarbonylation (DCN) refers to the removal of the carbonyl group in less H_2 environment to produce alkanes with one carbon lesser than the original fatty acid.

2.4.1.2 Decarboxylation (DCX)

Decarboxylation (DCX) refers to the removal of the carboxyl group from fatty acid to produce alkanes by the direct attack at C – C bond with no H_2 environment and high reaction temperature.

2.4.1.3 Hydrodeoxygenation (HDO)

Hydrodeoxygenation is an oxygen displacement process that depends on the use of pure hydrogen H_2 under specific temperature and high-pressure condition for direct scission of C–O bond, fatty acids are converted to saturated hydrocarbon and O_2 is removed in the form of water.

2503957090 CU iThesis 6171003063 thesis / recv: 27072563 17:27:35 / seq: 25

2503957090 CU iThesis 6171003063 thesis / recv: 27072563 17:27:35 / seq: 25

2.4.2 Methanation and Water-Gas-Shift Reactions

CO_2 methanation reaction can occur during deoxygenation reaction as the joining of two reactions: water-gas-shift reaction and CO methanation. The main gaseous products from the deoxygenation reaction of triglyceride-based vegetable oil are CO_2, CO, H_2, and C_3H_8. It is generally observed that the decarbonylation /decarboxylation pathway consumes less H_2 and produces C_{15} and C_{17} hydrocarbons. However, hydrodeoxygenation has higher hydrogen consumption which needs specific temperature and pressure and gives C_{16} and C_{18} hydrocarbons products. For decarboxylation reaction, the reaction releases more CO_2 as a by-product. After CO_2 reacts with four molecules of H_2, it will give methanation reaction and produces CH_4 with two H_2O molecules. Similarly, CO and three H_2 molecules react together, they form CH_4 and two molecules of H_2O. Furthermore, this reaction leads to the formation of lighter products. In addition, when CO and H_2O go through water-gas-shift reaction, CO_2 and H_2 are formed as shown in Table 2.5 and Figure 2.9 (Khan *et al.*, 2019).

Table 2.5 Methanation and water-gas-shift reactions (Feng *et al.*, 2019)

Reaction No.	**Reaction formula**	**$\Delta H_{298}K$ (kJ/mol)**	**Reaction type**
1)	$CO_2+4H_2 \leftrightarrow CH_4+2H_2O$	-165	Methanation reaction
2)	$CO+3H_2 \leftrightarrow CH_4+H_2O$	-206	Methanation reaction
3)	$CO+H_2O \leftrightarrow CO_2+H_2$	-42	Water-gas-shift reaction

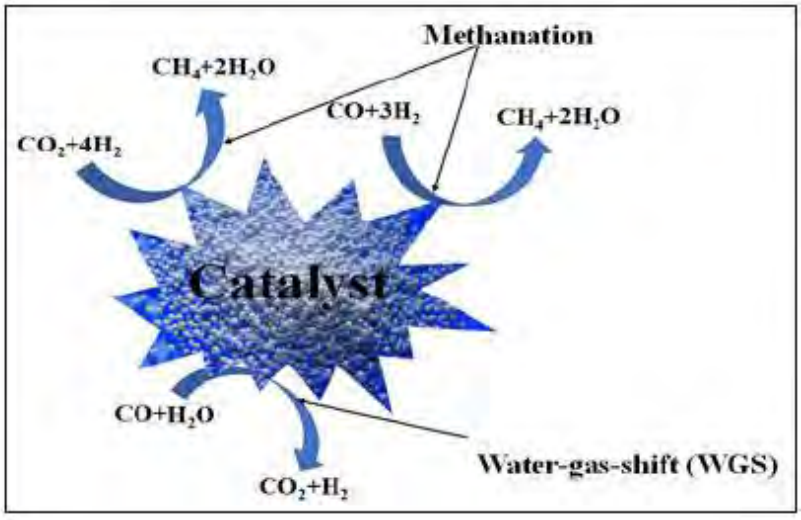

Figure 2.9 Methanation and water-gas-shift reactions (Khan *et al.*, 2019).

2.4.3 Hydrocracking and Isomerization Reactions

The deoxygenation process (DO) can be improved by adding more reactions. It usually produces alkane which gives a high cetane number. However, issues are occurred by these paraffin oils from their poor cold flow properties. Therefore, improving their physiochemical properties by hydrocracking and isomerization come into attention. Hydrocracking of alkanes is useful for the industrial process which is developed by petroleum refineries for producing gas hydrocarbons, gasoline, and kerosene from heavy fractions. Cracking reaction produces straight chain alkanes (C_{15} above) which need further cracking to be a suitable jet fuel range. After hydrocracking, normal long chain paraffins are converted to range C_9 to C_{14} hydrocarbon chains which are more suitable for jet fuel application. After hydroisomerization, the alkanes are maintained the high cetane number and improve the cold flow properties, the isomerization process converts *n*-paraffins or straight-chain hydrocarbons into iso-paraffin or branched structures to reduce the freezing point in order to meet the jet fuel specification and standard. The hydrocracking and isomerization reactions can be performed either together or respectively for the formation of hydrocarbons. Wei *et al.* suggested that hydrocracking is an important process before isomerization reaction to give a lighter alkane (Khan *et al.*, 2019).

2503957090 CU iThesis 6171003063 thesis / recv: 27072563 17:27:35 / seq: 25

There are several previous researches interesting to use vegetable as a feedstock for producing bio-jet fuel by the various metal catalyst.

De Sousa *et al*., 2016 used palm kernel oil (palmist oil) to produce bio-hydrocarbons in hydrocarbon range of diesel and jet fuel via hydrodeoxygenation and its hydrolyzed product by using Pd/C as a catalyst. It gave hydrodeoxygenation with conversion of up to 96% at 10 bar of H_2 pressure and 300 °C.

Lai *et al*., 2016 reported that the formation of Pd and Pt overlayer on Ni base metal would cause a negative shift of the d-band center of surface Pd or Pt and result in reducing the binding strength for adsorbed species. The resulting Pd and Pt active sites of overlayer catalysts significantly enhanced deoxygenation activity compared with that of Pd or Pt only catalysts.

Choi *et al*. 2018 showed that the bimetallic $WO_x/Pt/TiO_2$ catalyst enhances the performance of deoxygenation reaction. Bio-jet fuel range alkanes were prepared by using non-edible acid oils as a feedstock. For only WO_x metal or Pt metal on TiO_2 support had a low activity to deoxygenation reaction. Otherwise, WO_x addition to Pt/TiO_2 enhanced performance which gave a degree of deoxygenation of 86% C_{17} carbon selectivity which is more than two times higher than the Pt/TiO_2.

Thongkumkoon *et al*. 2019 presented trimetallic ReNiMo sulfide supported on γ-Al_2O_3 toward the deoxygenation of oleic acid, palm fatty acid distillate (PFAD), refined palm stearin (RPS) and refined palm olein (RPO). They found that using trimetallic catalysts had the highest diesel yield of 76.5% from oleic acid, 72.5% from PFAD, 69.7% from RPS, and 69.5% from RPO when compare to nanocatalyst. Moreover, adding some metal can promote characterization of catalyst like additional of Re increased the NiMo surface area by 20.4% and it reduced the metal particle size and gave high the metal dispersion on the support.

Hengsawad *et al*. 2018 studied the uses of Pd supported TiO_2 and Pd supported activated carbon catalysts for deoxygenation of triglycerides. They studied two different types of titania supports compose of mesoporous titania synthesized by a surfactant-assisted templating sol-gel method (SG-TiO_2) and commercial P25-TiO_2. It found that using TiO_2 support exhibited higher catalyst performance compare to

2503957090 CU iThesis 6171003063 thesis / recv: 27072563 17:27:35 / seq: 25

active carbon due to SMSI effect. SMSI effect give defect (oxygen vacancies and Ti^{3+}) on TiO_2. Furthermore, single-step sol-gel (SSSG) showed the highest conversion and selectivity to the diesel fuel ($C_{15} – C_{18}$) because of the well dispersion of Pd metal catalyst in support.

Zhang *et al*., 2016 studied Pd-Ni/HZSM-5 catalyst for Tandem Limonene dehydrogenation. The process involves the formation of *p*-cymene with generate H_2 as a by-product. Afterward, H_2 from the previous reaction is used for hydrodeoxygenation of stearic acid under low H_2 pressure (2 bar) to produce C_{17} and C_{18} alkane. The heterogeneous 5%Pd-10%Ni/HZSM-5 catalyst at 300 ^oC is effective for the full conversion of stearic acid and limonene via a cascade reaction sequence. In addition, the main route of limonene conversion is carbonylation reaction which leads to long-chain carbon 17 alkane formation and gas phase that present is H_2, CO, and CH_4. The process also occurred CO_2 methanation that reduces CO_2 in process.

Ameen *et al*., 2019 studied between non-sulphided monometallic Ni/γ-Al_2O_3 and Mo/γ-Al_2O_3 catalysts by conventional wet impregnation method to produce automotive clean fuel production via hydrodeoxygenation of rubber seed. They used 3 wt.%, 12 wt.%, and 15 wt.% Ni and Mo loading over γ-Al_2O_3 support. The result showed that the highest both Ni and Mo gave the highest yield. Moreover, nickel support had a higher surface area, small particle size, homogeneous dispersion of particles, higher crystallinity, lower reduction temperature, and low coke deposition due to CO_2 methanation appearance. The reaction mainly in decarboxylation (DCO_2) reaction. Otherwise, Mo loading enhanced hydrodeoxygenation reaction and gave a higher yield than Ni loading although it exhibited a high amount of coke deposition when compared to Ni supports catalyst.

2503957090 CU iThesis 6171003063 thesis / recv: 27072563 17:27:35 / seq: 25

2.5 The Catalyst for Bio-jet Fuel Production

The metal/acid bi-functional catalyst comes into attention for converting PFAD to high quality hydrocarbons in jet fuel range. The acid zeolite support with different porosity is an important effect on reaction activity and stability.

2503957090 CU iThesis 6171003063 thesis / recv: 27072563 17:27:35 / seq: 25

2.5.1 Zeolite as a Support Catalyst for Biojet Fuel Production

Zeolites are microporous crystalline aluminosilicates which have a high regular and open microporous (< 2 nm) structure. This structure is formed by a three-dimensional network of SiO_4 and $A10_4^-$ tetrahedral. The tetrahedral are linked to each other by shared oxygen atoms, to give cavities or cages, which are connected by ring or pore openings, with defined size and shape (Figure 2.10). There are several zeolites supports with different topology, channel structure, and pore size for various catalytic performance as shown in Table 2.6 (Ramsay *et al.*, 2000).

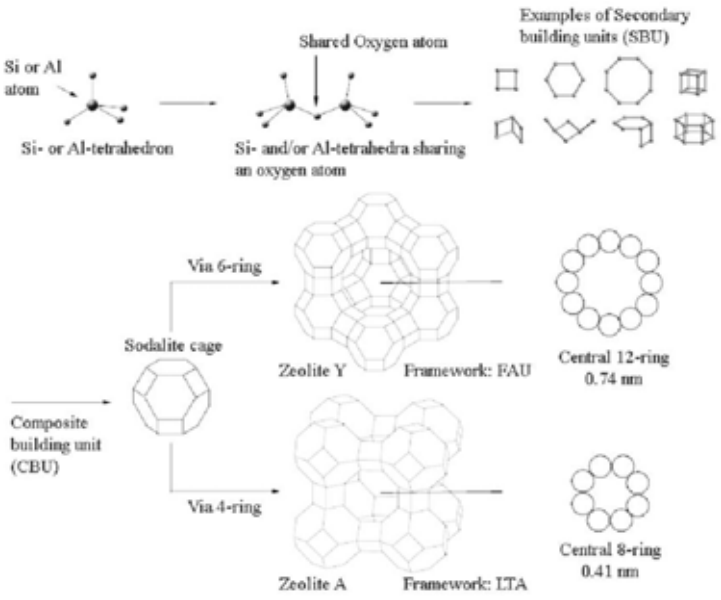

Figure 2.10 Composition of zeolites: from primary building unit to zeolite cage-like frameworks (Ramsay *et al.*, 2000).

Table 2.6 The topology, channel structure, size, and pore model of zeolites (Zhang *et al.*, 2016)

Material	Topology	Channel structure	Channel size	Pore model
ZSM-48	MRE	1D, 10-R	5.6 x 5.3 Å	Unimicro-pore
ZSM-12	MTW	1D, 12-R	5.6 x 6.0 Å	Unimicro-pore
ZSM-22	TON	1D, 10-R	5.7 x 4.6 Å	Unimicro-pore
ZSM-23	MTT	1D, 10-R	3.6 x 4.8 Å	Unimicro-pore
SAPO-11	AEL	1D, 10-R	4.3 x 7.0 Å	Unimicro-pore
SAPO-41	AFO	1D, 10-R	4.0 x 6.5 Å	Unimicro-pore
SAPO-35	LEV	2D, 8-R	3.6 x 4.8 Å	Unimicro-pore
SAPO-34	CHA	3D, 8-R	5.3 x 5.4 Å	Unimicro-pore
HY	FAU	3D, 12-R	7.4 x 7.4 Å	Unimicro-pore
ZSM-5	MFI	3D, 10-R	5.1 x 5.5 Å	Unimicro-pore

Zeolites are widespread applications in the petrochemical industry such as fluid catalytic cracking (FCC), aromatics conversion, and olefin production. There are more than two hundred zeolite frameworks have been defined and announced by the International zeolite association. The zeolite frameworks are described by using a three-letter code. However, even the natural zeolite is important for industrially applied zeo-catalysts in oil refining and the petrochemical process is still placed on zeolites Y (FAU), ZSM-5 (MFI), mordenite (MOR), beta (BEA), MCM-22 (MWW) and zeolite-like SAPO-34 (CHA), etc. The reason is their unique pore architectures that provide a perfect match with the requirement of target reactions, and their possessing suitable accessibility of active sites for guest molecules (Shi *et al.*, 2015).

2503957090 CU iThesis 6171003063 thesis / recv: 27072563 17:27:35 / seq: 25

Zeolites have the chemical composition: $M_{x/n}[(AlO_2)_x(SiO_2)_y]\cdot ZH_2O$ where x and y are integers, y/x equal to or greater than 1, n is the valency of cation M and Z is the number of water molecules in each unit cell. M is an extra-framework cation that balances the anionic charge of the framework. The Si/Al is an atomic ratio or molar ratio varies between 1 to ∞ ($M = SiO_2/Al_2O_3$). Zeolite can be occurred by nature and synthesis. Zeolite catalysts have various catalysis abilities because of their chemical composition, pore size distribution, and ion-exchange abilities. Furthermore, zeolite catalysts have both acidic and basic characteristics.

Zeolites are inexpensive and environmentally friendly, so they are widely used as heterogeneous catalysts in the industry. Generally, there are three types of zeolites, depending on their pore volume. There are small pore zeolites which have a diameter between 2.8 – 4 Å and containing rings with 6 – 8 members such as Sodalite and zeolite A, medium-pore zeolites which have diameter 5 – 6 Å and containing 10 membered rings (ZSM-type zeolites) and large-pore zeolites which have diameter more than 7 Å and constructed with 12 membered rings such as zeolites X and Y and faujasite-type zeolites (Shahinuzzaman *et al*., 2017)

The several types of zeolite supports have been studied in isomerization. One-dimensional structures such as ZSM-22, ZSM23, and SAPO-11 revealed shape selectivity while 12 membered rings such as ZSM-12, Beta, and USY are devoid shape selectivity and facilitated the formation of multi-branched isomers. The 10 membered rings zeolites have high shape selective called pore mouth selectivity which long chain hydrocarbon cannot diffuse inside the pore, leading to mono-branched products. The yield of multibranched isomers C10 is shown as a function of mono-brance C10 in Figure 2.11.

The optimal acidity linked to the occurrence of both isomerization and hydrocracking on Bronsted acid sites. More acidic catalyst has a trend to excessively cracking whereas less acidity allows only weak isomerization, resulting in low octane number. The acidity of zeolite can be adjusted by the SiO_2/Al_2O_3 ratio

2503957090 CU iThesis 6171003063 thesis / recv: 27072563 17:27:35 / seq: 25

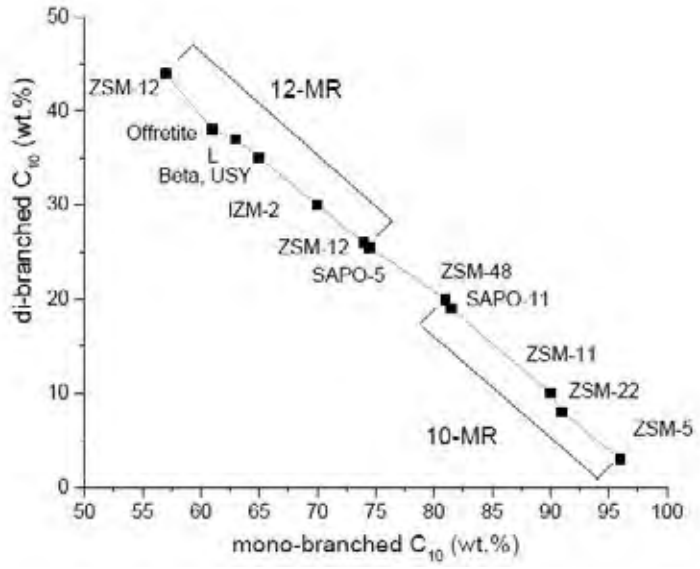

Figure 2.11 The yield of di-branched C10 as a function of monobranched C10 in n-decane hydroisomerization at 5% isomerization yield. Conditions: 4.5 bar, 300 °C, H_2/n-C_{10} molar ratio of 214, WHSV of 0.37 h^{-1} (Mäki-Arvela et al., 2018).

Ju *et al.*, 2016 integrates hydrotreating process and hydroisomerization to achieve the main specification requirement of jet fuel production though HEFA route. The results show that Pt/ZSM-12 has efficient converting *n*-C15 paraffin into multi-branched isomer and mono branched isomer with high weight yield 60% of algal oil to jet fuel rather than ZSM-22 and USY catalyst. Moreover, it gives a high multi/mono-isomers ratio which is satisfied with the ASTM specification of aviation biofuel. In addition, Marcelo *et al*., 2015 showed the result of HZSM-12 zeolite (Si/Al = 40), it was active in *n*-heptane catalytic cracking to C_1 to C_6 production. HZSM-12 with one dimensional and 12-member-ring channel system is interesting for application in several reactions of industrial interest due to its good stability, resistance to deposition of hard coke, and excellent performance in catalytic processes.

As-synthesized HZSM-5 zeolites with different Si/Al ratiosincluding 25, 90, 120, 240, and 400 used for dehydration of methanol to dimethyl ether (DME), which is a promising gaseous automotive fuel in the future. It was found that the Si/Al ratio of HZSM-5 had considerable impacts on its catalytic performance for

2503957090 CU iThesis 6171003063 thesis / recv: 27072563 17:27:35 / seq: 25

dehydration of methanol to DME and acidity increased with decreasing Si/Al ratio from 400 to 25 (Sameh *et al*., 2017).

2.5.2 Active Metal and Promoter

Support group VIII noble metal over support significantly affects on several deoxygenation reactions. Support group VIII noble metal is like a guide to what the reaction will be like. Thus, Pd catalyst comes into interest because proceeds mainly react via decarbonylation (DCN) and decarboxylation (DCX) pathways. Both pathways are favorable in terms of economic assessment. Pd/C catalyst shows completely converting steric acid to deoxygenated C_{17} products with high selectivity (98%) Moreover, The study found that activities for the deoxygenation of metals incorporated on the same support increased in the order of Os < Ru < Ir < Rh < Ni < Pt < Pd (Snåre *et al.*, 2006).

Cobalt is a very active non noble metal in deoxygenation reaction which mainly follows the hydrodeoxygenation reaction pathway at high reaction pressure. On the other hand, Cobalt has ability to go through decabonylation pathway at lower pressure. Cobalt loading is not only enhancing the deoxygenation but also shift the reaction towards the hydrocracking process to produce bio-jet fuel due to cobalt gives acid strength and amount acid site for cracking. Moreover, cobalt exhibits stability for the reaction without deactivation. (Cao *et al.*, 2018). Moreover, Srifa *et al*., 2015 also investigated the effect of Co with Ni, Pd, and Pt on alumina support for converting vegetable oil to replace petroleum diesel via deoxygenation reaction. The reaction tests show that the catalytic activity was in the order of Co > Pd > Pt > Ni respectively. Ni, Pd, and Pt catalysts gave more dominant in decarbonylation reaction whereas Co catalyst give hydrodeoxygenation reaction with occurred light hydrocarbon since the Co was partially selective to C–C cleavage in hydrocarbon chain.

2503957090 CU iThesis 6171003063 thesis / recv: 27072563 17:27:35 / seq: 25

2503957090 CU iThesis 6171003063 thesis / recv: 27072563 17:27:35 / seq: 25

CHAPTER 3
EXPERIMENTAL

3.1 Materials and Equipment

Material:

Feedstock

- Palm fatty acid distillate (obtained from Global Green Chemicals Public Co., Ltd., Thailand)

Chemical

- LUDOX HS-40 colloidal silica (40 wt.%, Dupont)
- Sodium aluminum oxide (Technical grade, Alfa Aesar)
- Tetraethylammonium hydroxide solution (TEAOH, 40 wt.% in water, Fluka)
- Palladium (II) chloride ReagentPlus ($PdCl_2$, 99% purity, Sigma Aldrich)
- Nickel nitrate hexahydrate ($NiNO_3.6H_2O$, Sigma Aldrich)
- Cobalt (II) nitrate hexahydrate ($Co(NO_3)_2.6H_2O$, Sigma Aldrich)
- Hydrochloric acid (HCl, 37 wt %, Emsure)
- Ammonium nitrate (NH_4NO_3, Ajex Finechem)
- HY zeolite (SiO_2/Al_2O_3 ratio of 100, Tosoh Company)
- ZSM-5 zeolite (SiO_2/Al_2O_3 ratio of 50, Zeolyst International Company)
- Dichloromethane (CH_2Cl_2, Honeywell)
- Pyridine (C_5H_5N, 98 % purity, Carlo Erba)
- N,O-bis(trimethylsilyl)-trifluoro acetamide (BSTFA, $C_8H_{18}F_3NOSi_2$, 99 % purity, Sigma Aldrich)
- Eicosane ($C_{20}H_{42}$, 99 % purity, Sigma Aldrich)
- Methanol (CH_3OH, 99.9 % purity, CT Chemical)
- Acetone (CH_3COCH_3, 99.5 % purity, CT Chemical)
- Hexane (C_6H_{14}, 99.9 % purity, CT Chemical)
- Deionized water

Gases

- Hydrogen (H_2, HP grade, 99.99 % purity)
- Helium (He, UHP grade, 99.999 % purity)
- Nitrogen (N_2, HP grade, 99.99 % purity)
- Air zero (HP grade, 99.99 % purity)

Equipment:

1. High pressure packed-bed continuous flow reactor system
2. Mass flow controller (Brooks instrument 5850E)
3. Teledyne ISCO syringe pumps 1000D
4. Back pressure regulator (Siemens)
5. ¾" O.D.x16" long stainless-steel reactor
6. Three-zone tubular furnace with a temperature controller (Cabolite)
7. Gas chromatograph (Agilent GC 7890 equipped with injector, DB-5HT column and FID)
8. Gas chromatograph (Hewlett Packard 5890 series II, HP-PLOT/Al_2O_3 column)
9. Chamber Furnace (Cabolite)
10. X-ray diffractometer (XRD)
11. Transmission electron microscopy (TEM)
12. Surface area analyzer (AS-3XR)
13. Temperature programmed reduction (TPR) apparatus
14. Temperature programmed desorption (TPD) apparatus
15. Temperature programmed oxidation (TPO) apparatus
16. CHNS analyzer (LECO / Truspec CHN/S)
17. X-Ray fluorescence spectrometer (WDXRF)
18. Hot & stirrer plate (Cole Parmer)
19. Wet test gas meter (Ritter)

2503957090 CU iThesis 6171003063 thesis / recv: 27072563 17:27:35 / seq: 25

3.2 Experimental Procedures

3.2.1 Catalyst Preparation

3.2.1.1 Synthesis of ZSM-12 Catalyst

The parent ZSM-12 (SiO_2/Al_2O_3 ratio of 100) was synthesized from hydrogel solutions with the following molar composition $100SiO_2$: $1Al_2O_3$: $1Na_2O$: 25TEAOH: $1500H_2O$ (Fang *et al*., 2008). TEAOH was mixed with deionized water and sodium aluminum oxide until the solid dissolved then added Ludox in solution and stirred at 250 rpm for 24 h until the gel became uniform. Next, the resultant gel was transferred to a 100 mL Teflon-lined stainless-steel autoclave and crystallized by thermal treatment under autogenous pressure and static conditions at 160 °C for 120 h (5 days). After hydrothermal synthesis, the autoclave was removed and cooled down to room temperature then recovered product by filtration with deionize water around 1500 mL. After that, product was dried at 120 °C overnight and removed the organic template by calcining in air flow at 550 °C for 5 h with a heating rate of 10 °C/min.

3.2.1.2 Treatment of ZSM-12 with Ammonium Nitrate

After the first calcination, the as-synthesized ZSM-12 was ion-exchanged with a 100 mL of 1 molar ammonium nitrate solution for three times at 80 °C, then washed with deionized water to remove the nitrate ions. Zeolite was dried at 120 °C overnight and calcined in air at 550 °C for 5 h with heating rate of 10 °C/min to obtain HZSM-12 (acidic form).

3.2.1.3 Preparation of HZSM-5 and HY Catalysts

The ZSM-5 and Y zeolite catalysts were dried at 120 °C overnight then the dried catalysts were calcined in air flow at 550 °C for 5 h with heating rate of 10 °C/min for removing impurity and obtaining H^+ form (HZSM-5 and HY) (Li *et al.*, 2016).

2503957090 CU iThesis 6171003063 thesis / recv: 27072563 17:27:35 / seq: 25

3.2.2 Metal Loading on Zeolite Supports

The metals were loaded in zeolite supports by incipient wetness impregnation method. $PdCl_2$ was firstly dissolved in HCl solution at 80 °C to afford H_2PdCl_4 solution. For Co metal loading, $Co(NO_3)_2 \cdot 6H_2O$ was firstly dissolved in water. The Pd and Co precursors were mixed and slowly dropped onto zeolite support, then the catalyst was dried at 80 °C overnight. The dried catalyst was calcined in an air flow at 500 °C for 6 h with a heating rate of 2 °C/min.

2503957090 CU iThesis 6171003063 thesis / recv: 27072563 17:27:35 / seq: 25

3.3 Catalyst Characterizations

3.3.1 X-ray Diffraction (XRD)

X-ray diffraction was used to determine the information of the crystalline phase of ZSM-12 synthesized catalyst before and after metal incorporation by a Rigaku X-ray diffractometer with Cu tube for generating CuK_α radiation (1.5406 Å) at room temperature. The sample was measured in the 2θ range of 5–50° with a scanning rate of 5°/min and a step of 0.02°.

3.3.2 X-ray Fluorescence (XRF)

X-ray fluorescence spectrometer (WDXRF) was used to determine its chemical or elemental composition. An X-ray beam with enough energy interacted with the atom by replacing electron from inner shell. Atom became unstable from missing inner electron then an outer electron replaced the missing inner electron. The replacement occurred the difference energy between the X-ray beam from analyzer and the binding energy that held electrons in their proper orbits.

3.3.3 Surface Analysis

Autosorb-1MP (AS-3XR) surface analyzer was used to measure surface properties of the prepared catalysts. Firstly, the sample was outgassed to remove humidity and volatile adsorbents adsorbed on the surface under vacuum at 250 °C for 10 h before the analysis. Then, N_2 was purged to adsorb on the surface then the quantity of gas adsorbed or desorbed from their solid surface was observed by static volumetric method at equilibrium vapor pressure. The solid sample was maintained at a constant temperature of the sample cell until the equilibrium was

established. This volume-pressure data would be used to calculate the BET surface area.

3.3.4 Temperature Programmed Reduction (TPR)

The reducibility of the catalysts was analyzed by a temperature-programmed reduction (H_2-TPR) under a reducing gas consists of 5% H_2 in N_2 with a thermal conductivity detector. Firstly, the calcined catalyst was dried at 120 °C overnight, then 0.1 g catalyst was packed inside a 1/4" O.D. quartz tubular reactor between the layers of quartz wools. After that, the sample would be exposed to a stream of 5% H_2 in N_2 with 30 mL/min then the sample was heated to 800 °C with a heating rate of 10 °C/min. The H_2 consumption was monitored and collected by an SRI model 110 TCD detector as a function of temperature.

3.3.5 Temperature Programmed Desorption (TPD)

The Thermo Finnigan temperature programmed desorption/reduction/ oxidation analyzer (TPDRO/TF) was used to analyze the acidity of the prepared catalysts. Initially, 0.2 g of sample was pretreated with nitrogen at 300 °C for 1h and adsorption ammonia at 100 °C for 1 h, then cooled down to 50 °C. After the pretreatment, the sample was heated in a flow of 30 mL/min helium to 900 °C with a heating rate of 10 °C/min and hold for 2 h then cooled down the catalyst. The desorbed ammonia was analyzed online using a TCD detector.

3.3.6 Transmission Electron Microscopy (TEM)

Transmission electron microscopy (JEM-1400) was used to observe the morphology of preparing catalysts. The catalyst was prepared by dispersing on the carbon film coating TEM grid then it was suspended in isopropanol solvent. After that, the sample was sonicated and dried overnight at room temperature.

3.3.7 Temperature Programmed Oxidation (TPO)

The Thermo Finnigan temperature programmed desorption/reduction/ oxidation analyzer (TPDRO/TF) was used to analyze coke of spent catalysts. Initially, 0.1 g of the sample was pretreatment with nitrogen at 250 °C and held for 30 min. After pretreatment, the sample was heated with a flow of 30 mL/min 5.27% oxygen in helium to 800 °C with a heating rate of 10 °C/min and hold for 2 h then cool down the

2503957090 CU iThesis 6171003063 thesis / recv: 27072563 17:27:35 / seq: 25

catalyst. The CO_x products from the oxidation were measured online using a TCD detector.

3.3.8 CHNS Analyzer

Leco CHNS analyzer was used to determine the amount of carbon by the combustion of sample in high temperature furnace with an infrared detector. The analyzer was heated to 950 °C and held for 4 h. Blank test and EDTA standard were performed to calibrate the instrument. After that, 0.2 g of sample was wrapped with tin foil and loaded in the machine. The combustion products were analyzed by infrared detection to determine carbon contents.

2503957090 CU iThesis 6171003063 thesis / recv: 27072563 17:27:35 / seq: 25

3.4 Catalytic Activity Testing

The schematic of the reactor system and the description of flow-diagram are shown in Figure 3.1 and Table 3.1. The reactions (i.e. hydrodeoxygenation, decarbonylation, decarboxylation, isomerization, and hydrocracking) were carried in a 3/4" O.D. stainless steel trickle-bed reactor. Firstly, the catalyst was reduced under pressure H_2 for 3 h at the reduction temperature of catalyst. Then, the temperature and pressure were set to the desired reduction temperature. After that, the PFAD stream was fed into the reactor by a Teledyne 1000D Isco syringe pump.

Mass flow controller and back-pressure regulator used for controlling the flow of carrier gas and the reaction pressure, respectively. During the process, the liquid product was trapped and collected in a condenser while the gas product was analyzed by using a Hewlett Packard 5890 series II gas chromatograph equipped with a capillary HP-PLOT/Al_2O_3 “S” deactivated column and FID detector. In addition, the amount of gas product was determined by a wet test gas meter (Ritter TG 05/2). Finally, the liquid product was analyzed by another gas chromatograph, Agilent 7890 equipped with a DB-5HT column and FID detector. Both gas and liquid product were collected and analyzed hourly.

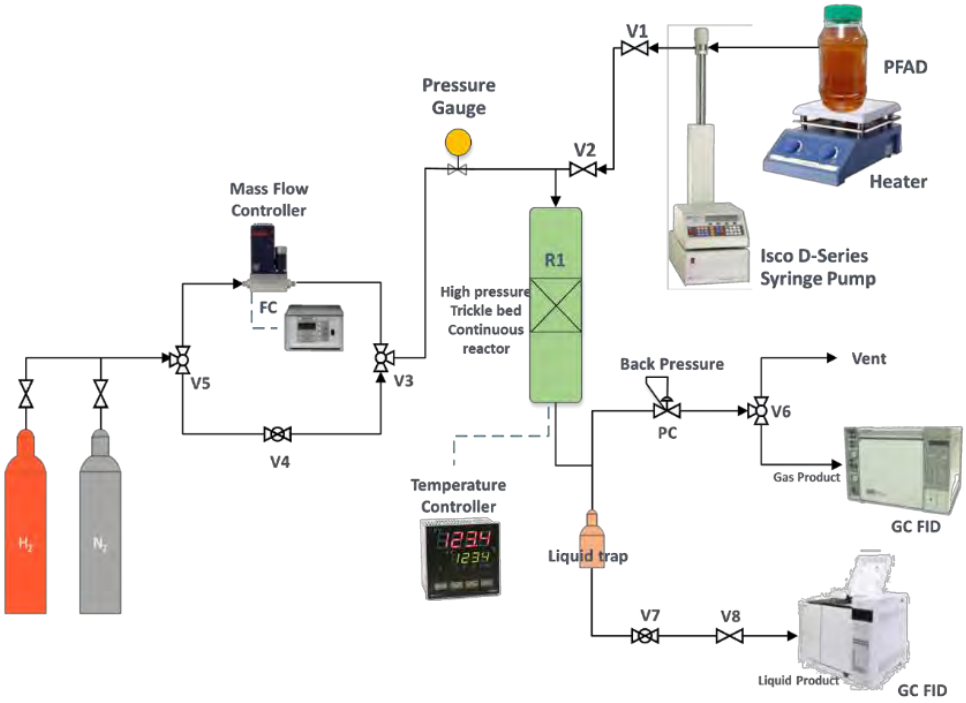

Figure 3.1 The schematic diagram of the reactor system.

Table 3.1 The description of system in flow diagram of the continuous flow trickle-bed reactor

No.	Part	Description
1	V1	On-off valve for feedstock from ISCO syringe pumps
2	V2	On-off valve for avoiding the backward flow of the feedstock
3	V3	Three ways valve for switching between gas flow meter controller and bypass
4	V4	Needle valve for releasing gas from bypass
5	V5	Three ways valve for switching between nitrogen gas and hydrogen gas flow
6	V6	Three ways valve for switching between vent gas and gas to GC lines
7	V7	Needle valve for gathering the liquid product from condenser
8	V8	On-off valve for collecting liquid product
9	R1	Continuous flow trickle-bed reactor where hydroprocessing reaction take place

CU iThesis 6171003063 thesis / recv: 27072563 17:27:35 / seq: 25
2503957090

Table 3.1 (cont.) The description of system in flow diagram of the continuous flow trickle-bed reactor

No.	Part	Description
10	FC	Flow controller to set flow rate for the desired H_2/feed molar ratio
11	PG	Pressure gauge for indicating pressure in packed bed reactor
12	PC	Back pressure regulator for controlling the pressure in reactor

2503957090 CU iThesis 6171003063 thesis / recv: 27072563 17:27:35 / seq: 25

The hydroprocessing reaction of PFAD was performed at temperature, pressure, liquid hourly space velocity (LHSV), and H_2/PFAD molar ratio as shown in Table 3.2.

Table 3.2 The reaction conditions for hydroprocessing of PFAD in continuous flow trickle-bed reactor

Parameter	Value
Reaction Tempearature (°C)	325 – 375
Reaction Pressure (bar)	10 – 30
LHSV (h^{-1})	1.5 – 2.5
Volume of Catalyst (mL)	4
Particle Size of Catalysts (mesh)	20 – 40
H_2/feed Molar Ratio	8

3.5 Product Analysis

3.5.1 Liquid Products Analysis

Gas chromatograph (Agilent 7890) equipped with FID detector was used to measure liquid product. Non-polar hydrocarbons liquid product from the hydrocracking of PFAD were determined by using a DB-5 column (non-polar column).

The GC operating condition was summarized as follows:

Injector temperature : 50 °C

Detector temperature : 380 °C

Carrier gas : He

Column type : Capillary column

(DB-5HT diameter 0.32 mm length 30 m)

The following chromatographic temperature program in Table 3.3 was used for liquid product analysis:

Table 3.3 The chromatographic temperature program for liquid product analysis

Step	Temperature (°C)	Rate (°C/min)	Holding time (min)
1	50	-	5
2	169	10	10
3	380	20	10

For the weight of the liquid product, the areas of each peak were analyzed hourly by a GC/FID (Agilent 7890) and were converted to gram unit by Equation 3.1.

$$Weight\ of\ product\ (g) = \frac{(areas\ of\ product\ i)x(grams\ of\ liquid\ product)}{total\ areas\ of\ liquid\ product} \qquad (3.1)$$

The conversion and selectivity of the product were measured by Equations 3.2 and 3.3, respectively:

$$Conversion\ (\%) = \frac{(weight\ of\ feed\ input - weight\ of\ feed\ remaining)x100}{weight\ of\ feed\ input} \qquad (3.2)$$

$$Selectivity\ of\ product\ i(\%) = \frac{moles\ of\ product\ i\ x100}{moles\ of\ overall\ products} \qquad (3.3)$$

2503957090 CU iThesis 6171003063 thesis / recv: 27072563 17:27:35 / seq: 25

3.5.2 Gas Products Analysis

GC/FID (Hewlett Packard 5890 series II) was used to analyze the composition of gas products. The GC operating condition was summarized as follows:

Injection temperature : 180 °C

Detector temperature : 250 °C

Carrier gas : He

Column type : capillary HP-PLOT/Al_2O_3 "S" deactivated column

The following chromatographic temperature program in Table 3.4 was used for gas product analysis:

Table 3.4 The chromatographic temperature program for gas-phase product analysis

Step	Temperature (°C)	Rate (°C/min)	Holding time (min)
1	40	-	3
2	70	15	0
3	170	5	0
4	190	1	0

For the quantitative calculation of gas product, the areas of each peak were analyzed hourly by GC/FID (Hewlett Packard 5890 series II) and were converted to gram unit by comparing with the area of methane from gas standard by mol% (equal to vol%), as shown in Equation 3.4.

$$Weight\ of\ product\ i(g) = \frac{(areas\ of\ product\ i\ per\ 1\ ml)x(mol\ of\ methane\ per\ 1\ ml)x\left(overall\ gas\ product\left(\frac{ml}{h}\right)\right)}{(mol\ of\ carbon\ atom)x(reference\ area\ of\ methane\ per\ 1\ ml)x\left(molecular\ weight\left(\frac{g}{mol}\right)\right)} \quad (3.4)$$

2503957090 CU iThesis 6171003063 thesis / recv: 27072563 17:27:35 / seq: 25

The calculations of conversion, selectivity, and yield of the product were defined as shown in Equations 3.5, 3.6 and 3.7, respectively.

$$Conversion\ (\%) = \frac{(weight\ of\ feed\ input - weight\ of\ feed\ remaining)x100}{weight\ of\ feed\ input} \quad (3.5)$$

$$Selectivity\ of\ product\ i(\%) = \frac{moles\ of\ product\ i\ x100}{moles\ of\ overall\ products} \quad (3.6)$$

$$Yield\ of\ product\ i(\%) = (conversion)x(selectivity\ of\ product\ i) \quad (3.7)$$

2503957090 CU iThesis 6171003063 thesis / recv: 27072563 17:27:35 / seq: 25

2503957090 CU iThesis 6171003063 thesis / recv: 27072563 17:27:35 / seq: 25

CHAPTER 4
RESULTS AND DISCUSSION

In this research, the monometallic (Co and Pd) and bimetallic (CoPd and NiPd) supported on HZSM-12 zeolite with various metal loadings and bimetallic CoPd with various zeolite supports (HZSM-12, HZSM-5, and HY) were synthesized by incipient wetness impregnation and characterized by X-ray diffraction (XRD), X-ray fluorescence (XRF), Brunauer-Emmett-Teller (BET), temperature programmed reduction (TPR), temperature programmed desorption (TPD) of ammonia, and transmission electron microscopy (TEM). The catalysts were tested for their catalytic activity in converting PFAD to bio-jet fuel. The spent catalysts were characterized by temperature programmed oxidation (TPO) and CHNS analyzer.

4.1 Characterization of Catalysts

4.1.1 X-ray Diffraction (XRD)

XRD patterns of the synthesized catalysts are shown in Figure 4.1. The synthesized ZSM-12 exhibited characteristic peaks at 2θ = 7.36°, 8.80°, 20.88°, 22.88°, and 23.20° which correspond to plane (2,0,0), (2,2,-2), (3,1,0), (3,1,-3), and (0,0,6). The positions and relative intensities of the parent ZSM-12 agreed with the data from previous studies (Marcelo *et al*., 2005). Moreover, the XRD peak intensity was slightly lower after the ZSM-12 was changed to acid form. The monoclinic cell parameters of HZSM-12 are shown in Table 4.1. The synthesized catalysts had similar lattice constants with a previous study (Fyfe *et al*., 1990) so it can confirm that the synthesized catalysts are HZSM-12 zeolite supports. The characteristic peaks of palladium oxide (PdO) appeared at 29.26° (1,0,0) and 33.84° (1,0,1), cobalt oxide (CoO) peaks appeared at 31.22° (2,2,0) and 36.65° (3,1,1), and nickel oxide (NiO) peaks appeared at 37.07° (1,1,1) and 43.09° (2,0,0), corresponding to previous study (Ma *et al.*, 2019), (Guo *et al.*, 2010), and (Qiao *et al.*, 2009), respectively. For bimetallic 10Co1Pd/HZSM-12, 10Ni1Pd/HZSM-12, 10Co1Pd/HZSM-5, and 10Co1Pd/HY catalysts, the palladium oxide peaks were not clearly observed while

cobalt oxide and nickel oxide exhibited obvious peak because the higher metal loading resulted in an intense peak of the metal oxide (Ameen *et al.*, 2019). The results exhibited that XRD peaks were lower after loading metal because the framework structure was destroyed and had defects on zeolite during the thermal treatment according to the previous study (Kathrina *et al.*, 2013).

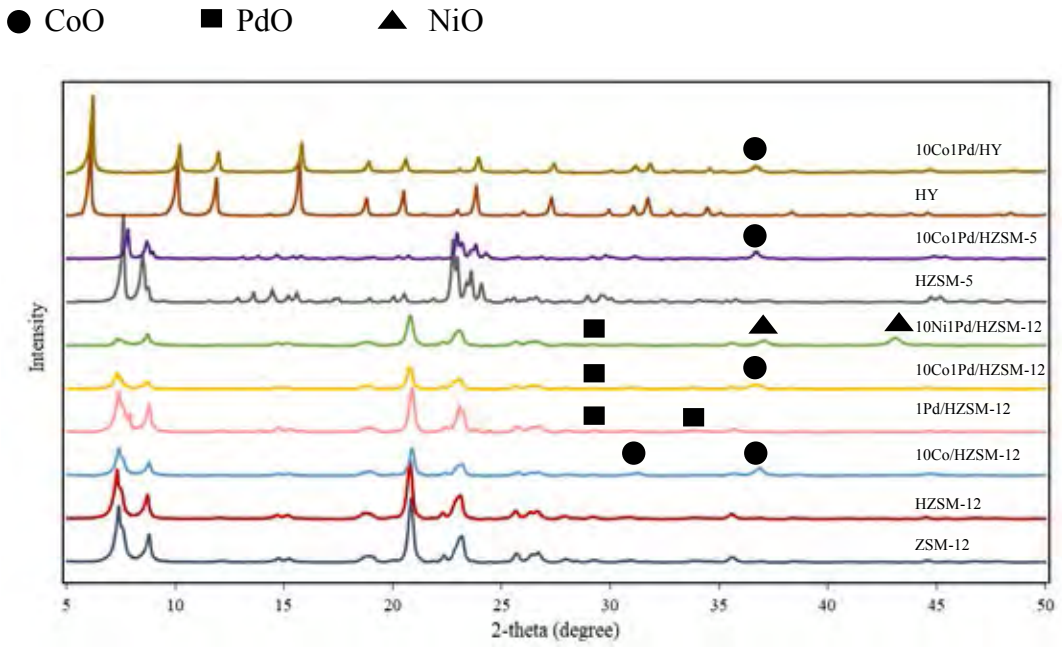

Figure 4.1 XRD patterns of synthesized catalysts.

Table 4.1 XRD data of the prepared HZSM-12

Catalysts	Theory				XRD			
	a (Å)	b (Å)	c (Å)	β (°)	a (Å)	b (Å)	c (Å)	β (°)
HZSM-12					25.20	5.08	24.66	107.7
10Co/HZSM-12	24.86	5.01	24.33	107.7	24.94	5.03	24.41	107.7
1Pd/HZSM-12					24.91	5.02	24.38	107.7

2503957090 CU iThesis 6171003063 thesis / recv: 27072563 17:27:35 / seq: 25

Table 4.1 (cont.) XRD data of the prepared HZSM-12

Catalysts	Theory				XRD			
	a (Å)	b (Å)	c (Å)	β (°)	a (Å)	b (Å)	c (Å)	β (°)
10Co1Pd/HZSM-12	24.86	5.01	24.33	107.7	25.07	5.05	24.53	107.7
10Ni1Pd/HZSM-12					25.20	5.08	24.66	107.7

2503957090 CU iThesis 6171003063 thesis / recv: 27072563 17:27:35 / seq: 25

4.1.2 X-ray Fluorescence (XRF)

X-ray fluorescence is a bulk analysis that was utilized to study the chemical composition of the synthesized HZSM-12. As shown in Table 4.2, the results showed that the Pd contents in the prepared 1Pd/HZSM-12, 5Co1Pd/HZSM-12, 10Co1Pd/HZSM-12, and 15Co1Pd/HZSM-12 catalysts were 0.51%, 0.60%, 0.65%, and 0.65%, respectively. Co contents in the prepared 10Co/HZSM-12, 5Co1Pd/HZSM-12, 10Co1Pd/HZSM-12, and 15Co1Pd/HZSM-12 catalysts were 8.43%, 4.32%, 8.19%, and 11.4%, respectively. The unexpected lower amount could be due to the loss during the preparation process.

Table 4.2 Chemical composition of the prepared catalysts

Catalysts	Co (wt. %)		Pd (wt. %)	
	Theory	XRF	Theory	XRF
10Co/HZSM-12	10	8.43	0	0
1Pd/HZSM-12	0	0	1	0.51
5Co1Pd /HZSM-12	5	4.32	1	0.60
10Co1Pd/HZSM-12	10	8.19	1	0.65
15Co1Pd /HZSM-12	15	11.4	1	0.65

4.1.3 Brunauer-Emmett-Teller (BET)

Brunauer-Emmett-Teller (BET) was used to explain the physical adsorption of gas molecules on a solid surface to find textural properties of the prepared catalyst. As shown in Table 4.3, the surface area of synthesized catalysts was measured by BET equation. External surface area and micropore volume were derived by V-t method, and total pore volume was obtained by Barrett-Jayner-Halenda (BJH). The results indicated that total surface area, external surface area, micropore volume, and total pore volume were decreased after metals loading which could block some micropore and mesopore of zeolite support (Silva *et al*., 2004). 1Pd/HZSM-12 had the highest surface area and pore volume due to its low metal loading. 5Co1Pd/HZSM-12 had a higher surface area and pore volume than 10Co1Pd/HZSM-12 and 15Co1Pd/HZSM-12. The textural properties of 10Co/HZSM-12 and 10Co1Pd/HZSM-12 were not significantly different. In addition, different zeolite supports have different textural properties from their structures. The results exhibited that 10Co1Pd/HY had the highest surface area, followed by 10Co1Pd/HZSM-5, and 10Co1Pd/HZSM-12.

Table 4.3 Physical characteristics of the prepared catalysts

Catalysts	**S_{BET}** **(m^2/g)**	**S_{ext}** **(m^2/g)**	**V_{micro}** **(cm^3/g)**	**V_{total}** **(cm^3/g)**
HZSM-12	313	104	0.114	0.4036
1Pd/HZSM-12	297	104	0.105	0.3561
10Co/HZSM-12	243	82	0.088	0.3435
5Co1Pd/HZSM-12	254	82	0.094	0.3874
10Co1Pd/HZSM-12	244	84	0.088	0.3546
15Co1Pd/HZSM-12	224	79	0.079	0.3542
10Ni1Pd/HZSM-12	264	99	0.090	0.3946
10Co1Pd/HZSM-5	289	119	0.094	0.5469
10Co1Pd/HY	480	122	0.195	0.5158

2503957090 CU iThesis 6171003063 thesis / recv: 27072563 17:27:35 / seq: 25

2503957090 CU iThesis 6171003063 thesis / recv: 27072563 17:27:35 / seq: 25

4.1.4 Temperature Programmed Reduction (TPR)

The temperature programmed reduction was performed to determine the reduction temperature of catalysts. The TPR profiles of the different catalysts are shown in Figure 4.2. Initially, 10Co/HZSM-12 exhibited two peaks at approximately 300 – 360 °C and 360 – 530 °C, corresponded to the reducibility of Co_3O_4 to CoO and CoO to metal Co, respectively (Cao *et al.*, 2018). Furthermore, 1Pd/HZSM-12 had two TPR peaks at 50 – 60 °C from H_2 consumption to reduce both PdO and $Pd(OH)_2$ to form Pd hydride. Moreover, the negative peak demonstrated palladium hydride decomposition through H-diffusion into palladium crystallites because PdO species can reversibly transform to $Pd(OH)_2$ in the presence of water, this was similar to the previous study (Kim *et al.*, 2018). Bimetallic 10Co1Pd/HZSM-12 had two reduction temperature peaks. Firstly, the reduction temperature at 100 – 260 °C presented the reduction of Pd oxide species (either PdO or $Pd(OH)_2$) combined with cobalt oxide (Co_3O_4). Secondly, the reduction temperature at 260 – 360 °C referred to the reduction of cobalt oxide (CoO). The reduction temperature was shifted to lower temperature as compared to monometallic 10Co/HZSM-12. This indicated that cobalt and palldium have a strong interaction and the reducibility of metal oxide is facilitated after loading palladium in the catalyst (Dao *et al.*, 2015). Moreover, 10Ni1Pd/HZSM-12 showed reduction temperature at 250 – 360 °C.

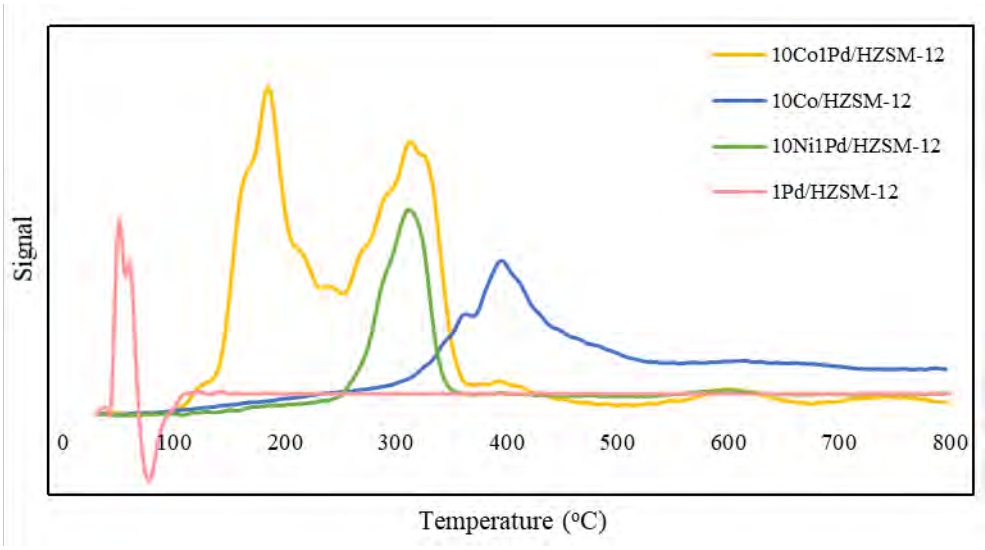

Figure 4.2 H_2-TPR profiles of 10Co1Pd/HZSM-12, 10Co/HZSM-12, 1Pd/HZSM-12, and 10Ni1Pd/HZSM-12.

4.1.5 Temperature Programmed Desorption (TPD) of Ammonia

The acidic properties of the calcined catalysts were characterized by temperature programmed desorption of ammonia. As shown in Figure 4.3, 1Pd/HZSM-12 exhibited peaks at 100 – 260 °C which referred to the desorption of NH_3 on weak acid site. 10Co/HZSM-12 exhibited two NH_3 desorption peaks 100 – 300 °C (weak acid site) and 350 – 540 °C (strong acid site). 10Co1Pd/HZSM-12 peak showed the same trend as 10Co/HZSM-12 but it had an intermediate peak at 260 – 360 °C because the transition metal has ability to introduce a new acid site. Both intermediate and strong acid peaks referred to difficult for desorption NH_3 on the acid sites (Gao *et al.*, 2019). 10Co1Pd/HY showed two NH_3 desorption peaks which consisted of a weak acid site at 100 – 250 °C and strong acid site at 250 – 400 °C. 10Co1Pd/HZSM-5 showed three peaks which are 100 – 320 °C (weak acid site), 350 – 490 °C (intermediate acid site), and 490 – 580 °C (strong acid site). Table 4.4 illustrates the SiO_2/Al_2O_3 molar ratio of zeolite supports from XRF and the acidity of synthesized catalysts from NH_3-TPD. HZSM-12 was synthesized with a molar composition of $100SiO_2$: $1Al_2O_3$: $1Na_2O$: 25TEAOH: $1500H_2O$. The XRF results showed SiO_2/Al_2O_3 molar ratios of all zeolite supports were higher than the theory, indicating lower acidity than expected. However, the SiO_2/Al_2O_3 molar ratios of all catalysts were not significantly different. Furthermore, the NH_3-TPD results showed that the acidity of catalysts increased after metal loading. 1Pd/HZSM-12 had the highest acidity, followed by 10Co1Pd/HZSM-12 and 10Co/HZSM-12, respectively. In addition, 1Pd/HZSM-12 had a high amount of weak acid sites while others had both weak and strong acid sites. As compared to different zeolite supports, 10Co1Pd/HZSM-5 catalyst had higher acidity than 10Co1Pd/HZSM-12, and 10Co1Pd/HY, respectively. The acidity is important for hydrocracking and isomerization reactions.

2503957090 CU iThesis 6171003063 thesis / recv: 27072563 17:27:35 / seq: 25

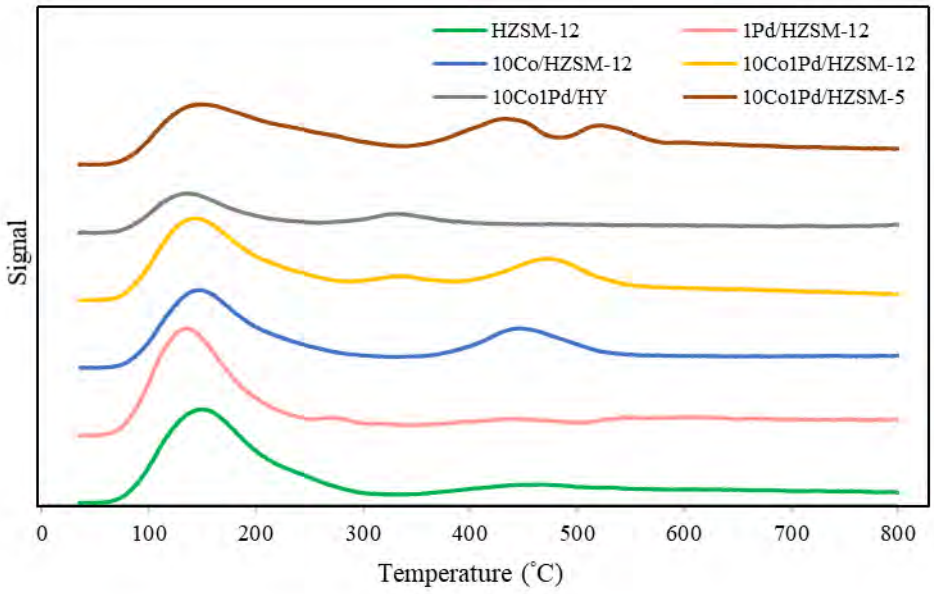

Figure 4.3 NH_3-TPD profiles of parent HZSM-12, 1Pd/HZSM-12, 10Co/HZSM-12, 10Co1Pd/HZSM-12, 10Co1Pd /HZSM-5, and 10Co1Pd /HY catalysts.

Table 4.4 Acidity of parent HZSM-12, 10Co1Pd/HZSM-12, 10Co/HZSM-12, 1Pd/HZSM-12, 10Ni1Pd/HZSM-12, 10Co1Pd/HZSM-5, and 10Co1Pd/HY from NH_3-TPD

Catalysts	**SiO_2/Al_2O_3 molar ratio from XRF**		**Acidity from NH_3-TPD (mmol/g)**
	Theory	**XRF**	
HZSM-12	100	N/A	2.287
10Co/HZSM-12	100	114.49	2.359
1Pd/HZSM-12	100	122.29	3.227
10Co1Pd/HZSM-12	100	118.80	2.571
10Co1Pd/HZSM-5	100	N/A	2.987
10Co1Pd/HY	100	N/A	1.118

2503957090 CU iThesis 6171003063 thesis / recv: 27072563 17:27:35 / seq: 25

4.1.6 Transmission Electron Microscopy (TEM)

Transmission electron microscopy images of the prepared catalysts are illustrated in Figure 4.4. In Figure 4.4 (a), the parent HZSM-12 had a cubic shape with crystal size approximately equal to 600 nm (Silva *et al.*, 2019). Figures 4.4 (b) – (d) show metal dispersion of 5%, 10%, and 15% wt. Co loading with 1% wt. Pd loading on HZSM-12 supports. Cobalt showed a big spot due to its large particle size while palladium had a dark spot because of its high mass number. In Figures 4.4 (b) and 4.4 (c), 5Co1Pd/HZSM-12 and 10Co1Pd/HZSM-12 catalysts showed high metal dispersion which is auxiliary to occur deoxygenation reaction while 15Co1Pd/ HZSM-12 catalyst had some cobalt aggregation in the support as shown in Figure 4.4 (d).

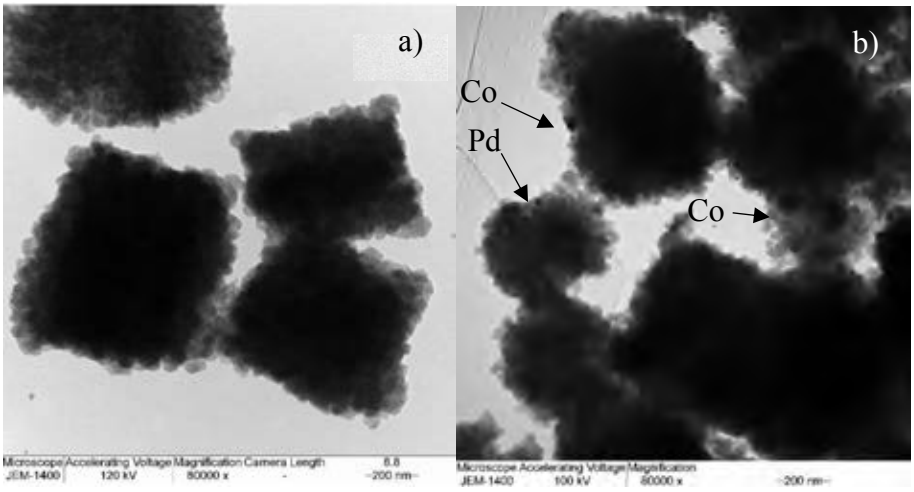

Figure 4.4 TEM images of (a) calcined HZSM-12 zeolite, (b) 5Co1Pd/ HZSM-12 zeolite, (c) 10Co1Pd/ HZSM-12 zeolite, and (d) 15Co1Pd/ HZSM-12 catalysts.

2503957090 CU iThesis 6171003063 thesis / recv: 27072563 17:27:35 / seq: 25

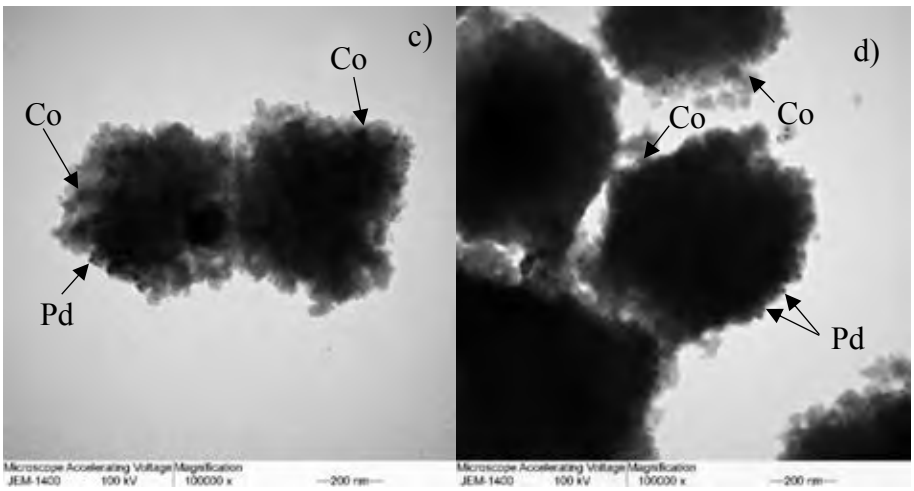

Figure 4.4 (cont.) TEM images of (a) calcined HZSM-12 zeolite, (b) 5Co1Pd/ HZSM-12 zeolite, (c) 10Co1Pd/ HZSM-12 zeolite, and (d) 15Co1Pd/ HZSM-12 catalysts.

4.1.7 Temperature Programmed Oxidation (TPO)

Temperature Programmed Oxidation (TPO) profiles of spent catalysts are presented in Figure 4.5. 1Pd/HZSM-12 exhibited a peak at 320 – 420 °C which is due to the oxygen uptake for soft coke combustion. 10Co/HZSM-12 showed two peaks at 280 – 480 °C and 500 – 610 °C which corresponded to poorly and highly polymerized coke deposition on the catalyst, respectively. Meanwhile, 10Co1Pd/HZSM-12 exhibited peak from oxygen consumption at 200 – 360 °C. Because cobalt and palladium had strong interaction, the peak was shifted to the lower temperature as compared to monometallic Co or Pd on the same zeolite supports which referred to the ease of coke removal. 10Ni1Pd/HZSM-12 revealed the low intensity peak at 270 – 500 ° C. 10Co1Pd/HZSM-5 exhibited two peaks from soft coke (280 – 450 °C) and hard coke (520 – 610 °C). 10Co1Pd/HY had a broad peak at 300 – 800 °C, indicating a high amount of hard coke according to the previous study (Rihko-Struckmann *et al.*, 2006).

2503957090 CU iThesis 6171003063 thesis / recv: 27072563 17:27:35 / seq: 25

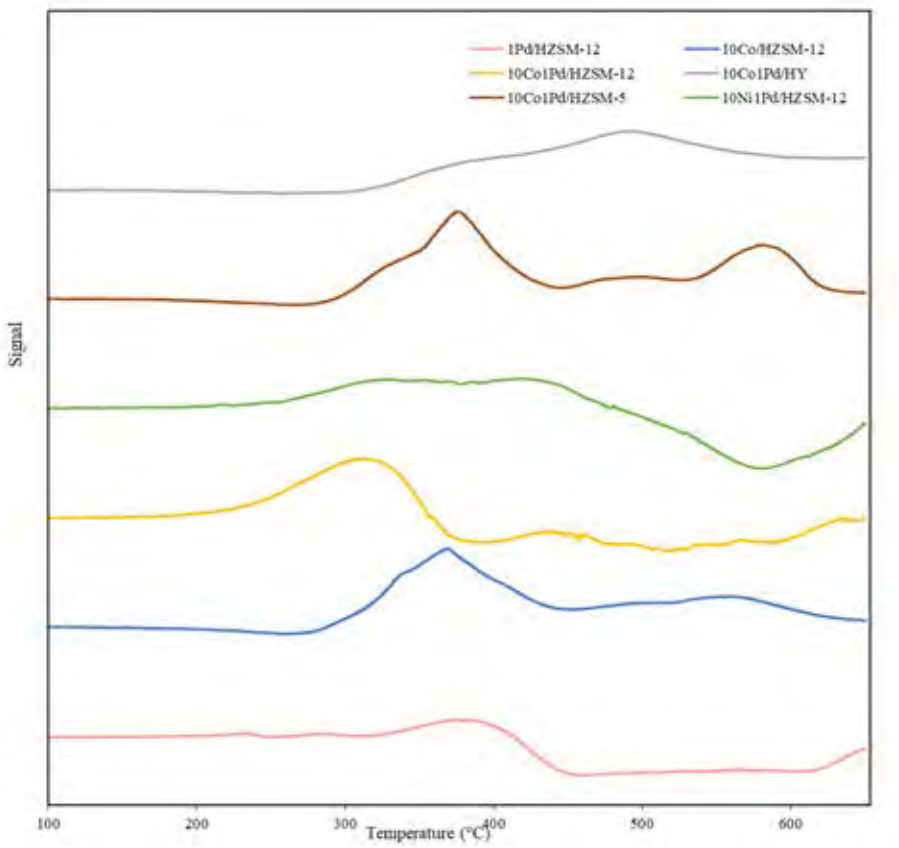

Figure 4.5 Temperature Programmed Oxidation of 1Pd/HZSM-12, 10Co/HZSM-12, 10Co1Pd/HZSM-12, 10Ni1Pd/HZSM-12, 10Co1Pd/HZSM-5, and 10Co1Pd/HY catalysts.

4.1.8 CHNS Analyzer

Table 4.5 shows the quantities of carbon in catalysts. The amount of coke deposition was lower than carbon contents on spent catalysts since fresh catalysts also had some carbon deposition. Among HZSM-12 supported catalysts, the coke deposition in spent catalysts tended to decrease in the following order: 10Co1Pd/HZSM-12 > 10Co/HZSM-12 > 10Ni1Pd/HZSM-12 > 1Pd/HZSM-12. The strong acidity plays a significant role in coke formation. According to TPD-NH_3 profiles, both 10Co1Pd/HZSM-12 and 10Co/HZSM-12 catalysts had strong acid sites, leading to the ease of coke deposition (Gao *et al.*, 2016). Moreover, the interaction of Co and Pd presented the high activity that tends to form coke. Bimetallic

2503957090 CU iThesis 6171003063 thesis / recv: 27072563 17:27:35 / seq: 25

10Ni1Pd/HZSM-12 had a low coke since nickel mainly took part in the hydrogenation reaction. Therefore, it had a side reaction like methanation for converting carbon monoxide to methane. The low coke deposition is related to the removal of carbon in the form of CO_x during the reaction (Ameen *et al.*, 2019). The different zeolite supports were also studied, the amounts of the coke tended to decrease in the following order: 10Co1Pd/HY > 10Co1Pd/HZSM-5 > 10Co1Pd/HZSM-12. 10Co1Pd/HZSM-12 showed the lowest coke deposition since one-dimensional channel does not allow coke precursor penetrating inside (Zhang *et al.*, 1999) and 10Co1Pd/HZSM-5 also had shaped selective that limits coke into the pores (Weigert *et al*., 1986). However, the HZSM-5 in this work had high acidity from Si/Al molar ratio of 50 which affects high coke formation according to the previous study (Gao *et al.*, 2016). 10Co1Pd/HY exhibited the highest amount of coke because it had large cavities of the pores that coke can be placed inside the pores (Schulz *et al*., 2004).

2503957090 CU iThesis 6171003063 thesis / recv: 27072563 17:27:35 / seq: 25

Table 4.5 Amount of carbon deposits on spent catalysts from CHNS analyzer

Catalysts	Carbon of fresh catalysts (wt. %)	Carbon of spent catalysts (wt. %)
10Co/HZSM-12	1.642	20.50
1Pd/HZSM-12	1.655	16.53
10Co1Pd/HZSM-12	1.633	22.79
10Ni1Pd/HZSM-12	N/A	18.67
10Co1Pd/HZSM-5	N/A	24.66
10Co1Pd/HY	1.672	28.44

4.2 Gas Chromatography of Feed and Standard Analysis

4.2.1 Feed Analysis

The chromatogram and composition of PFAD, analyzed by GC/FID (Agilent 7890A) are shown in Figure 4.6, and Table 4.6, respectively. It was observed that PFAD contained palmitic acid and oleic acid as the main components (retention

times are 16.043 and 17.509, respectively), it also contained other components i.e. hexadecane, octadecane, steric acid, hexadecanol, monoglyceride, diglyceride, and triglyceride (retention times are 11.903, 13.898, 15.190, 17.737, 28.831, 32.960 – 34.377 and 35.937 – 37.254, respectively).

Table 4.6 Composition of PFAD feedstock

Feed components	**Amount (% wt.)**
Palmitic acid	46.48
Oleic acid	43.41
Stearic acid	4.00
Hexadecane	0.38
Octadecane	1.14
Monoglyceride	1.45
Diglyceride	2.28
Triglyceride	0.86

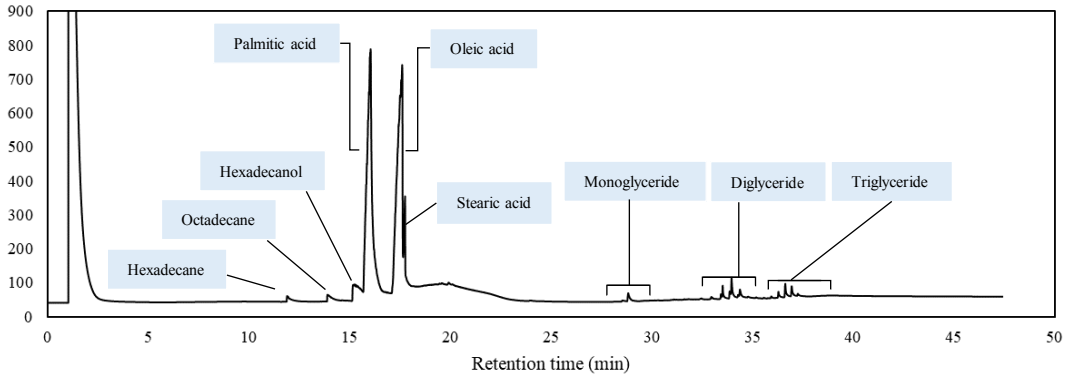

Figure 4.6 The chromatogram of various components in PFAD range analyzed by a GC/FID.

4.2.2 Standard Analysis

The chromatograms of liquid standards were analyzed by an Agilent 7890 gas chromatograph equipped with an FID detector to identify the peaks of non-polarity liquid standards (*n*-alkanes) and the polarity liquid standards (oxygenated

2503957090 CU iThesis 6171003063 thesis / recv: 27072563 17:27:35 / seq: 25

compounds). Figure 4.7 shows chromatograms of *n*-alkanes from ASTM 2887 standards, consisting of hexane (C6), heptane (C7), octane (C8), nonane (C9), decane (C10), undecane (C11), dodecane (C12), tetradecane (C14), hexadecane (C16), octadecane (C18), and eicosane (C20) (retention times are 1.056, 1.067, 1.127, 1.236, 1.481, 2.067, 3.446, 8.294, 11.125, 13.292, and 15.122, respectively). In addition, other *n*-alkanes; tridecanes (C13), and heptadecane (C17) had retention times at 6.35 and 12.233.

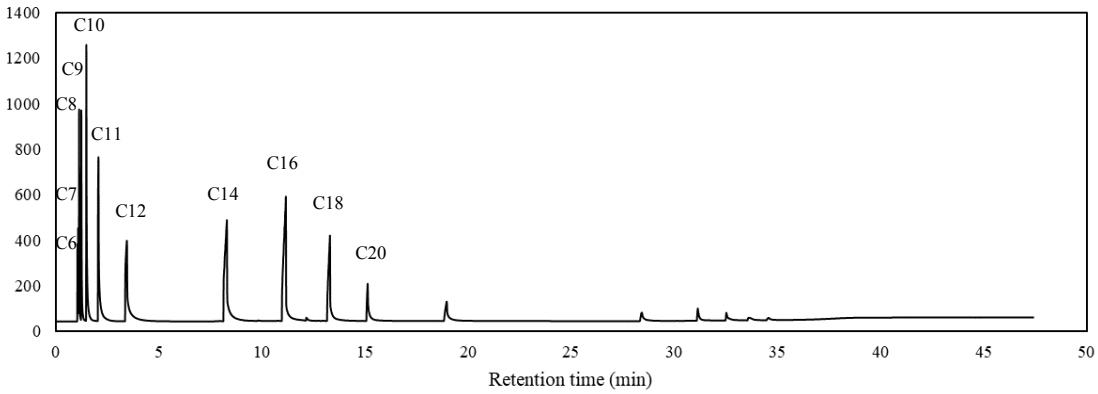

Figure 4.7 The chromatogram of various *n*-alkane components in ASTM 2887 standard analyzed by a GC/FID.

The chromatogram of oxygenated compounds standards is shown in Figure 4.8, consisting of hexadecanol, C20 internal standard, palmitic acid, octadecanol, oleic acid, and stearic acid (retention times are 14.828, 15.104, 15.662, 16.616, 17.079, and 17.376, respectively).

2503957090 CU iThesis 6171003063 thesis / recv: 27072563 17:27:35 / seq: 25

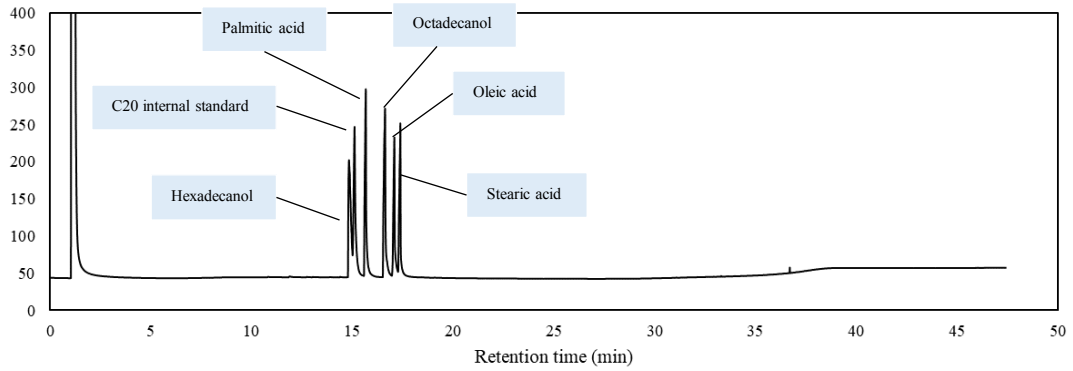

Figure 4.8 The chromatogram of oxygenated compounds standard analyzed by a GC/FID.

4.3 Catalyst Activity Testing

This section exhibits the performance of the prepared catalysts in terms of conversion of PFAD and product yield. Monometallic (Co and Pd) and bimetallic (CoPd and NiPd) supported on HZSM-12 zeolite with various metal loadings and bimetallic CoPd with various zeolite supports (HZSM-12, HZSM-5, and HY) were studied. The optimum reaction conditions (i.e. temperature, pressure, and LHSV) were also investigated.

4.3.1 Effect of Metal Loading

This section is divided into 3 parts including 1) Effect of mono- and bi-metallic CoPd supported on HZSM-12 2) Effect of Co loading on CoPd/HZSM-12and 3) Comparison of CoPd/HZSM-12 and NiPd/HZSM-12.

4.3.1.1 Effect of Mono- and Bi-metallic CoPd Supported on HZSM-12

Figure 4.9 shows conversion and yield of products over 1Pd/HZSM-12, 10Co/HZSM-12, and 10Co1Pd/HZSM-12 catalyts at 350°C, 30 bar, LHSV= 1.5 h^{-1}, and H_2/feed molar ratio of 8. All catalysts gave high conversion of PFAD (closed to 100%). After operating the system for 7 h, the conversion of 1Pd/HZSM-12 deactivated from 99.15% to 76.87% while other catalysts still gave high conversion almost 100%. Moreover, 1Pd/HZSM-12 exhibited the highest bio-jet fuel yield of 70.53% at TOS of 4 h then deactivated, giving bio-jet fuel 3.94% at TOS of 8 h. 10Co/HZSM-12 exhibited good stability at first 6 h with a yield higher than 30%. Finally, 10Co1Pd/HZSM-12 exhibited great stability without deactivation at

2503957090 CU iThesis 6171003063 thesis / recv: 27072563 17:27:35 / seq: 25

first 7 h with a conversion of 99.98% and yield of bio-jet fuel of 50.92%. According to CHNS results, the 1Pd/HZSM-12 catalyst activity dropped faster than 10Co/HZSM-12 and 10Co1Pd/HZSM-12 catalysts even though it had the lowest coke formation. Because the presence of cobalt in catalyst facilitates hydrogen adsorption on active sites (Dao *et al*., 2015), hydrogen can further react with the nearby coke to stabilize the catalysts (Yang *et al.*, 2009). Moreover, 10Co/HZSM-12 and 10Co1Pd/HZSM-12 catalysts presented high PFAD conversion after 6 and 7 h, respectively. But, the yield of bio-jet decreased with the increasing of diesel. It can be expected that metal still had high activity in deoxygenation reaction but the acidity for hydrocracking was lower. The lower acidity could be from the sintering after the course of reaction at high temperature. The sintering process resulted in crystal agglomeration and further pore blocking, thus lowering catalyst active site for hydrocracking reaction (Nasrallah M, 2018).

2503957090 CU iThesis 6171003063 thesis / recv: 27072563 17:27:35 / seq: 25

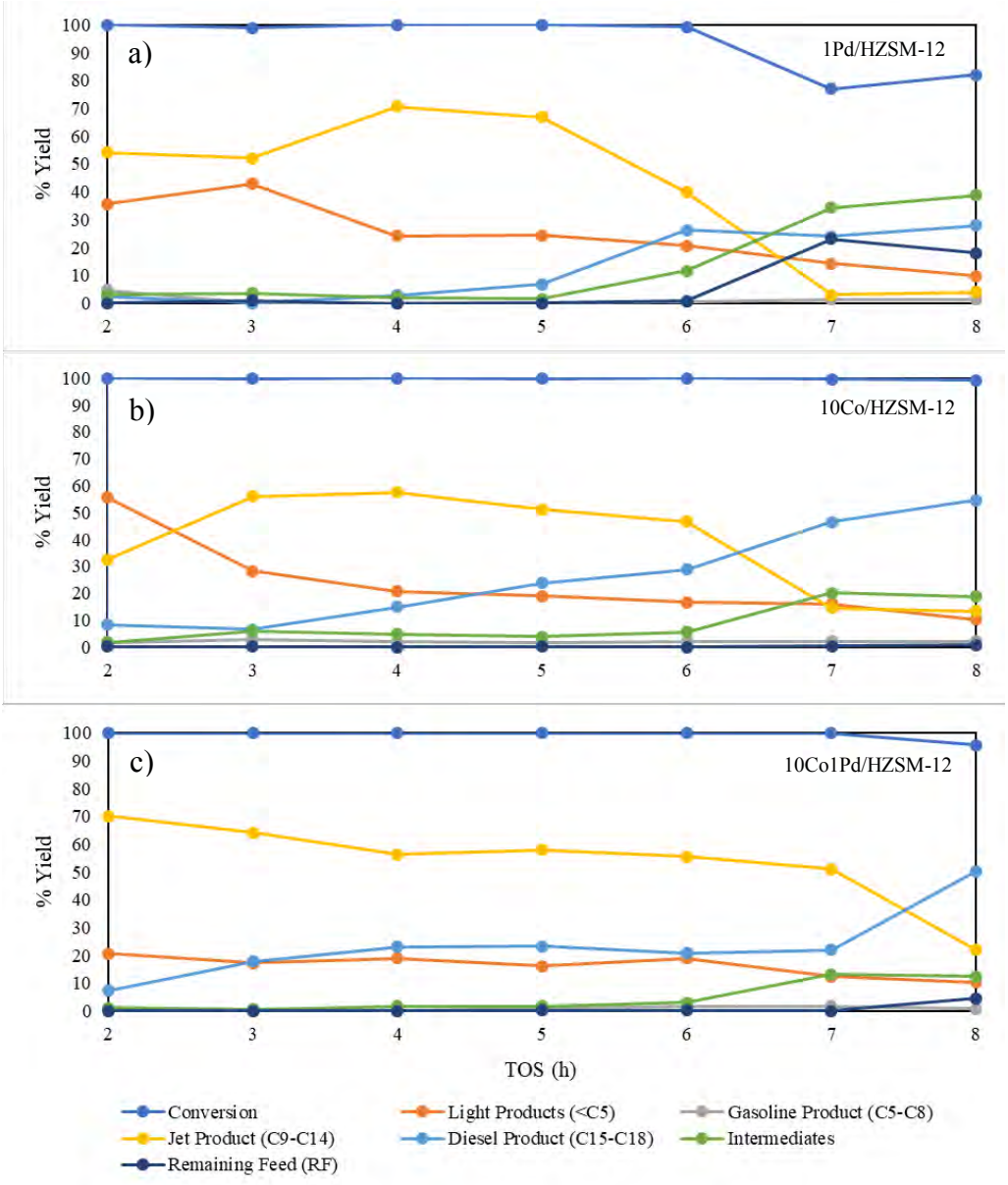

Figure 4.9 The conversion of PFAD and product yield obtained over (a) 1Pd/HZSM-12, (b) 10Co/HZSM-12, and (c) 10Co1Pd/HZSM-12 (Reaction condition: 350°C, 30 bar, LHSV= 1.5 h^{-1}, and H_2/feed molar ratio of 8).

The conversion of PFAD and products yield over 1Pd/HZSM-12, 10Co1Pd/HZSM-12, and 10Co/HZSM-12 catalysts are presented in Figure 4.10. All catalysts gave high fraction of *i*-paraffins. Although 1Pd/HZSM-12 was highly active as shown in Figure 4.8, it produced 39.98 % bio-jet fuel which is lower than 10Co/HZSM-12 and 10Co1Pd/HZSM-12 (46.62% and 55.46%, respectively) at 6 h.

CU iThesis 6171003063 thesis / recv: 27072563 17:27:35 / seq: 25
2503957090

Moreover, the presence of bimetallic CoPd on HZSM-12 zeolite support not only enhanced the deoxygenation and hydrocracking for bio-jet fuel production, but also showed the highest stability as compared to the other catalysts.

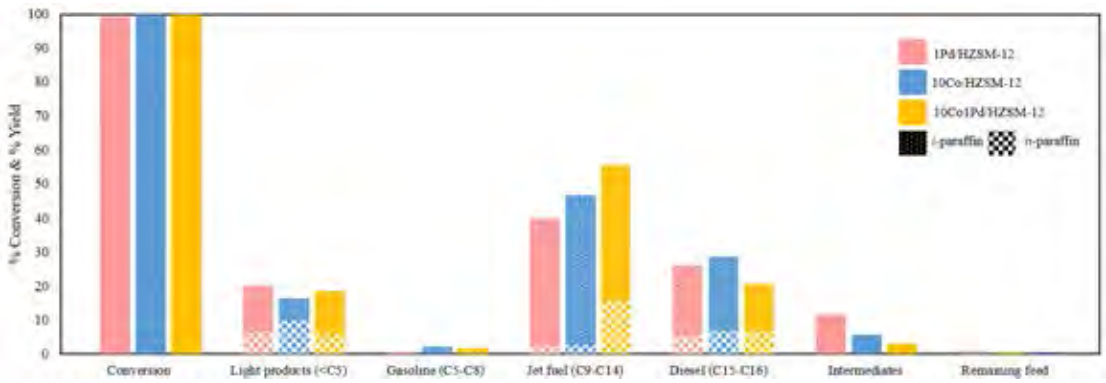

Figure 4.10 The conversion and yield of products over 1Pd/HZSM-12, 10Co /HZSM-12, and 10Co1Pd/HZSM-12 catalysts (Reaction condition: 350°C, 30 bar, LHSV= 1.5 h^{-1}, H_2/feed molar ratio of 8, and TOS= 6 h).

4.3.1.2 Effect of Co Loading on CoPd/HZSM-12 Catalysts

The conversion and yield of products over 5Co1Pd/HZSM-12, 10Co1Pd/HZSM-12, and 15Co1Pd/HZSM-12 catalysts at 350 °C, 30 bar, LHSV= 1.5 h^{-1}, and H_2/feed molar ratio of 8 are presented in Figure 4.11. 5Co1Pd/HZSM-12 and 10Co1Pd/HZSM-12 gave high conversions of PFAD which were 93.90 % and 99.91 %, respectively while 15Co1Pd/HZSM-12 gave 84.73%. 5Co1Pd/HZSM-12 produced bio-jet fuel as well as biodiesel. On the other hand, 15Co1Pd/HZSM-12 produced higher biodiesel yield than bio-jet fuel. It is possible that metal agglomerates and blocks pore size of support as shown in TEM image so the catalyst had a lower ability for cracking. It can be summarized that 10Co1Pd/HZSM-12 had a suitable Co loading as compared to the others.

2503957090 CU iThesis 6171003063 thesis / recv: 27072563 17:27:35 / seq: 25

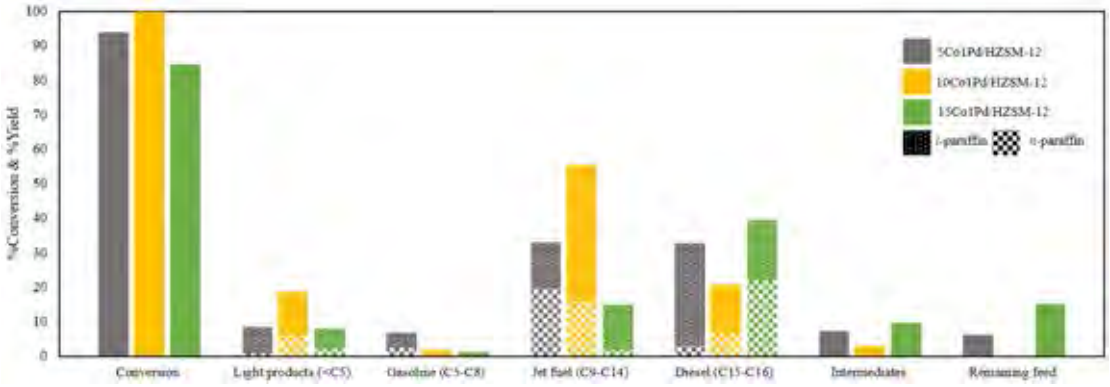

Figure 4.11 The conversion and yield of products over 5Co1Pd/HZSM-12, 10Co1Pd/HZSM-12, and 15Co1Pd/HZSM-12 catalysts (Reaction condition: 350°C, 30 bar, LHSV= 1.5 h^{-1}, H_2/feed molar ratio of 8, and TOS= 6 h).

4.3.1.3 Comparison CoPd/HZSM-12 and NiPd/HZSM-12 Catalysts

The conversion and yield of products over 10Co1Pd/HZSM-12 and 10Ni1Pd/HZSM-12 catalysts at 350 °C, 30 bar, LHSV of 1.5 h^{-1}, and H_2/feed molar ratio of 8 are shown in Figure 4.12. Both 10Co1Pd/HZSM-12 and 10Ni1Pd/HZSM-12 exhibited almost complete conversion and produced high *i*-paraffins. Cobalt demonstrated C – C hydrogenolysis that produced 55.46% bio-jet fuel while nickel exhibited high deoxygenation route, but it showed the lower hydrocracking, so it produced biodiesel similar to bio-jet fuel which were 43.96% and 43.25%, respectively. The results were similar to the previous study (Zhang *et al.*, 2014). It can be concluded that cobalt is an appropriated non-noble metal for this reaction.

2503957090 CU iThesis 6171003063 thesis / recv: 27072563 17:27:35 / seq: 25

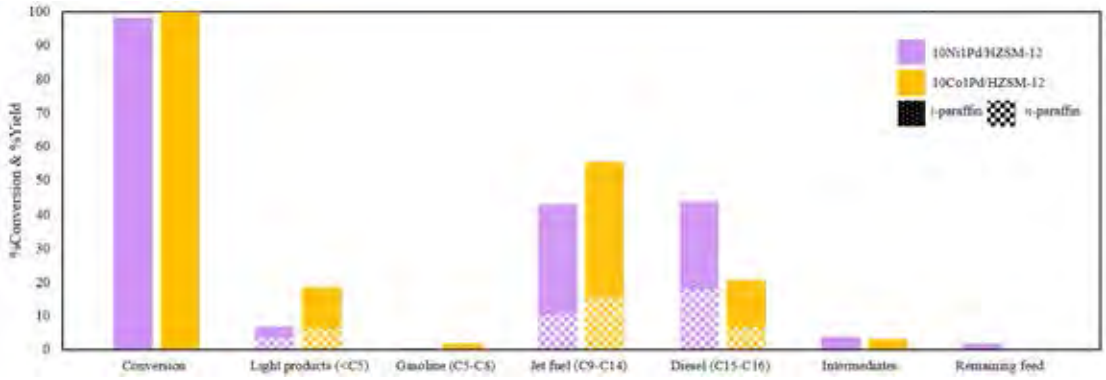

Figure 4.12 The conversion and yield of products over 10Ni1Pd/HZSM-12 and 10Co1Pd/HZSM-12 catalysts (Reaction condition: 350°C, 30 bar, LHSV= 1.5 h^{-1}, H_2/feed molar ratio of 8, and TOS= 6 h).

4.3.2 Effect of Zeolite Supports

In this section, the effect of different zeolite supports including HZSM-12, HZSM-5, and HY on the catalytic activity of CoPd catalysts was investigated. Figure 4.13 shows the appearance of liquid products obtained over the catalysts with different supports as a function of time. The liquid products obtained from 10Co1Pd/HZSM-12 were clear at first 5 h while those from 10Co1Pd/HZSM-5 and 10Co1Pd/HY were yellow and brown. After TOS of 5 h, the product obtained over 10Co1Pd/HZSM-12 exhibited an orange color. 10Co1Pd/HZSM-5 products gave a lower amount of liquid product than other catalysts and changed color to orange in TOS = 7 h, and further became dark brown. The color of 10Co1Pd/HY products continuously changed from dark brown to light brown and white solid was observed after 6 h.

2503957090 CU iThesis 6171003063 thesis / recv: 27072563 17:27:35 / seq: 25

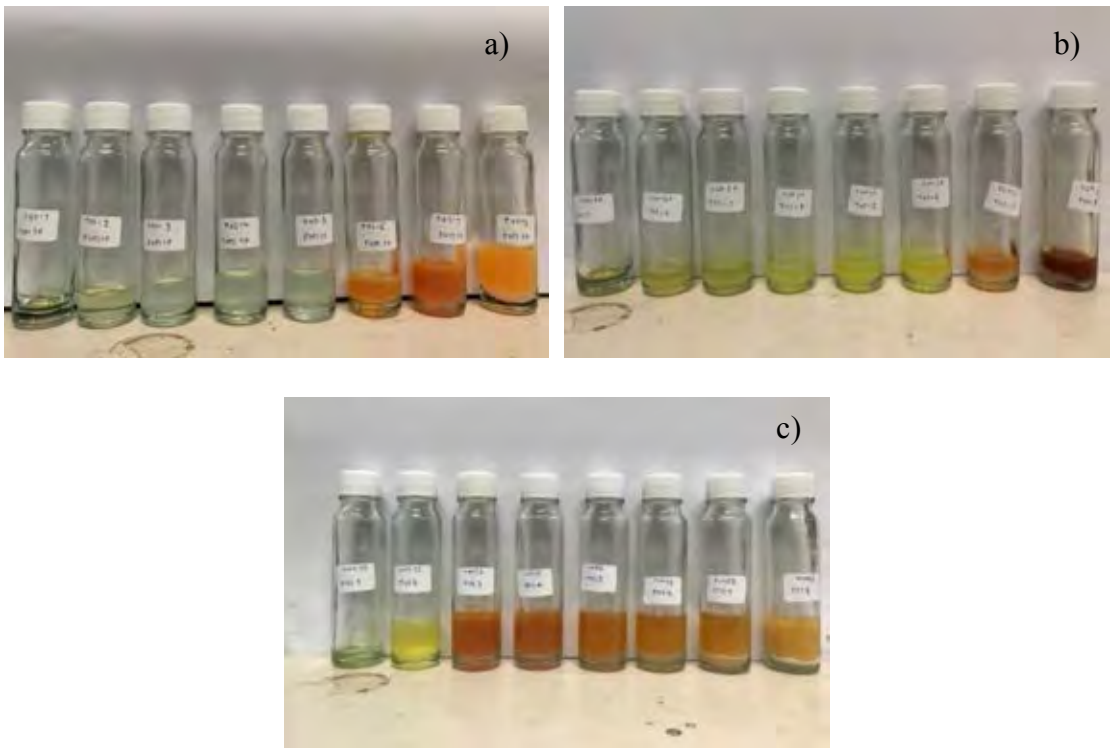

Figure 4.13 The appearance of liquid products obtained over different supports (a) 10Co1Pd/HZSM-12, (b) 10Co1Pd/HZSM-5, and (c) 10Co1Pd/HY (Reaction condition: 350°C, 30 bar, LHSV= 1.5 h^{-1}, and H_2/feed molar ratio of 8).

The conversion and yield of products over 10Co1Pd/HZSM-12, 10Co1Pd/HZSM-5, and 10Co1Pd/HY are shown in Figure 4.14. 10Co1Pd/HZSM-12 provided high bio-jet fuel which is higher than 50% at first 7 h. After that, intermediates were firstly observed. 10Co1Pd/HZSM-5 produced higher light gases than bio-jet fuel at first 5 h. After that, both light gases and bio-jet fuel became almost equal at 38%. For 10Co1Pd/HY, the high yield of gasoline occurred at first 2 h. After that, it decreased continuously while biodiesel product was increased sharply with time on stream, giving bio-jet fuel lower than 10 %.

2503957090 CU iThesis 6171003063 thesis / recv: 27072563 17:27:35 / seq: 25

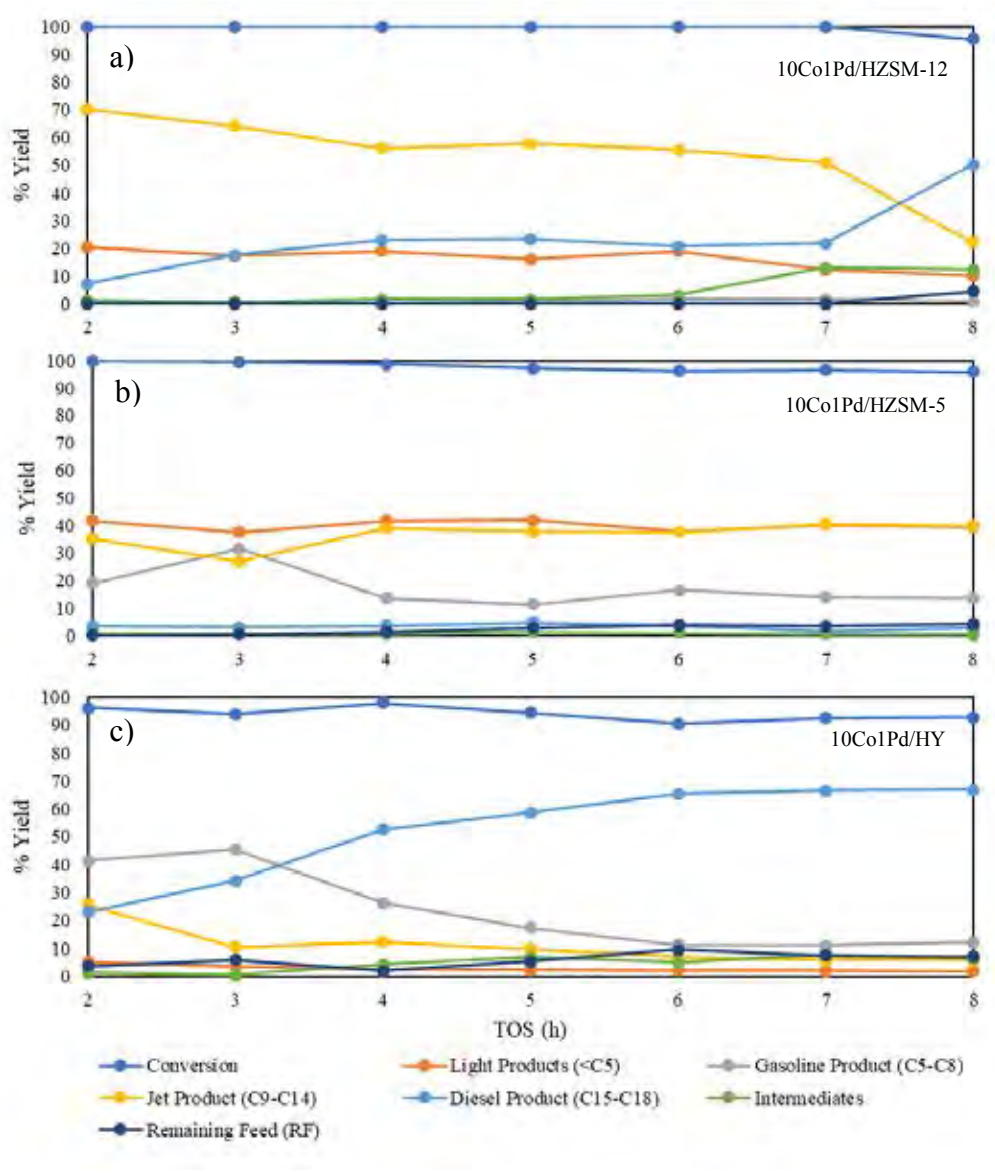

Figure 4.14 The Conversion of PFAD and product yield obtained over (a) 10Co1Pd/HZSM-12, (b) 10Co1Pd/HZSM-5, and (c) 10Co1Pd/HY (Reaction condition: 350°C, 30 bar, LHSV= 1.5 h^{-1}, and H_2/feed molar ratio of 8).

Figure 4.15 demonstrates the conversion of PFAD and yield of products obtained over 10Co1Pd/HZSM-12, 10Co1Pd/HZSM-5, and 10Co1Pd/HY at 350°C, 30 bar, LHSV= 1.5 h^{-1}, H_2/feed molar ratio of 8, and time on stream of 6. All catalysts gave high conversion. The product distributions were directly affected by the structure of the zeolite catalysts. HZSM-12 has MTW structure that has high stability and resists to deposition of coke (Marcelo *et al*., 2005). It produced 55.46% bio-jet

2503957090 CU iThesis 6171003063 thesis / recv: 27072563 17:27:35 / seq: 25

fuel with high *i*-paraffin since the pore mouth of HZSM-12 is suitable for transforming *n*-paraffin to *i*-paraffin (Ju *et al.*, 2016). HZSM-5 has MFI structure which is high stability because its channel does not allow the formation of the aromatic compound for leading coke (Weigert *et al.*, 1986). However, HZSM-5 has high acidity that affects excessive cracking with low isomerization thus it produced a high amount of light gases about 36.95% (Peng *et al.*, 2012). On the other hand, HY catalyst produced bio-jet fuel of 6.77% since FAU structure of HY has a big pore size that easily forms coke and causes low selective hydrocracking to produce a lighter product as bio-jet fuel. Moreover, it also had low isomerization (Castaño *et al.*, 2011). It can be expected that HZSM-12 is achieved catalyst support for jet fuel production purposes.

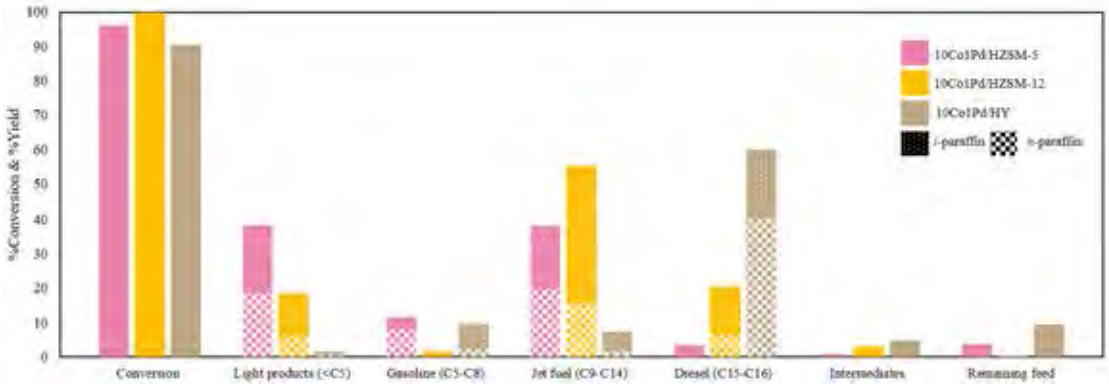

Figure 4.15 The conversion and yield of products over 10Co1Pd/HZSM-5, 10Co1Pd/HZSM-12, and 10Co1Pd/HY catalysts (Reaction condition: 350°C, 30 bar, LHSV= 1.5 h^{-1}, H_2/feed molar ratio of 8, and TOS= 6 h).

4.3.3 Effect of Reaction Temperature

In this section, the effect of reaction temperature was investigated. Figure 4.16 shows the conversion of PFAD and yield of products over 10Co1Pd/HZSM-12 catalyst at 30 bar, LHSV= 1.5 h^{-1}, and H_2/feed molar ratio of 8. The reaction temperature was varied from 325 – 375 °C. At 325 °C, PFAD was not completely converted and high amount of intermediates (42.02%) was observed. The yield of bio-jet fuel significantly increased at 350 °C with completely converting

2503957090 CU iThesis 6171003063 thesis / recv: 27072563 17:27:35 / seq: 25

PFAD because this temperature was high enough to crack the longer chain product like biodiesel and intermediates to bio-jet fuel. Moreover, at 375 °C almost complete conversion was observed. Although high amount of both intermediates and diesel were cracked, bio-jet fuel obtained only 37.37% and gasoline increased to 38.14%. It can be concluded that the reaction temperature significantly affected product selectivity. The optimal temperature for bio-jet fuel production is 350 °C (Wei *et al.*, 1996).

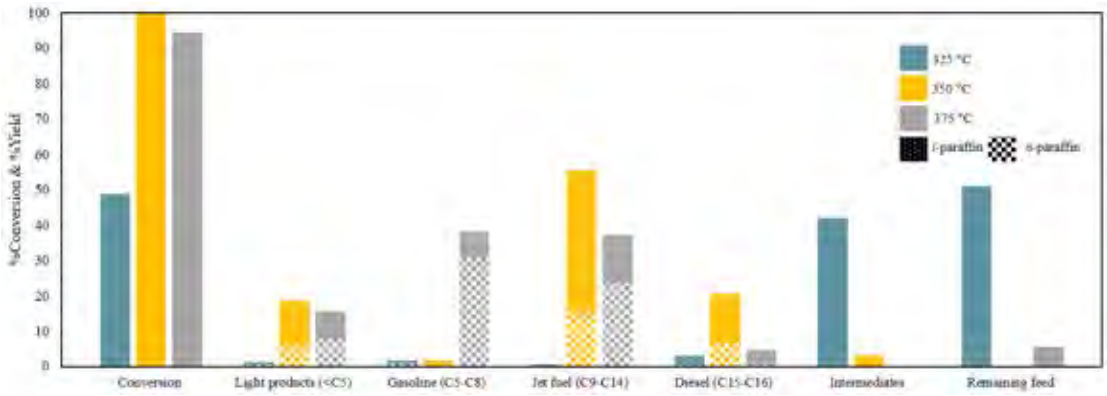

Figure 4.16 The conversion and yield of products over 10Co1Pd/HZSM-12 catalyst with different temperatures (Reaction condition: 30 bar, LHSV= 1.5 h^{-1}, H_2/feed molar ratio of 8, and TOS= 6 h).

4.3.4 Effect of Reaction Pressure

In this section, the effect of reaction pressure was investigated. Figure 4.17 shows the conversion of PFAD and products yield over 10Co1Pd/HZSM-12 catalyst at 350 °C, LHSV= 1.5 h^{-1}, and H_2/feed molar ratio of 8 with various pressures (10 – 30 bar). The results showed that the conversion of PFAD and bio-jet fuel yield increased with pressure. The reaction at 30 bar exhibited the highest conversion at 99.91% with the highest bio-jet fuel yield at 55.46% while 10 and 20 bar demonstrated bio-jet fuel yield of 17.35%, and 38.93%, respectively. Moreover, high *i*-paraffin products were observed at 20 and 30 bar. High pressure had auxiliary to adsorb hydrogen on active site and dissolve hydrogen in PFAD on the catalyst which

2503957090 CU iThesis 6171003063 thesis / recv: 27072563 17:27:35 / seq: 25

is necessary for deoxygenation, hydrocracking, and isomerization reactions (Srifa *et al.*, 2014).

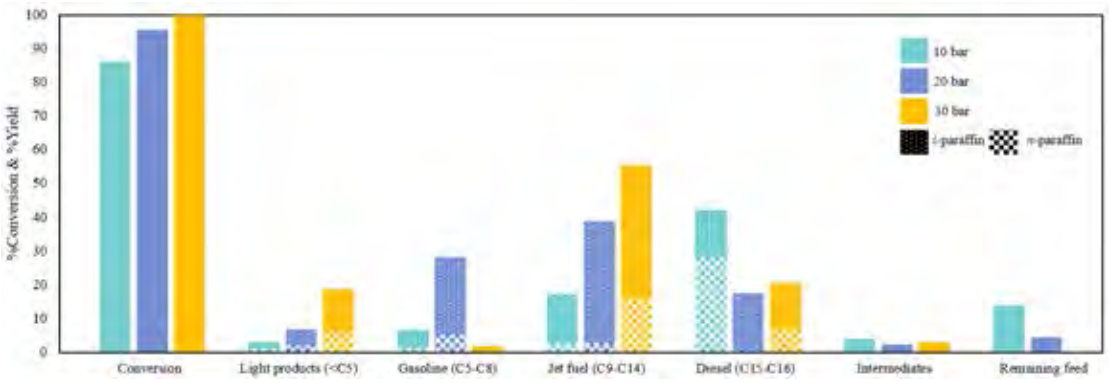

Figure 4.17 The conversion and yield of products over 10Co1Pd/HZSM-12 catalyst with different pressure (Reaction condition: 350°C, LHSV= 1.5 h^{-1}, H_2/feed molar ratio of 8, and TOS= 6 h).

4.3.5 Effect of Liquid Hourly Space Velocity (LHSV)

In this section, the effect of LHSV for bio-jet fuel production was investigated. Figure 4.18 shows the conversion and yield of products over 10Co1Pd/HZSM-12 catalysts at 350 °C, 30 bar, and H_2/feed molar ratio of 8. LHSV varied from 1.5 to 2.5 h^{-1}. Decreasing LHSV led to the lower intermediates and diesel and the higher bio-jet fuel yield with high isomer products since the catalyst had more contact time with PFAD so the intermediates can be cracked and produced lighter products like bio-jet fuel.

2503957090 CU iThesis 6171003063 thesis / recv: 27072563 17:27:35 / seq: 25

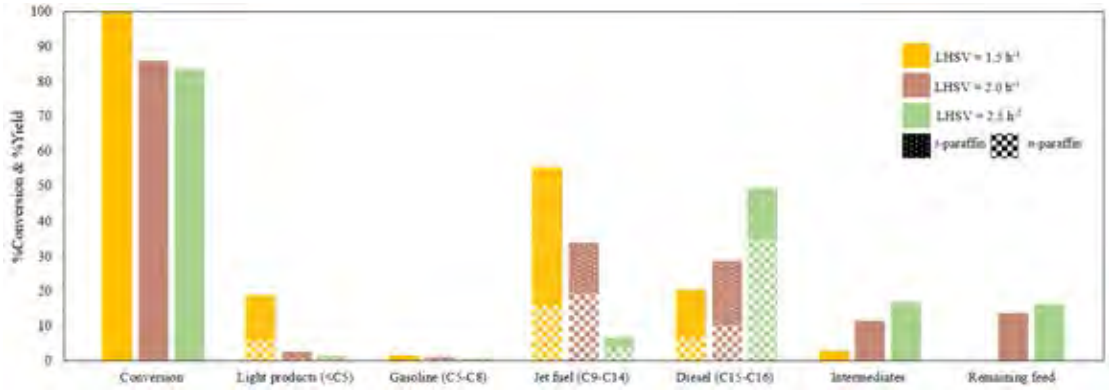

Figure 4.18 The conversion and yield of products over 10Co1Pd/HZSM-12 catalysts with different LHSV (Reaction condition: 350°C, 30 bar, H_2/feed molar ratio of 8, and TOS= 6 h).

4.4 The Proposed Reaction Pathway

The proposed reaction pathway of palmitic acid which is a major component of palm fatty acid distillate is illustrated in Figure 4.19. Palmitic acid can be further converted into saturated hydrocarbons in diesel range by deoxygenation reaction. During the deoxygenation process, oxygen is removed from fatty acid then forms to H_2O and/or CO_x. Deoxygenation reaction can be divided into three types, consisting of hydrodeoxygenation (HDO), decarboxylation (DCO_2), and decarbonylation (DCO) (Coumans *et al.*, 2017). First, hydrodeoxygenation reaction (HDO) is oxygen exclusion process which is necessary to consume high hydrogen pressure and temperature to direct scission of C – O bond. Palmitic acid is transformed to hexadecanal via hydrogenolysis. Hexadecanal is converted to 1-hexadecanol by hydrogenated. After that, hexadecane is further produced from 1-hexadecanol through dehydrogenated reaction. Second, decarbonylation reaction (DCO) is the removal of carbonyl group, the primary reaction to form hexadecanal is firstly occurred hydrogen consumption. Subsequently, hexadecanal has transformed to pentadecane and CO by C – C bond scission. Moreover, 1-hexadecanol can also transform to pentadecane though decarbonylation reaction by removing CO and water. Third, decarboxylation reaction (DCO_2) is the removal of carboxyl group with no hydrogen consumption and

2503957090 CU iThesis 6171003063 thesis / recv: 27072563 17:27:35 / seq: 25

directly form pentadecane. Furthermore, hydrocracking reaction converts straight long chain-like diesel range to bio-jet fuel product by adding hydrogen. Moreover, the isomerization process converted straight-chain (*n*-paraffin) to branched-chain (*i*-paraffin) by removing hydrogen to form olefin and further produce various isomer products (Srifa *et al.*, 2015).

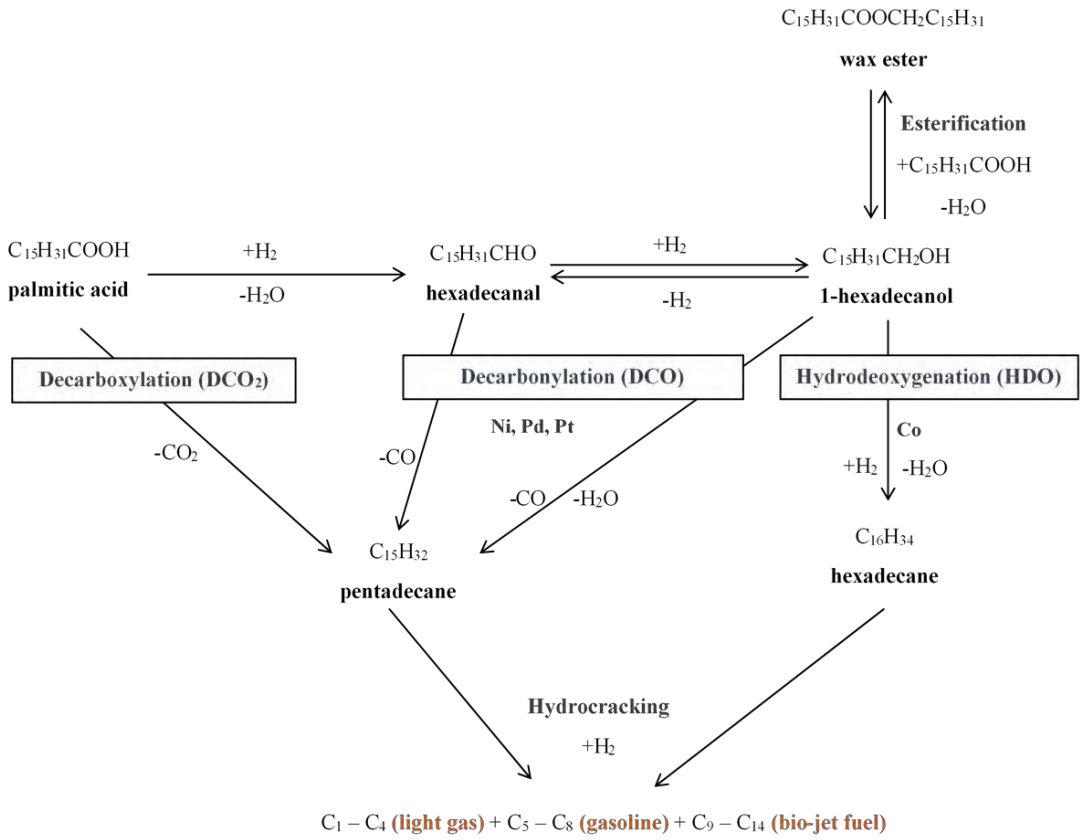

Figure 4.19 The proposed reaction pathway of bio-jet fuel production from palmitic acid over bi-functional catalysts.

2503957090 CU iThesis 6171003063 thesis / recv: 27072563 17:27:35 / seq: 25

CHAPTER 5
CONCLUSIONS AND RECOMMENDATIONS

5.1 Conclusions

In this study, monometallic (Co and Pd) and bimetallic (CoPd and NiPd) supported on HZSM-12 zeolite with various metal loadings and bimetallic CoPd with various zeolite supports (HZSM-12, HZSM-5, and HY) were investigated to find the suitable catalyst for converting PFAD to bio-jet fuel product. The synthesized catalysts were confirmed by XRD, XRF, and TEM images. The acidity of catalysts enhanced after metals were loaded to zeolite support as shown in the TPD results. 10Co1Pd/HZSM-12 exhibited high catalyst activity and stability as compared to monometallic (Co or Pd) and bimetallic (NiPd) with the same zeolite supports. This could be due to its suitable acidity for cracking and isomerization to the product in jet fuel range. Moreover, 10Co1Pd/HZSM-12 exhibited low coke formation as compared to other zeolite supports since its pore size does not allow penetration of coke precursor, according to TPO and CHNS analyzer. 10Co1Pd/HZSM-5 demonstrated high acidity, resulting in a low bio-jet fuel. 10Co1Pd/HY had a large pore size and low acidity thus presenting low hydrocarbons in jet fuel range. The optimum reaction conditions for 10Co1Pd/HZSM-12 was found at 350 °C, 30 bar, LHSV of 1.5 h^{-1}, and H_2/Feed molar ratio of 8, giving 55.46% bio-jet fuel yield.

5.2 Recommendations

The 10Co1Pd/HZSM-12 catalyst exhibited high conversion until TOS = 7. However, the intermediates began to increase after TOS = 6 h. It is possible that catalyst began to deactivation, as a result, this catalyst should be further studied.

Carbon monoxide and carbon dioxide should be considered to investigate the production pathway.

2503957090 CU iThesis 6171003063 thesis / recv: 27072563 17:27:35 / seq: 25

2503957090 CU iThesis 6171003063 thesis / recv: 27072563 17:27:35 / seq: 25

APPENDICES

Appendix A1 Overall Mass Balance of Deoxygenation-hydroprocessing at Mono- and Bi-metallic CoPd supported on HZSM-12

Table A1 Overall mass balance of deoxygenation-hydroprocessing one-pot reaction over 10Co/HZSM-12, 1Pd/HZSM-12, and 10Co1Pd/HZSM-12 catalysts (Reaction conditions: 350°C, 30 bar, H_2/Feed molar ratio of 8, LHSV of 1.5 h^{-1}, and TOS = 6 h)

Metal loading		**10Co/HZSM12**	**1Pd/HZSM12**	**10Co1Pd/HZSM12**
Selectivity of product (wt.%)	C1	5.246986	0.339572	0.857380
	C2	0.649201	0.976038	0.650933
	Ethylene	0.000000	0.000000	0.000000
	C3	4.363975	8.876373	9.153071
	Propylene	4.072942	5.691452	4.800060
	iso-C4	2.259293	4.918437	3.453046
	n-C4	0.004409	0.000000	0.009590
	iso-C5	1.494013	0.588912	1.652352
	n-C5	0.589756	0.000000	0.000000
	iso-C6	0.045742	0.011570	0.047857
	n-C6	0.071243	0.013229	0.010054
	iso-C7	0.008435	0.003790	0.002499
	n-C7	0.000000	0.000000	0.000000
	iso-C8	0.000000	0.000000	0.000000
	n-C8	0.000391	0.000000	0.000000
	iso-C9	0.000235	8.967363	0.000000
	n-C9	0.001387	1.155683	0.000297
	iso-C10	32.836648	22.984698	37.307341
	n-C10	0.739924	0.387210	14.518271
	iso-C11	3.897054	1.208956	0.945268
	n-C11	0.463927	0.298135	0.743261

Table A1 (Cont.) Overall mass balance of deoxygenation-hydroprocessing one-pot reaction over 10Co/HZSM-12, 1Pd/HZSM-12, and 10Co1Pd/HZSM-12 catalysts (Reaction conditions: 350°C, 30 bar, H_2/Feed molar ratio of 8, LHSV of 1.5 h^{-1}, and TOS = 6 h)

Metal loading		**10Co/HZSM12**	**1Pd/HZSM12**	**10Co1Pd/HZSM12**
Selectivity of product (wt.%)	*iso*-C12	2.967439	0.438892	0.744055
	n-C12	0.844959	0.147564	0.503653
	iso-C13	1.874997	0.818054	0.426182
	n-C13	0.058881	0.024221	0.006159
	iso-C14	2.422689	3.334241	0.259802
	n-C14	0.548883	0.559745	0.051783
	iso-C15	7.210888	3.197237	1.407418
	n-C15	6.794290	4.208786	1.091614
	iso-C16	11.045163	5.012418	5.920185
	n-C16	0.026774	0.784873	0.068034
	iso-C17	2.172126	6.849027	1.261768
	n-C17	0.211576	0.189992	5.359984
	iso-C18	1.367321	5.727621	5.450335
	n-C18	0.008629	0.442789	0.161249
Intermediates		5.668985	11.583036	3.004438
Feed Remaining		0.030837	0.260085	0.132061
%Conversion		99.912461	99.150405	99.912222

2503957090 CU iThesis 6171003063 thesis / recv: 27072563 17:27:35 / seq: 25

Appendix A2 Overall Mass Balance of Deoxygenation-hydroprocessing at Different Co loading on CoPd/HZSM-12 Catalysts

Table A2 Overall mass balance of deoxygenation-hydroprocessing one-pot reaction over 5Co1Pd/HZSM-12, 10Co1Pd/HZSM-12, and 15Co1Pd/HZSM-12 catalysts (Reaction conditions: 350°C, 30 bar, H_2/Feed molar ratio of 8, LHSV of 1.5 h^{-1}, and TOS = 6 h)

Percent Co Loading		**5 wt.%**	**10 wt.%**	**15 wt.%**
Selectivity of product (wt.%)	C1	0.559765	0.857380	0.539730
	C2	0.485965	0.650933	0.307238
	Ethylene	0.000048	0.000000	3.117325
	C3	2.788100	9.153071	0.000000
	Propylene	0.020588	4.800060	0.010651
	iso-C4	5.342473	3.453046	3.563622
	n-C4	0.000000	0.009590	1.878578
	iso-C5	1.431589	1.652352	1.093960
	n-C5	0.656645	0.000000	0.401432
	iso-C6	0.178414	0.047857	0.038188
	n-C6	0.031871	0.010054	0.006956
	iso-C7	1.934233	0.002499	0.001964
	n-C7	0.859370	0.000000	0.000000
	iso-C8	1.176657	0.000000	0.000000
	n-C8	0.998835	0.000000	0.000000
	iso-C9	13.461656	0.000000	0.000000
	n-C9	0.085343	0.000297	0.000000
	iso-C10	2.619685	37.307341	6.577045
	n-C10	0.049835	14.518271	0.000000
	iso-C11	2.394300	0.945268	5.355324
	n-C11	0.056265	0.743261	1.432255

2503957090 CU iThesis 6171003063 thesis / recv: 27072563 17:27:35 / seq: 25

Table A2 (Cont.) Overall mass balance of deoxygenation-hydroprocessing one-pot reaction over 5Co1Pd/HZSM-12, 10Co1Pd/HZSM-12, and 15Co1Pd/HZSM-12 catalysts (Reaction conditions: 350°C, 30 bar, H_2/Feed molar ratio of 8, LHSV of 1.5 h^{-1}, and TOS = 6 h)

Percent Co Loading		**5 wt.%**	**10 wt.%**	**15 wt.%**
Selectivity of product (wt.%)	*iso*-C12	2.008977	0.744055	2.214378
	n-C12	0.093066	0.503653	0.042350
	iso-C13	1.448025	0.426182	1.105847
	n-C13	0.107335	0.006159	0.151859
	iso-C14	12.240362	0.259802	0.380266
	n-C14	0.485923	0.051783	0.456600
	iso-C15	1.393072	1.407418	0.024439
	n-C15	1.178540	1.091614	24.696296
	iso-C16	11.099892	5.920185	17.342538
	n-C16	0.538642	0.068034	0.162581
	iso-C17	9.180391	1.261768	1.900136
	n-C17	0.767843	5.359984	0.887589
	iso-C18	10.198445	5.450335	1.437369
	n-C18	0.602381	0.161249	0.043168
Intermediates		7.317326	3.004438	9.413614
Feed Remaining		6.208140	0.132061	15.416701
%Conversion		93.900167	99.912222	84.728233

2503957090 CU iThesis 6171003063 thesis / recv: 27072563 17:27:35 / seq: 25

Appendix A3 Overall Mass Balance of Deoxygenation-hydroprocessing at CoPd/HZSM-12 and NiPd/HZSM-12 Catalysts

Table A3 Overall mass balance of deoxygenation-hydroprocessing one-pot reaction over 10Co1Pd/HZSM-12 and 10Ni1Pd/HZSM-12 catalysts (Reaction conditions: 350°C, 30 bar, H_2/Feed molar ratio of 8, LHSV of 1.5 h^{-1}, and TOS = 6 h)

Co and Ni Loading		10Co1Pd/HZSM-12	10Ni1Pd/HZSM-12
Selectivity of product (wt.%)	C1	0.857380	2.453971
	C2	0.650933	0.350749
	Ethylene	0.000000	0.000000
	C3	9.153071	2.231191
	Propylene	4.800060	0.015146
	iso-C4	3.453046	1.146331
	n-C4	0.009590	0.751278
	iso-C5	1.652352	0.191624
	n-C5	0.000000	0.095514
	iso-C6	0.047857	0.020738
	n-C6	0.010054	0.007294
	iso-C7	0.002499	0.008602
	n-C7	0.000000	0.000061
	iso-C8	0.000000	0.000102
	n-C8	0.000000	0.000098
	iso-C9	0.000000	0.000087
	n-C9	0.000297	0.002578
	iso-C10	37.307341	30.131004
	n-C10	14.518271	0.000000
	iso-C11	0.945268	5.008269
	n-C11	0.743261	0.933028

2503957090 CU iThesis 6171003063 thesis / recv: 27072563 17:27:35 / seq: 25

Table A3 (Cont.) Overall mass balance of deoxygenation-hydroprocessing one-pot reaction over 10Co1Pd/HZSM-12 and 10Ni1Pd/HZSM-12 catalysts (Reaction conditions: 350°C, 30 bar, H_2/Feed molar ratio of 8, LHSV of 1.5 h^{-1}, and TOS = 6 h)

Co and Ni Loading		**10Co1Pd/HZSM-12**	**10Ni1Pd/HZSM-12**
Selectivity of product (wt.%)	*iso*-C12	0.744055	2.593336
	n-C12	0.503653	0.270377
	iso-C13	0.426182	1.943106
	n-C13	0.006159	0.064803
	iso-C14	0.259802	2.995759
	n-C14	0.051783	0.120629
	iso-C15	1.407418	4.100417
	n-C15	1.091614	14.786899
	iso-C16	5.920185	7.551282
	n-C16	0.068034	1.135997
	iso-C17	1.261768	10.760776
	n-C17	5.359984	1.208080
	iso-C18	5.450335	4.234605
	n-C18	0.161249	1.006522
Intermediates		3.004438	3.561848
Feed Remaining		0.132061	0.317898
%Conversion		99.912222	98.153510

2503957090 CU iThesis 6171003063 thesis / recv: 27072563 17:27:35 / seq: 25

Appendix A4 Overall Mass Balance of Deoxygenation-hydroprocessing at Different Zeolite Supports

Table A4 Overall mass balance of deoxygenation-hydroprocessing one-pot reaction over 10Co1Pd/HY, 10Co1Pd/HZSM-12, and 10Co1Pd/HZSM-5 catalysts (Reaction conditions: 350°C, 30 bar, H_2/Feed molar ratio of 8, LHSV of 1.5 h^{-1}, and TOS = 6 h)

Support Catalysts		**HY**	**HZSM-12**	**HZSM-5**
Selectivity of product (wt.%)	C1	0.586482	0.857380	3.159819
	C2	0.129284	0.650933	6.740948
	Ethylene	0.000000	0.000000	0.000000
	C3	0.660323	9.153071	18.522268
	Propylene	0.001585	4.800060	0.034591
	iso-C4	0.320676	3.453046	0.000000
	n-C4	0.269689	0.009590	8.171146
	iso-C5	0.277765	1.652352	0.000000
	n-C5	0.114779	0.000000	0.527732
	iso-C6	0.041282	0.047857	0.075869
	n-C6	0.110534	0.010054	0.004956
	iso-C7	2.322251	0.002499	14.756847
	n-C7	0.346782	0.000000	0.755662
	iso-C8	7.465660	0.000000	0.000000
	n-C8	0.051619	0.000000	0.010062
	iso-C9	1.379081	0.000000	24.479598
	n-C9	0.048797	0.000297	0.024077
	iso-C10	1.386763	37.307341	4.397850
	n-C10	0.021436	14.518271	0.138669
	iso-C11	0.923088	0.945268	2.103287
	n-C11	0.063909	0.743261	0.511875

2503957090 CU iThesis 6171003063 thesis / recv: 27072563 17:27:35 / seq: 25

Table A4 (Cont.) Overall mass balance of deoxygenation-hydroprocessing one-pot reaction over 10Co1Pd/HY, 10Co1Pd/HZSM-12, and 10Co1Pd/HZSM-5 catalysts (Reaction conditions: 350°C, 30 bar, H_2/Feed molar ratio of 8, LHSV of 1.5 h^{-1}, and TOS = 6 h)

Support Catalysts		**HY**	**HZSM-12**	**HZSM-5**
Selectivity of product (wt.%)	*iso*-C12	1.067914	0.744055	1.441949
	n-C12	0.058576	0.503653	0.096046
	iso-C13	0.467632	0.426182	1.464471
	n-C13	0.022071	0.006159	0.130116
	iso-C14	0.969375	0.259802	1.640348
	n-C14	0.143208	0.051783	0.085159
	iso-C15	8.437586	1.407418	0.992539
	n-C15	0.700219	1.091614	0.040892
	iso-C16	23.207444	5.920185	0.803009
	n-C16	0.470155	0.068034	0.043005
	iso-C17	9.894960	1.261768	0.904136
	n-C17	0.893218	5.359984	0.027395
	iso-C18	17.863429	5.450335	0.612915
	n-C18	1.139428	0.161249	0.030269
Intermediates		4.623338	3.004438	0.789549
Feed Remaining		13.519663	0.132061	6.482945
%Conversion		90.500606	99.912222	96.203812

2503957090 CU iThesis 6171003063 thesis / recv: 27072563 17:27:35 / seq: 25

Appendix A5 Overall Mass Balance of Deoxygenation-hydroprocessing at Different in Temperature

Table A5 Overall mass balance of deoxygenation-hydroprocessing one-pot reaction over 10Co1Pd/HZSM-12 catalyst in different temperature (Reaction conditions: 30 bar, H_2/Feed molar ratio of 8, LHSV of 1.5 h^{-1}, and TOS = 6 h)

Temperature (ºC)		**325**	**350**	**375**
Selectivity of product (wt.%)	C1	0.064472	0.857380	1.805180
	C2	0.190148	0.650933	0.780369
	Ethylene	0.000000	0.000000	4.795606
	C3	0.663755	9.153071	0.128168
	Propylene	0.001142	4.800060	4.021611
	iso-C4	0.706384	3.453046	3.725326
	n-C4	0.000000	0.009590	0.000000
	iso-C5	0.000000	1.652352	1.304073
	n-C5	0.094456	0.000000	0.498155
	iso-C6	0.366299	0.047857	0.354562
	n-C6	0.251196	0.010054	0.008366
	iso-C7	0.878456	0.002499	16.060817
	n-C7	0.444579	0.000000	5.431521
	iso-C8	0.208534	0.000000	12.889825
	n-C8	0.039452	0.000000	1.111454
	iso-C9	0.379238	0.000000	23.964055
	n-C9	0.023785	0.000297	0.183087
	iso-C10	0.140639	37.307341	3.460338
	n-C10	0.061723	14.518271	0.065914
	iso-C11	0.176757	0.945268	2.926052
	n-C11	0.010575	0.743261	0.121024

2503957090 CU iThesis 6171003063 thesis / recv: 27072563 17:27:35 / seq: 25

Table A5 (Cont.) Overall mass balance of deoxygenation-hydroprocessing one-pot reaction over 10Co1Pd/HZSM-12 catalyst in different temperature (Reaction conditions: 30 bar, H_2/Feed molar ratio of 8, LHSV of 1.5 h^{-1}, and TOS = 6 h)

Temperature (ºC)		**325**	**350**	**375**
Selectivity of product (wt.%)	*iso*-C12	0.158612	0.744055	2.179395
	n-C12	0.011339	0.503653	0.086393
	iso-C13	0.210803	0.426182	1.249003
	n-C13	0.010418	0.006159	0.415717
	iso-C14	0.197130	0.259802	1.786690
	n-C14	0.009363	0.051783	0.081774
	iso-C15	1.010467	1.407418	2.777113
	n-C15	0.012805	1.091614	0.075603
	iso-C16	1.147813	5.920185	0.630494
	n-C16	0.067207	0.068034	0.028958
	iso-C17	1.463293	1.261768	0.788609
	n-C17	0.106842	5.359984	0.060845
	iso-C18	2.023194	5.450335	0.180545
	n-C18	0.793647	0.161249	0.014851
Intermediates		72.583466	3.004438	0.268027
Feed Remaining		15.492010	0.132061	5.740482
%Conversion		48.875178	99.912222	94.483429

2503957090 CU iThesis 6171003063 thesis / recv: 27072563 17:27:35 / seq: 25

Appendix A6 Overall Mass Balance of Deoxygenation-hydroprocessing at Different in Pressure

Table A6 Overall mass balance of deoxygenation-hydroprocessing one-pot reaction over 10Co1Pd/HZSM-12 catalyst in different pressure (Reaction conditions: 350°C, H_2/Feed molar ratio of 8, LHSV of 1.5 h^{-1}, and TOS = 6 h)

Pressure		**10 bar**	**20 bar**	**30 bar**
Selectivity of product (wt.%)	C1	0.033347	0.666731	0.857380
	C2	0.007402	0.226886	0.650933
	Ethylene	0.000027	0.000059	0.000000
	C3	0.045236	1.390670	9.153071
	Propylene	0.008244	0.029172	4.800060
	iso-C4	0.065645	3.614048	3.453046
	n-C4	0.014583	0.000000	0.009590
	iso-C5	0.009711	0.000000	1.652352
	n-C5	0.009074	1.063813	0.000000
	iso-C6	0.060977	1.536850	0.047857
	n-C6	0.004600	0.255828	0.010054
	iso-C7	0.125702	16.073235	0.002499
	n-C7	0.063935	4.039026	0.000000
	iso-C8	0.101502	6.495961	0.000000
	n-C8	0.005226	0.074152	0.000000
	iso-C9	0.158638	24.390613	0.000000
	n-C9	0.007543	0.176533	0.000297
	iso-C10	0.136520	4.792189	37.307341
	n-C10	0.002817	0.026740	14.518271
	iso-C11	0.146736	3.778385	0.945268
	n-C11	0.021242	0.065625	0.743261

2503957090 CU iThesis 6171003063 thesis / recv: 27072563 17:27:35 / seq: 25

Table A6 (Cont.) Overall mass balance of deoxygenation-hydroprocessing one-pot reaction over 10Co1Pd/HZSM-12 catalyst in different pressure (Reaction conditions: 350°C, H_2/Feed molar ratio of 8, LHSV of 1.5 h^{-1}, and TOS = 6 h)

Pressure		**10 bar**	**20 bar**	**30 bar**
Selectivity of product (wt.%)	*iso*-C12	0.105104	2.280886	0.744055
	n-C12	0.012265	0.089673	0.503653
	iso-C13	0.101185	0.897913	0.426182
	n-C13	0.004504	0.047187	0.006159
	iso-C14	0.088951	1.706192	0.259802
	n-C14	0.014451	0.283177	0.051783
	iso-C15	1.258929	6.988325	1.407418
	n-C15	0.032233	0.203576	1.091614
	iso-C16	0.379441	6.902938	5.920185
	n-C16	0.030588	0.018298	0.068034
	iso-C17	0.382023	2.343647	1.261768
	n-C17	0.006404	0.054364	5.359984
	iso-C18	0.267743	1.593551	5.450335
	n-C18	0.077304	0.145403	0.161249
Intermediates		0.185684	2.235634	3.004438
Feed Remaining		0.968962	5.512722	0.132061
%Conversion		86.118969	95.576319	99.912222

2503957090 CU iThesis 6171003063 thesis / recv: 27072563 17:27:35 / seq: 25

Appendix A7 Overall Mass Balance of Deoxygenation-hydroprocessing at Different Liquid Hourly Space Velocity

Table A7 Overall mass balance of deoxygenation-hydroprocessing one-pot reaction over 10Co1Pd/HZSM-12 catalyst in different liquid hourly space velocity (Reaction conditions: 350°C, 30 bar, H_2/Feed molar ratio of 8, and TOS = 6 h)

LHSV (h^{-1})		**1.5**	**2**	**2.5**
Selectivity of product (wt.%)	C1	0.857380	0.139818	0.318389
	C2	0.650933	0.243182	0.073002
	Ethylene	0.000000	0.000000	0.000060
	C3	9.153071	0.982158	0.569029
	Propylene	4.800060	0.000000	0.018230
	iso-C4	3.453046	1.720810	0.536367
	n-C4	0.009590	0.000000	0.205872
	iso-C5	1.652352	0.532338	0.139740
	n-C5	0.000000	0.344671	0.086080
	iso-C6	0.047857	0.233305	0.143914
	n-C6	0.010054	0.241387	0.033928
	iso-C7	0.002499	0.080694	0.068495
	n-C7	0.000000	0.001109	0.376728
	iso-C8	0.000000	0.000000	0.003116
	n-C8	0.000000	0.000635	0.002868
	iso-C9	0.000000	12.578225	1.706050
	n-C9	0.000297	1.585696	0.092261
	iso-C10	37.307341	2.511772	1.262607
	n-C10	14.518271	3.303845	0.022095
	iso-C11	0.945268	2.434516	1.094958
	n-C11	0.743261	0.735991	0.035361

2503957090 CU iThesis 6171003063 thesis / recv: 27072563 17:27:35 / seq: 25

Table A7 (Cont.) Overall mass balance of deoxygenation-hydroprocessing one-pot reaction over 10Co1Pd/HZSM-12 catalyst in different liquid hourly space velocity (Reaction conditions: 350°C, 30 bar, H_2/Feed molar ratio of 8, and TOS = 6 h)

LHSV (h^{-1})		**1.5**	**2**	**2.5**
Selectivity of product (wt.%)	*iso*-C12	0.744055	1.979094	0.778480
	n-C12	0.503653	0.687938	0.009236
	iso-C13	0.426182	0.800512	0.914531
	n-C13	0.006159	0.934495	0.304753
	iso-C14	0.259802	1.881758	1.448203
	n-C14	0.051783	4.310389	0.294556
	iso-C15	1.407418	6.339104	8.911426
	n-C15	1.091614	9.108420	3.646249
	iso-C16	5.920185	10.196519	7.197420
	n-C16	0.068034	5.611524	27.111879
	iso-C17	1.261768	3.375009	5.416115
	n-C17	5.359984	2.196797	0.563076
	iso-C18	5.450335	1.421102	5.964975
	n-C18	0.161249	0.908908	0.332300
Intermediates		3.004438	14.755645	17.702752
Feed Remaining		0.132061	7.822635	12.614899
%Conversion		99.912222	85.468920	84.952311

2503957090 CU iThesis 6171003063 thesis / recv: 27072563 17:27:35 / seq: 25

REFERENCES

Ab Gapor Md, T. (2010). Production and utilization of palm fatty acid distillate (PFAD). Lipid Technology 22(1), 11-13.

Ameen, M., Azizan, M.T., Ramli, A., Yusup, S. and Abdullah, B. (2019). The effect of metal loading over Ni/γ-Al2O3 and Mo/γ-Al2O3 catalysts on reaction routes of hydrodeoxygenation of rubber seed oil for green diesel production. Catalysis Today.

C. A. Fyfe, H.G., G. T. Kokotailo, B. Marler, and D. E. Cox (1990). Crystal Structure of Silica-ZSM-12 by the Combined Use of High-Resolution Solid-State

MAS NMR Spectroscopy and Synchrotron X-ray Powder Diffraction. The Journal of Physical Chemistry, 94.

Cao, Y., Shi, Y., Bi, Y., Wu, K., Hu, S., Wu, Y. and Huang, S. (2018). Hydrodeoxygenation and hydroisomerization of palmitic acid over bi-functional Co/H-ZSM-22 catalysts. Fuel Processing Technology 172, 29-35.

Castaño, P., Elordi, G., Olazar, M., Aguayo, A.T., Pawelec, B. and Bilbao, J. (2011). Insights into the coke deposited on HZSM-5, Hβ and HY zeolites during the cracking of polyethylene. Applied Catalysis B: Environmental 104(1-2), 91-100.

Choi, I.-H., Lee, J.-S., Kim, C.-U., Kim, T.-W., Lee, K.-Y. and Hwang, K.-R. (2018). Production of bio-jet fuel range alkanes from catalytic deoxygenation of Jatropha fatty acids on a WOx/Pt/TiO2 catalyst. Fuel 215, 675-685.

Coumans, A.E. and Hensen, E.J.M. (2017). A model compound (methyl oleate, oleic acid, triolein) study of triglycerides hydrodeoxygenation over alumina-supported NiMo sulfide. Applied Catalysis B: Environmental 201, 290-301.

de Sousa, F.P., Cardoso, C.C. and Pasa, V.M.D. (2016). Producing hydrocarbons for green diesel and jet fuel formulation from palm kernel fat over Pd/C. Fuel Processing Technology 143, 35-42.

Feng, F., Song, G., Xiao, J., Shen, L. and Pisupati, S.V. (2019). Carbon deposition on Ni-based catalyst with TiO2 as additive during the syngas methanation process in a fluidized bed reactor. Fuel 235, 85-91.

Gao, Y., Jiang, W., Luan, T., Li, H., Zhang, W., Feng, W. and Jiang, H. (2019). High-Efficiency Catalytic Conversion of NOx by the Synergy of Nanocatalyst and Plasma: Effect of Mn-Based Bimetallic Active Species. Catalysts 9(1).

Gao, Y., Zheng, B., Wu, G., Ma, F. and Liu, C. (2016). Effect of the Si/Al ratio on the performance of hierarchical ZSM-5 zeolites for methanol aromatization. RSC Advances 6(87), 83581-83588.

Guo, Q., Guo, X. and Tian, Q. (2010). Optionally ultra-fast synthesis of CoO/Co3O4 particles using CoCl2 solution via a versatile spray roasting method. Advanced Powder Technology 21(5), 529-533.

2503957090 CU iThesis 6171003063 thesis / recv: 27072563 17:27:35 / seq: 25

H. Schulz, M.W. (2004). Regimes Of Methanol Conversion On Zeolites. Surface Science and Catalysis 154.

Han, H.S., Kim, C.J., Cho, C.H., Sohn, C.H. and Han, J. (2018). Ignition delay time and sooting propensity of a kerosene aviation jet fuel and its derivative blended with a bio-jet fuel. Fuel 232, 724-728.

Hengsawad, T., Jindarat, T., Resasco, D.E. and Jongpatiwut, S. (2018). Synergistic effect of oxygen vacancies and highly dispersed Pd nanoparticles over Pd-loaded TiO2 prepared by a single-step sol–gel process for deoxygenation of triglycerides. Applied Catalysis A: General 566, 74-86.

Ju, C., Zhou, Y., He, M., Wu, Q. and Fang, Y. (2016). Improvement of selectivity from lipid to jet fuel by rational integration of feedstock properties and catalytic strategy. Renewable Energy 97, 1-7.

Kallio, P., Pasztor, A., Akhtar, M.K. and Jones, P.R. (2014). Renewable jet fuel. Curr Opin Biotechnol 26, 50-55.

Kathrina D., M., Rizalinda L. de Leon (2013). Characterization and catalytic performance of potassium loaded on rice husk silica and zeolite nay for transesterification of jatropha seed oil. Quim. Nova 36, 1116-1120.

Khan, S., Kay Lup, A.N., Qureshi, K.M., Abnisa, F., Wan Daud, W.M.A. and Patah, M.F.A. (2019). A review on deoxygenation of triglycerides for jet fuel range hydrocarbons. Journal of Analytical and Applied Pyrolysis 140, 1-24.

Kiatkittipong, W., Phimsen, S., Kiatkittipong, K., Wongsakulphasatch, S., Laosiripojana, N. and Assabumrungrat, S. (2013). Diesel-like hydrocarbon production from hydroprocessing of relevant refining palm oil. Fuel Processing Technology 116, 16-26.

Kim, Y., Kim, J. and Kim, D.H. (2018). Investigation on the enhanced catalytic activity of a Ni-promoted Pd/C catalyst for formic acid dehydrogenation: effects of preparation methods and Ni/Pd ratios. RSC Advances 8(5), 2441-2448.

Kousoulidou, M. and Lonza, L. (2016). Biofuels in aviation: Fuel demand and CO2 emissions evolution in Europe toward 2030. Transportation Research Part D: Transport and Environment 46, 166-181.

Lai, Q., Zhang, C. and Holles, J.H. (2016). Hydrodeoxygenation of guaiacol over Ni@Pd and Ni@Pt bimetallic overlayer catalysts. Applied Catalysis A: General 528, 1-13.

Li, T., Cheng, J., Huang, R., Yang, W., Zhou, J. and Cen, K. (2016). Hydrocracking of palm oil to jet biofuel over different zeolites. International Journal of Hydrogen Energy 41(47), 21883-21887.

Ma, Yuan, Jiang, Zhu, Lu and Li (2019). Pd4S/SiO2: A Sulfur-Tolerant Palladium Catalyst for Catalytic Complete Oxidation of Methane. Catalysts 9(5).

Marcelo J. B. Souzaa, A.O.S.S., Anne M. Garrido Pedrosab and Antonio S. Araujob

2503957090 CU iThesis 6171003063 thesis / recv: 27072563 17:27:35 / seq: 25

(2005). Catalytic properties of hzsm-12 zeolite in n-heptane catalytic cracking. Reaction Kinetics, Mechanisms, and Catalysis 84.

Nasrallah M, D. (2018). Sintering process and catalysis. International Journal of Nanomaterials, Nanotechnology and Nanomedicine, 001-003.

Ong, H.C., Mahlia, T.M.I., Masjuki, H.H. and Norhasyima, R.S. (2011). Comparison of palm oil, Jatropha curcas and Calophyllum inophyllum for biodiesel: A review. Renewable and Sustainable Energy Reviews 15(8), 3501-3515.

Pattanaik, B.P. and Misra, R.D. (2017). Effect of reaction pathway and operating parameters on the deoxygenation of vegetable oils to produce diesel range hydrocarbon fuels: A review. Renewable and Sustainable Energy Reviews 73, 545-557.

Peng, B., Yao, Y., Zhao, C. and Lercher, J.A. (2012). Towards quantitative conversion of microalgae oil to diesel-range alkanes with bifunctional catalysts. Angew Chem Int Ed Engl 51(9), 2072-2075.

Qiao, H., Wei, Z., Yang, H., Zhu, L. and Yan, X. (2009). Preparation and Characterization of NiO Nanoparticles by Anodic Arc Plasma Method. Journal of Nanomaterials 2009, 1-5.

Ramsay, J.D.F. and Kallus, S. (2000). Zeolite Membranes. Recent Advances in Gas Separation by Microporous Ceramic Membranes**:** 373-395.

Regnskogfondet (2016). Palm Fatty Acid Distillate (PFAD) in biofuels. ZERO and Rainforest Foundation Norway.

Rihko-Struckmann, L.K., Ye, Y., Chalakov, L., Suchorski, Y., Weiss, H. and Sundmacher, K. (2006). Bulk and Surface Properties of a VPO Catalyst Used in an Electrochemical Membrane Reactor: Conductivity-, XRD-, TPO- and XPS-study. Catalysis Letters 109(1-2), 89-96.

Sameh M.K. Aboul-Fotouh, L.I.A., Mona A. Naghmash, Noha A. K. Aboul-Gheit (2017). Effect of the Si/Al ratio of HZSM-5 zeolite on the production of dimethyl ether before and after ultrasonication. FUEL CHEMISTRY AND TECHNOLOGY 45.

Shahinuzzaman, M., Yaakob, Z. and Ahmed, Y. (2017). Non-sulphide zeolite catalyst for bio-jet-fuel conversion. Renewable and Sustainable Energy Reviews 77, 1375-1384.

Shi, J., Wang, Y., Yang, W., Tang, Y. and Xie, Z. (2015). Recent advances of pore system construction in zeolite-catalyzed chemical industry processes. Chem Soc Rev 44(24), 8877-8903.

Shi, Y., Xing, E., Wu, K., Wang, J., Yang, M. and Wu, Y. (2017). Recent progress on upgrading of bio-oil to hydrocarbons over metal/zeolite bifunctional catalysts. Catalysis Science & Technology 7(12), 2385-2415.

Silva (2004). Acid Properties Of The Hzsm-12 Zeolite With Different Si-Al Ratio By

2503957090 CU iThesis 6171003063 thesis / recv: 27072563 17:27:35 / seq: 25

Thermo-Programmed Desorption. 76.

Silva, L.S.d., Araki, C.A., Marcucci, S.M.P., Silva, V.L.d.S.T.d. and Arroyo, P.A. (2019). Desilication of ZSM-5 and ZSM-12 Zeolites with Different Crystal Sizes: Effect on Acidity and Mesoporous Initiation. Materials Research 22(2).

Snåre, M., Kubičková, I., Mäki-Arvela, P., Eränen, K. and Murzin, D.Y. (2006). Heterogeneous Catalytic Deoxygenation of Stearic Acid for Production of Biodiesel. Industrial & Engineering Chemistry Research 45(16), 5708-5715.

Srifa, A., Faungnawakij, K., Itthibenchapong, V. and Assabumrungrat, S. (2015). Roles of monometallic catalysts in hydrodeoxygenation of palm oil to green diesel. Chemical Engineering Journal 278, 249-258.

Srifa, A., Faungnawakij, K., Itthibenchapong, V., Viriya-Empikul, N., Charinpanitkul, T. and Assabumrungrat, S. (2014). Production of bio-hydrogenated diesel by catalytic hydrotreating of palm oil over NiMoS2/gamma-Al2O3 catalyst. Bioresour Technol 158, 81-90.

Sun, J., Niu, W., Taguchi, A., Abe, T., Yoneyama, Y. and Tsubaki, N. (2014). Combining wet impregnation and dry sputtering to prepare highly-active CoPd/H-ZSM5 ternary catalysts applied for tandem catalytic synthesis of isoparaffins. Catalysis Science & Technology 4(5).

Thi Kim Thoa Dao, C.L.L. (2015). n-Hexane hydro-isomerization over promoted Pd/HZSM-5 catalysts. Nanoscience and Nanotechnology 6.

Thongkumkoon, S., Kiatkittipong, W., Hartley, U.W., Laosiripojana, N. and Daorattanachai, P. (2019). Catalytic activity of trimetallic sulfided Re-Ni-Mo/γ-Al2O3 toward deoxygenation of palm feedstocks. Renewable Energy 140, 111-123.

Thrän, D. and Ponitka, J. (2016). Government Policy on Delivering Biofuels for the Aviation Sector. Biofuels for Aviation**:** 295-313.

Wang, M., Dewil, R., Maniatis, K., Wheeldon, J., Tan, T., Baeyens, J. and Fang, Y. (2019). Biomass-derived aviation fuels: Challenges and perspective. Progress in Energy and Combustion Science 74, 31-49.

Wei, J. (1996). Adsorption and cracking of N-alkanes over ZSM-5: Negative activation energy of reaction. Chemical Engineering Science 51(11), 2995-2999.

Weigert, F.J. (1986). HZSM-5-catalyzed isomerization of alkylanilines. J. Org. Chem. 52, 3296-3298.

Yang, Y.-C. and Weng, H.-S. (2009). The role of H2 in n-butane isomerization over Al-promoted sulfated zirconia catalyst. Journal of Molecular Catalysis A: Chemical 304(1-2), 65-70.

Yunming Fang, H.H., and Guohua Chen (2008). In Situ Assembly of Zeolite Nanocrystals into Mesoporous Aggregate with Single-Crystal-Like Morphology without Secondary Template. Chemistry of Materials 20.

2503957090 CU iThesis 6171003063 thesis / recv: 27072563 17:27:35 / seq: 25

Zhang, C., Hui, X., Lin, Y. and Sung, C.-J. (2016). Recent development in studies of alternative jet fuel combustion: Progress, challenges, and opportunities. Renewable and Sustainable Energy Reviews 54, 120-138.

Zhang, H., Lin, H. and Zheng, Y. (2014). The role of cobalt and nickel in deoxygenation of vegetable oils. Applied Catalysis B: Environmental 160-161, 415-422.

Zhang, J. and Zhao, C. (2016). Development of a Bimetallic Pd-Ni/HZSM-5 Catalyst for the Tandem Limonene Dehydrogenation and Fatty Acid Deoxygenation to Alkanes and Arenes for Use as Biojet Fuel. ACS Catalysis 6(7), 4512-4525.

Zhang, W.M. and Smirniotis, P.G. (1999). Effect of zeolite structure and acidity on the product selectivity and reaction mechanism for n-octane hydroisomerization and hydrocracking. Journal of Catalysis 182(2), 400-416.

2503957090 CU iThesis 6171003063 thesis / recv: 27072563 17:27:35 / seq: 25

VITA

NAME	Jarujit Chaowichitra
DATE OF BIRTH	30 April 1996
PLACE OF BIRTH	Bangkok
INSTITUTIONS ATTENDED	Department of Chemical Technology, Faculty of Science
HOME ADDRESS	91/567 Rattanathibet road City Mueng Stat Nonthaburi Postcode 11000 Country Thailand

2503957090
CU iThesis 6171003063 thesis / recv: 27072563 17:27:35 / seq: 25